Analysis of external influences on an OTEC cycle

V. Gudjónsdóttir





ANALYSIS OF EXTERNAL INFLUENCES ON AN OTEC CYCLE

by

V. Gudjónsdóttir

in partial fulfillment of the requirements for the degree of

Master of Science

in Mechanical Engineering

at the Delft University of Technology, to be defended on Tuesday July 14, 2015 at 10:00 AM.

Supervisor: Dr. ir. C. A. Infante Ferreira

Thesis committee: Prof. Dr. ir. B. J. Boersma TU Delft

Prof. Dr. ir. T. J. H. Vlugt, TU Delft Ir. B. J. Kleute Bluerise

Report number: 2674



ABSTRACT

Ocean Thermal Energy Conversion (OTEC) is a promising renewable energy technology that has vast potential in the tropics. The technology uses the temperature difference between different ocean layers to run a power cycle. The effects of temperature variations for a fixed design of the thermodynamic cycle is one of the questions that has to be answered for this technology. These effects are here analysed for three different working fluids, pure ammonia, ammonia - water mixture and R32 - R134a mixture. An off design model is implemented in MATLAB to analyse the effects. Experiments were performed with pure ammonia in an OTEC experimental set up to validate the model. The heat exchangers in the thermodynamic cycle are one of the most important components since they are large and costly in comparison to other components because of the small temperature difference in the system. Based on the experiments performed, suitable heat transfer correlations were selected. It is still a question if these correlations are suitable for other working fluids especially mixtures. This has to be confirmed with further experiments. The results of the model suggest that in all cases the net power output and the thermal efficiency are proportional to the temperature difference of the ocean layers. Fluctuations in the warm and cold seawater temperature seem to have similar effect on the outcome. Fluctuation of one degree for a 25 MW plant will result in approximately 10% fluctuation in the net power output. This is considerable and has to be taken into account in economical evaluations for each suitable location. To minimize negative effects the mass flow of the working fluid can be varied however that will only improve the performance to a small degree.

CONTENTS

Ał	stra	ct	iii
Ac	knov	wledgements	vii
1	Intr	roduction	1
	1.1 1.2 1.3 1.4 1.5 1.6 1.7	OTEC Bluerise BV OTEC History. OTEC Technology Objective Method Thesis outline	1 1 2 3 5 5 6
2	2.1 2.2 2.3 2.4 2.5 2.6	thermodynamics of an OTEC power cycle Heat exchangers	7 9 11 20 26 26 27 28 28
3	The 3.1 3.2	Assumptions	31 31 32
4	Des 4.1	ign of Experiments Sensors	37 38 38 39 40
5	Exp 5.1	5.1.1 Complications during experiments5.1.2 Results5.1.3 Uncertainty analysis	41 41 43 45
	5.2	Heat exchangers validation	46 46 49 51

VI

67 68 71 72
 64 67 68 71
 64 67 68
 64 67
64

ACKNOWLEDGEMENTS

I would first of all like to thank my main supervisor Carlos Infante Ferreira for his valuable and constructive suggestions during the development of this thesis. He was always willing to answer any questions I had, question things and guide me in the right direction with my work.

I also want to thank everyone at Bluerise for all the help and the table tennis brakes. Special thanks to Berend Jan Kleute and Joost Kirkenier who were always open to answer questions and assist with the thesis work. Additionally I would like to thank Bram Harmsen and the staff from the Process & Energy lab, especially Duncan, with all their help regarding the OTEC experimental set up.

NOMENCLATURE

- A Area, $[m^2]$
- B Width, [m]
- *b* Plate spacing, [m]
- *Bo* Boiling number (eq. 2.29)
- c_p Heat capacity, [J kg⁻¹ K⁻¹]
- Co Convective number (eq. 2.34)
- d_e Equivalent diameter, [m]
- *f* Fanning friction factor
- G Mass flux, $[kg m^{-2} s^{-1}]$
- g Gravity constant, $[m s^{-2}]$
- Ga Galileo number, (eq. 2.23)
- h Enthalpy, [J kg⁻¹]
- L Length, [m]
- \dot{m} Mass flow [kg s⁻¹]
- P Pressure, [Pa]
- *p* Plate pitch, [m]
- p_{co} Corrugated pitch
- Q Heat duty, [W]
- *Pr* Prandtl number
- q Vapor fraction
- $q^{''}$ Average imposed wall heat flux, [W m $^{-2}$]
- *Re* Reynolds number
- T Temperature [K]

X NOMENCLATURE

- U Overall heat transfer coefficient, [W m⁻²K⁻¹]
- u Velocity, [m s⁻¹]/uncertainty
- V Liquid molar volume [$m^3 \text{ mol}^{-1}$]
- v Specific volume [m³ kg⁻¹]
- W Specific work, $[J kg^{-1}]$
- \dot{W}_{net} The net power of the cycle, [W]
- \dot{W}_{T-G} The power output from the turbine connected with the generator, [W]
- \dot{W}_{TP} The total electricity consumption of the pumps, [W]
- x Mole fraction of mixture component, [mol mol $^{-1}$]
- X_{tt} The Martinelli parameter
- z Ammonia concentration, $[kg kg^{-1}]$

Greek Symbols

- α Convective heat transfer coefficient, [W m⁻²K⁻¹]
- β Chevron angle of the heat exchanger plates, measured from the horizontal
- ΔP Pressure drop, [Pa]
- Δq Vapor quality difference
- ΔT Temperature difference, [K]
- δ Thickness, [m]
- η Efficiency

 η_{Carnot} The Carnot efficiency of the cycle

 η_{cycle} The thermal efficiency of the cycle

- λ Thermal conductivity, [W m⁻¹ K⁻¹]/corrugation wavelength [m]
- μ Dynamic viscosity, [Pa s]
- ω Acentric factor
- Φ Surface enlargement factor/two phase multiplier
- ρ Density, [kg m⁻³]
- φ Chevron angle of the heat exchanger plates, measured from the vertical
- ξ Friction factor

Nomenclature xi

Subscripts

acc Acceleration

avg Average

c Critical

cond Condenser

cw Cold water side

cwp Cold water pump

des Design

ele Elevation

eq Equivalent

evap Evaporator

f Saturated liquid

fouling Fouling

frict Frictional

G Generator

g Saturated vapor

hw How water side

hwp Hot water pump

i Heat exchanger control volume

in Inlet

j/k Component j/k of a mixture

l Liquid

lm Logarithmic mean

lv latent: liquid to vapor

m Mixture

man Manifolds

off Off design

out Outlet

xii Nomenclature

P Pump

p Heat exchanger plate

recup Recuperator

red Reduced

seawater Seawater side

sp Single phase

Turbine

total Total

v Vapor

VDI VDI Heat Atlas [64]

wf Working fluid

wfp Working fluid pump

Abbreviations

DCNS Direction des Constructions Navales Services (a French naval defence company)

LCOE Levelized Cost of Electricity

LMTD Logarithmic mean temperature difference

OTEC Ocean Thermal Energy Conversion

P&ID Process and Instrumentation Diagram

SIDS Small Island Devoloping States

SWAC Seawater Air Conditioning

1

INTRODUCTION

1.1. OTEC

With global warming, rising oil prices and increasing population there is need to re-estimate the solutions to the worlds energy needs. Renewable energy technologies are an important factor to that solution. Most renewables have a fluctuating nature like wind and solar energy and can therefore not be used as base loads without an energy storage. Ocean thermal energy conversion (OTEC) is a promising renewable energy technology that can be a base load energy source in the tropics. OTEC uses the temperature difference in the ocean to produce energy. The sun heats up the ocean surface in the tropics that stores solar energy. The surface ocean layer and a much colder layer at around 1000 m depth can be used as a heat source and sink, respectively, for a power cycle. In the tropics this temperature difference between these layers is over 20 K which is the normal limit used for OTEC power cycles [43].

The potential of OTEC is vast. At least 98 nations and territories have been identified with OTEC thermal resources within their nautical economical zone [29]. The total estimated potentials of OTEC have been from 10,000 TWh/yr [54] up to about 60,000 TWh/yr [50] power production. When compared with the world electricity consumption in 2011, 19,397 TWh/yr, the potentials of OTEC are at least half if not exceeding the total electricity consumption [63]. OTEC is especially a compelling option for Small Island Developing States (SIDS) which most are dependent on fossil fuels [29, 44, 69]. Additionally SIDS are especially vulnerable to climate change [13]. OTEC can not only provide clean energy for SIDS but the islands can also greatly benefit from other usages of the technology like air conditioning with the cold ocean water and distillation of seawater. The deep ocean water is also full of nutrients that can be used for aquaculture [17, 34].

1.2. BLUERISE BV

Bluerise BV is a startup company situated in Delft, the Netherlands. Bluerise BV focuses on OTEC, seawater air conditioning (SWAC) and other related deep sea water applications. Bluerise BV can provide the technology and development plan for these technologies.

2 1. Introduction

They have a working experimental set up situated at the Technical University of Delft that is a proof of principle and is used for further development of OTEC technology. They are working together with the Curaçao Airport for development of OTEC and related technologies as part of their future plans [8]. Curaçao is a small development island situated in the Caribbean and is therefore optimal for OTEC technology as explained in section 1.1. The Curaçao Airport will have deep sea water air conditioning and a Deep Seawater Ecopark that utilizes the deep seawater. Among the technologies that are suitable for the Ecopark are aquaculture, algae, desalination, and Data Centers cooling. The goal of the Ecopark is to create economic growth, reduce import dependency, stimulate industries on the island and educate the public about renewable energy technologies [1]. The next step for Bluerise is to develop and build a 10-25 MW offshore OTEC power plant [33]. The analysis in this report is a part of that development.

1.3. OTEC HISTORY

The idea of OTEC was presented over one hundred years ago even though no commercial plants have been realized up to date. The idea was presented by a French physicist, J. D'Arsonval in 1881 [34]. The first OTEC plant was then constructed in 1930 in Cuba by his student Georges Claude. The plant failed to produce net power but operated for several weeks [66]. Since then many attempts have been made and a couple of small scale plants have been successfully constructed. Especially in the 1970's and 80's during the oil crisis OTEC got increased interest by the U.S, Japan and France [4]. In 1979 an OTEC pilot plant was made on a barge off the coast of Hawaii producing 50 kW gross power and 18 kW net power [66]. Another successful pilot plant was built in the republic of Nauru and in 1981 it produced at maximum load 120 kW gross power and 31.5 kW net power [43]. The largest OTEC plant so far was a land based one in Hawaii that operated between 1993 to 1998. The plant produced up to 255 kW gross power corresponding to 103 kW net power [66]. The only operating OTEC plant today is a pilot plant operating in Okinawa, Japan, that has been operating from June 2013. The plant has two units, both of them are Rankine cycles with R134a as a working fluid. One of the units can produce maximum amount of 50 kW while the other one is used for experiments of elemental technology and is without a turbine. [24]

Even though the principle of OTEC has been demonstrated with successful small scale pilot plants, a commercial scale OTEC plant does not exist at this time. One of the reasons is that the pilot plants that have been made do not provide enough data for a commercial plant [17]. Couple of authors seem to agree that an OTEC plant on the scale of around 5 MW is the next step that is needed before commercial scale OTEC plants can be a reality [17, 34, 66]. There has been interest in building these plants but lack of funding has for example been an issue so far because of low fossil fuel prices [65]. The next step for OTEC seems to be on the horizon with several OTEC projects being developed around the world. One of them is a 5.7 MW onshore OTEC plant in Martinique planned by Akuo Energy, DCNS (a French naval defence company) and Entrepose [47]. This plant along with other planned plants can be the intermediate step that is needed to take OTEC to the commercial scale.

1.4. OTEC TECHNOLOGY

Different types of OTEC systems have been researched since D'Arsonval presented the idea. The first plant built by Claude mentioned in section 1.3 was an open cycle OTEC system [66]. In the open cycle the surface seawater is flash-evaporated in a vacuum chamber and the resulting steam drives a turbine. The steam is then condensed with the relatively cold seawater. Fresh water can be a by-product of the open cycle system [66, 77]. Recent research and development has been mainly on the closed cycle [34]. The closed cycle is typically a Rankine cycle or a modification of the Rankine cycle. In the typical Rankine cycle a working fluid is evaporated in an evaporator using the warm surface water. The vapor is used to drive a turbine and the working fluid is condensed in a condenser using the cold seawater. A pump increases the pressure of the working fluid after the condenser and feeds it to the evaporator. A hybrid cycle has also been proposed where attributes of the closed and the open cycle are combined. After the heating of the closed cycle working fluid part of the warm seawater is desalinated in a flash evaporator. Both electricity and desalinated water are produced [55].

Since OTEC uses low temperature difference the thermal efficiency is low. Various researches have been performed to improve the cycle and the efficiency. One research direction has been in developing variations of the closed cycle to enhance the efficiency. One of them is the Kalina cycle proposed by Kalina [28]. The Kalina cycle uses an ammonia water mixture instead of a pure working fluid. The benefit of the mixture is that the evaporation and condensation do not happen at a fixed temperature like for a pure fluid. Instead the temperature gradually changes and therefore more closely follows the temperature of the seawater. Uehara [62] proposed yet another cycle in 1990 which he based on the one made by Kalina. The cycle also uses ammonia-water mixture as the working fluid and has additionally an extraction process that extracts part of the vapor from the turbine to enhance the thermal efficiency [34, 77]. Other cycles have been proposed to enhance the efficiency of OTEC. A cycle proposed by Yoon et al. [75] is supposed to give even better efficiency than the Kalina and the Uehara cycle. The cycle runs on pure ammonia and the major difference between the common Rankine Cycle is addition of a second turbine, regenerator, cooler and a separator. Yet another cycle proposed by Yuan et al. [77] proposes an absorption power cycle with two ejectors working on ammonia-water mixture to be used for OTEC. The cycle reduces the energy consumption of the cold water pump. It was not reported if it performed better than previously proposed cycles.

Another research direction has been towards increasing the temperature difference between the surface and deep seawater by utilizing renewable energy technologies like solar, geothermal or waste energy [5]. Research made by Kim et al. showed that the efficiency of an OTEC cycle improved by approximately 2 % by using the condenser effluent from a nuclear power plant instead of surface water [30]. Soto and Vergara [55] studied the possibility of coupling OTEC with a coal fired power plant located at latitude 28 °S. The proposed cycle is a hybrid cycle, consisting of a closed Rankine cycle, and uses the discharge water from the coal fired power plant instead of surface water. This application enhances the possibilities of OTEC since for normal OTEC system the location of the plant would not be feasible since the temperature difference of the seawater would

4 1. Introduction

be too small. The OTEC system additionally cools the discharge water and thereby reduces the local thermal pollution. The possiblity of coupling OTEC with solar collectors has also been researched. Aydin et al. [5] compared the options of preheating the surface seawater and direct superheating of the working fluid before the turbine with solar collectors. Both methods increased the power generation of the cycle but the thermal efficiency only increased with the direct superheating and then it improved about 60 %. With the superheating the working fluid can be heated to approximately 50 °C, compared to the 26 °C surface sea water. This temperature increase explains the increase in thermal efficiency.

Another research direction has been on a suitable working fluid for OTEC. In most cases ammonia has been the fluid of choice for closed cycle OTEC systems [7]. Other working fluids, mostly refrigerants and binary mixtures have also been researched. In 1980 Ganic and Wu compared ammonia, propane and freon-114 as possible working fluids for OTEC and concluded that ammonia was the best fit [18]. Yang and Yeh [74] also compared different refrigerants for an OTEC plant using an organic Rankine cycle. The working fluids they tested were R717 or ammonia, R600a, R245fa, R152a and R134a. The ammonia performed best in objective parameter evaluation, which was the ratio of net power output to the total heat exchanger area, but R600a gave higher thermal efficiency. As mentioned above, ammonia-water mixture has been proposed by a couple of researchers to increase the efficiency of OTEC. Other mixtures like ammonia-ethane have been proposed to increase the efficiency of the cycle [12]. The advantage of using zeotropic mixtures is the temperature glide during evaporation and condensation which more closely matches the source and sink temperature profiles and therefore increases the efficiency of the cycle. The disadvantage is that the heat transfer coefficient is lower than when using pure refrigerants because of non-linear behaviour of thermodynamic properties of refrigerant mixtures and mass transfer effect caused by composition change during the evaporation of zeotropic refrigerant mixtures [52].

Some research has gone into sensitivity analysis of OTEC and off-design operation. Research done by Gritton et al. in 1980 [19] took the seasonal variations of surface temperature in the Gulf of Mexico into account in their design. They selected a suitable cycle that maximized the average power over the year based on these variations. Hiroyuki et al. [22] did a sensitivity analysis on an ocean based closed cycle OTEC system in 1987. They analysed the effects of temperature variations and water intake flow rate variations. In 2012 Najafi et al. [45] made a sensitivity analysis of a closed cycle OTEC system. They analysed the effect of varied seawater temperature, diameter and velocity of the seawater pipes and evaporation and condensation temperature.

All OTEC technologies can be land-based or sea based [29]. The most critical components of an offshore OTEC plant were determined by Muralidharan as the following: [44]:

- Platform
- Platform mooring system
- Platform/pipe interface
- Heat exchangers

1.5. Objective 5

- Cold water pipe
- Pumps and turbines
- · Power cables

Most components have already been tested and are commercially available in the offshore industry for OTEC plants under 10 MW. For a larger scale modular design can be used for all of the components except for marine power cables, cold water pipe and the platform/pipe interface. These components present fabrication and deployment challenges for larger scale facilities [44]. More details about the components of the thermodynamic cycle can be viewed in Chapter 2.

1.5. OBJECTIVE

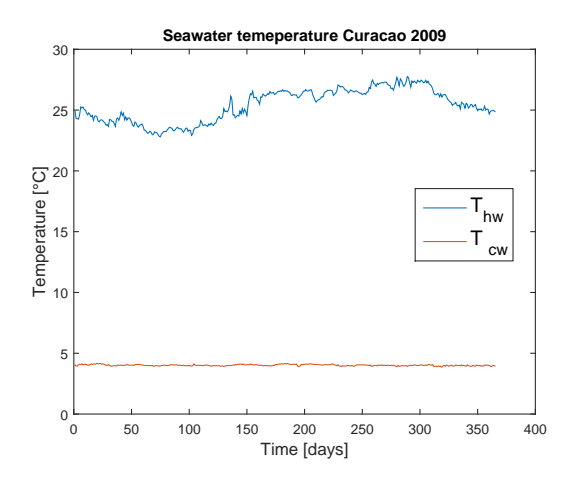
As stated before one of Bluerise goals is to build a 10 - 25 MW offshore OTEC plant. The design has been optimized for set conditions by Kirkenier for different working fluids [31]. The main objective of this thesis is to analyse the effects of fluctuations in seawater temperature for the proposed plant. The seawater temperature can differ because of seasonal fluctuations or because of different geographical setting than originally planned. In the tropical region between 15° north and 15° south the annual average temperature of the surface seawater varies from about 27 °C to about 29 °C while the seawater at 1000 m depth is fairly stable at 4.4 °C [4]. Another possible location for an OTEC plant is in Hawaii. The surface seawater temperature ranges from 24 to 28 °C while the seawater temperature at 1000 m depth is fairly constant at 4.5 °C throughout the year [65]. The temperature at 1000 m depth can be higher at certain locations that are still suitable for OTEC. An example is Sri Lanka where the temperature is around 7 °C at 1000 m depth ¹. A yearly fluctuations in seawater temperatures, for the year 2009, for the tropical island Curação where Bluerise has interest is shown in figure 1.1. The data is received from the World Ocean Atlas [38]. These temperature fluctuations at each locations have potentially a high impact on the performance of an OTEC plant since the overall temperature difference is relatively low.

1.6. METHOD

To achieve the goal of this research a new model is made. The results from Kirkeniers' optimization are used as inputs, specifically the heat exchanger geometry, mass flows and the concentration in the case of a mixture. The model made by Kirkenier calculates the most optimal design for fixed operating conditions. The warm seawater temperature was fixed at 27 °C and the cold seawater temperature at 5 °C, which are typical temperatures for the tropics. If these temperatures are changed Kirkeniers model will calculate a new optimized cycle design. In practice it is not practical to change the design to adjust to fluctuations, for example it is not economically feasible to change the heat

¹Joost Kirkenier, personal communication, April, 2015

6 1. Introduction



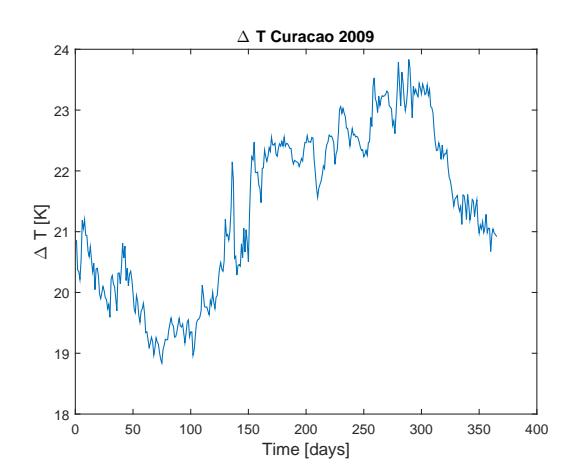


Figure 1.1: Seawater temperatures in Curaçao during 2009. On the left the warm seawater temperature at 20 m below sea level and cold water from 1000 m below sea level are displayed. On the figure on the right the temperature difference over the year is displayed.

exchanger size depending on the temperatures. To analyse the effects of the temperature fluctuations a new model is implemented in MATLAB [59]. To validate the model, experiments are executed with the OTEC experimental set up that Bluerise has available at the Technical University of Delft. The set up is in principle the Kalina cycle and has been operating with ammonia. The working fluids that are researched are therefore ammonia, the working fluid that showed the best results in Kirkenier's work which is the fully evaporating mixture R32-R134a and the partially evaporating mixture ammonia-water that also showed promising results in the work of Kirkenier. Additionally, to validate heat transfer correlations for the condenser when using ammonia water mixture, data is used from a former geothermal plant located in Húsavík, Iceland.

1.7. THESIS OUTLINE

The steps to achieve the goal of the research are listed below in each relevant chapter.

- Chapter 2: The thermodynamics of the OTEC cycle are explained and relevant correlations are reviewed.
- Chapter 3: The modelling approach and the solution procedure of the new model are described.
- Chapter 4: Experimental plan is designed to be performed with the OTEC experimental set up.
- Chapter 5: Results from the experiments and validation of the model.
- Chapter 6: Sensitivity analysis of the system is performed with regards to seawater temperature.
- Chapter 7: Conclusions and recommendations for future work.

2

THE THERMODYNAMICS OF AN OTEC POWER CYCLE

In this chapter the thermodynamics of the OTEC system that is being modelled are described. An overview of the system can be seen in figure 2.1. The principles of the thermodynamic cycle of the OTEC experimental set up and for the proposed 10 - 25 MW plant are similar. The only noticeable difference between the models of the systems is the scale and efficiencies. Also instead of seawater normal water is used as heating and cooling media. The cycle used in the OTEC experimental set up is the Kalina cycle, more specifically a cycle that has been called KCS 34g. This cycle is suited for plants operating with temperatures below 121°C [78]. The same cycle is the base for the larger plant. The cycle is shown in figure 2.1. From state 1 to 2 the working fluid pressure is increased by a means of a pump. From state 2 to 3 the working fluid is partly heated in the recuperator. From state 3 to 4 the working fluid is partly or fully evaporated in the evaporator by the means of the warm seawater. From state 4 in the cycle the working fluid is then separated in a separator into its liquid and vapor parts, that are shown in states 4w and 4r respectively. The vapor is expanded between state 4r and 5r in a turbine and work is produced. The liquid from the separator enters the recuperator in state 4w to 5w where it is used to heat up the working fluid coming from the pump. The liquid is then expanded between state 5w and 6w in an expansion valve to the same pressure as in state 5r. The liquid and vapor are then mixed in a mixer to state 7 in the cycle. Between states 7 and 1 the working fluid is condensed in a condenser by the means of the cold seawater.

In the thermo-economic optimization of the larger plant made by Kirkenier [31] other working fluids were also researched. The ones that gave the best results were all mixtures, see figure 2.2. The benefits of using mixtures is a temperature glide during evaporation and condensation opposed to pure fluids. The mixtures can therefore follow the slopes of the hot and cold seawater more closely than pure fluids which results in a better heat transfer [3]. Some of those mixtures fully evaporated in the evaporator and performed better than the ammonia-water mixture. With these fully evaporating mixtures the cycle design can be simpler by becoming the commonly used Rankine cycle. The mixture that showed the best result was R32-R134a. This mixture will therefore be analysed later in chapter 6. The most common working fluid so far in OTEC cycles has been ammonia which is also a common

working fluid in industry [44]. Ammonia is also used in the experiments that are executed to validate the model and will therefore also be used in the analysis in chapter 6. Ammonia water which is a partly evaporating mixture showed promising results in the thesis by Kirkenier [31]. Ammonia water has also been implemented in geothermal applications with a similar thermodynamic cycle for example in Húsavík, Iceland [56]. Ammonia water is therefore the third working fluid that is analysed in chapter 6.

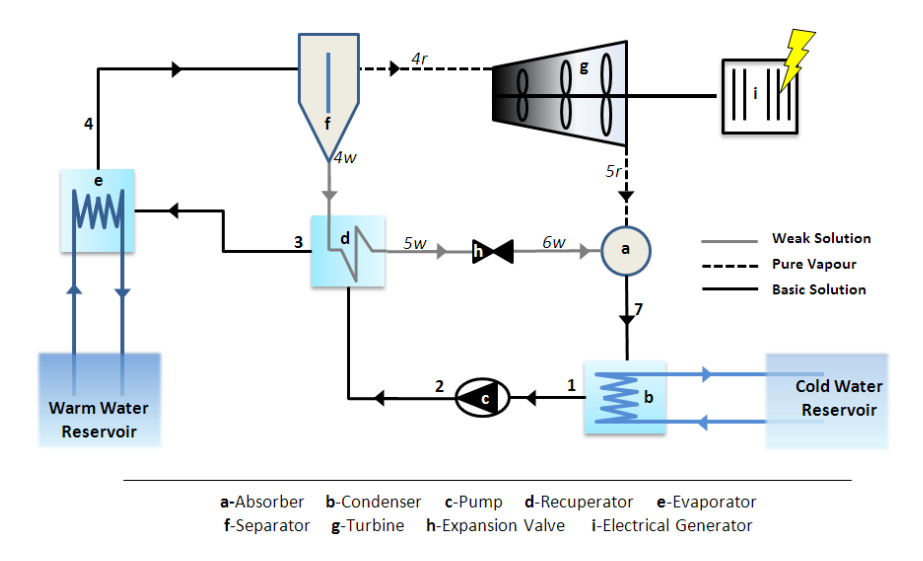


Figure 2.1: Layout of the OTEC system. From point 1 to 2 the working fluid pressure is increased by means of a pump. From point 2 to 3 the working fluid is partly preheated in the recuperator. From point 3 to 4 the working fluid is partly or fully evaporated in the evaporator by the means of the warm seawater. From point 4 in the cycle the working fluid is then separated in a separator into its liquid and vapor parts, that are shown in points 4w and 4r, respectively. The vapor is expanded between point 4r and 5r in a turbine and work is produced. The liquid from the separator enters the recuperator in point 4w to 5w where it is used to heat up the working fluid coming from the pump. The liquid is then expanded between point 5w and 6w in an expansion valve to the same pressure as in point 5r. The liquid and vapor are then mixed in an absorber to point 7 in the cycle. Between point 7 and 1 the working fluid is condensed in a condenser by the means of the cold seawater. Image courtesy of Bluerise BV.

2.1. HEAT EXCHANGERS 9



Figure 2.2: Specific and Levelized Cost of Electricity (LCOE)¹ from the optimization of the 10 to 25 MW OTEC system. The best results gave the fully evaporating mixture R32-R134a, ammonia water (R717-H₂O) is among the most promising mixtures and ammonia (R717) is among the most promising pure fluids for OTEC applications. Image courtesy of J. A. Kirkenier [31]

The sections below give an overview of each component of the system. Note that in case of an Rankine cycle the separator and the recuperator are unnecessary. The thermodynamic properties of the fluids are acquired from the REFPROP database [36].

2.1. HEAT EXCHANGERS

The heat exchangers in the system are the evaporator, the condenser and the recuperator. The heat exchangers are one of the most important components of an OTEC plant. Because of the small temperature difference between the sink and the source the necessary heat exchangers are large compared to the other components of the cycle and costly. The type of heat exchangers suitable for OTEC has been one of the research topics regarding OTEC technology. Experiments made by Journoud et al. [26] in 2012 showed that a vertical plate-type evaporator exchanged more heat per square meter and the system produced more electricity than with a shell and tube one. The working fluid they used was ammonia. The same conclusion was obtained at the OTEC laboratory of the Saga University in Japan [34]. They made a combined economic assessment of heat transfer capacity, pressure loss and seawater flow rate and their conclusion was that plate type heat exchangers are best suited for OTEC applications. The OTEC plant in Japan which is in operation uses titanium plate heat exchangers [24]. The heat exchangers in the OTEC experimental set up are also plate heat exchangers and in the optimization of a larger plant by Kirkenier plate heat exchangers were also used [31]. Plate-fin and plate-channel heat exchangers are also promising for OTEC systems but there is less operational experience with these heat exchangers [33].

¹Levelized Cost of Electricity seeks to capture the average cost of output over a plants entire life cycle [25].

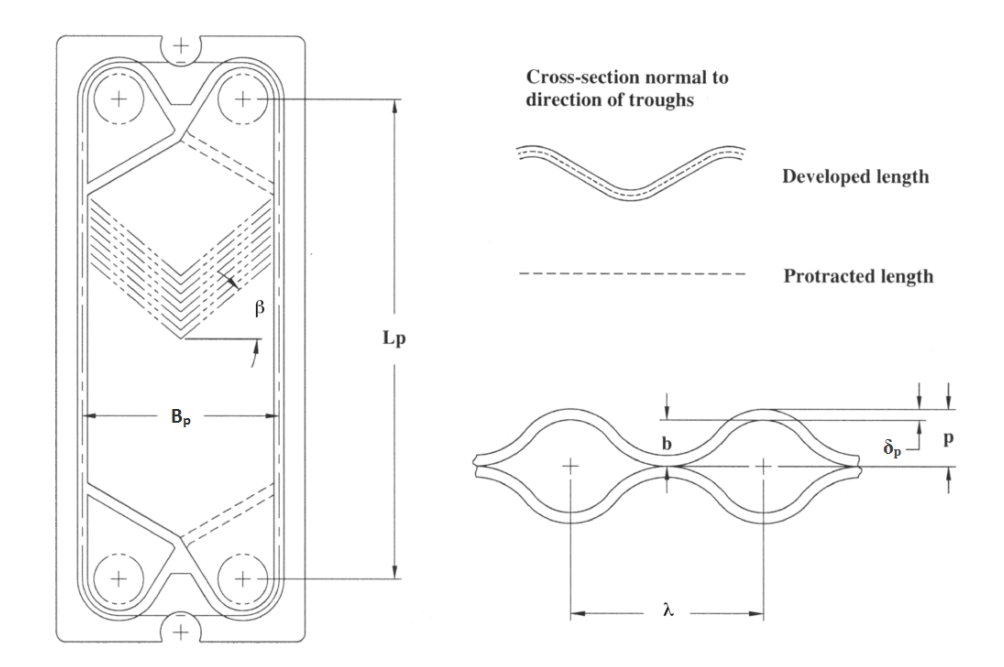


Figure 2.3: Plate parameters: B_p is the width of the plate, L_p is the length of the plate from each port center, β is the chevron angle, δ_p is the thickness of the plate, p the plate pitch, p the plate spacing and p the corrugation wavelength. Figure from Ayub [6].

For all the heat exchangers the Logarithmic Mean Temperature Difference (LMTD) method is used. The LMTD method is based on the assumption that the properties of the working fluid remain unchanged. That is not the case during two phase flow and therefore the heat exchangers are divided into N equal sections to make the calculations more accurate. This is similar to what was done by Li and Dai for Kalina cycle calculations [37]. The heat duty for each zone is then:

$$\dot{Q}_i = U_i A_i \Delta T_{lm,i} \tag{2.1}$$

Where the subscript i indicates the heat exchanger control volume, A the heat transfer area, ΔT_{lm} the Logarithmic Mean Temperature Difference (LMTD), and U the overall heat transfer coefficient. The heat transfer area of each plate in the heat exchanger can be defined as [64]

$$A_p = \Phi B_p L_p \tag{2.2}$$

Where Φ is the surface enhancement factor, this value is typically around 1.22 [64], B_p is the width of the plate and L_p is the length of each plate from each port center. The LMTD is calculated according to the following equation:

$$\Delta T_{lm} = \frac{\Delta T_{in} - \Delta T_{out}}{ln(\frac{\Delta T_{in}}{\Delta T_{out}})}$$
(2.3)

The overall heat coefficient is defined as:

$$\frac{1}{U_i} = \frac{1}{\alpha_{seawater,i}} + \frac{1}{\alpha_{fouling}} + \frac{\delta_p}{\lambda_p} + \frac{1}{\alpha_{wf,i}}$$
 (2.4)

2.1. HEAT EXCHANGERS

Here $\alpha_{seawater}$ is the convective heat transfer coefficient for the seawater side, α_{wf} is the convective heat transfer coefficient for the working fluid side, $\alpha_{fouling}$ is the heat transfer coefficient due to the effect of fouling on the seawater side, δ_p is the plate thickness, and λ_p is the thermal conductivity of the plate material.

Ayub [6] pointed out in 2003 that very few correlations for two phase flow in plate heat exchangers have been published and that manufacturers keep their correlations confidential. Even for single phase flow the available correlations apply for specific geometry, fluid and experimental range of operation and all of the correlations are of empirical nature. In the following sections some of the proposed correlations for heat transfer and pressure drop in plate heat exchangers are reviewed.

2.1.1. HEAT TRANSFER CORRELATIONS

The heat transfer correlations can be divided into single phase flow correlations and two phase flow correlations where the two phase flow correlations divide into correlations for evaporation and condensation.

2.1.1.1 Single phase flow

There is single phase flow on the seawater side of the evaporator and the condenser and as well as in the recuperator and the subcooled part of the evaporator. As pointed out in Coulson and Richardson's Chemical Engineering Design the heat transfer coefficient depends on the type of plate being used [53]. Table 2.1 shows a review of couple of heat transfer correlations for single phase flow. All of the correlations are empirical power law curve fits where the heat transfer coefficient is a function of the Reynolds and Prandtl number. The Reynolds number, *Re* is defined as

$$Re_i = \frac{Gd_e}{\mu_i} \tag{2.5}$$

Where G is the mass flow rate per unit cross-sectional area, μ is the dynamic viscosity and d_e is the equivalent diameter that can be estimated as twice the gap between the plates. The Prandtl number, Pr, is given as:

$$Pr_i = \frac{c_{p,i}\mu_i}{\lambda_i} \tag{2.6}$$

Where c_p is the heat capacity of the fluid.

Note that in the correlation from the VDI Heat Atlas [64] the equivalent diameter is calculated as twice the gap between the plates divided by the surface enhancement factor (Φ) . The Reynolds number is therefore different than the Reynolds number in equation 2.5 and is referred to as Re_{VDI} . In the same correlation ξ is the friction factor, see equation 2.46.

Comparison between the correlations can be seen in figure 2.4. There is a significant difference between the correlations even though they all show a similar trend. For the comparison the plate geometry of the heat exchangers from the OTEC experimental set up

is used, this geometry will be introduced in chapter 4 (table 4.1). Properties of water have been obtained at atmospheric pressure and 27°C which is typical operating conditions of the warm water side of the evaporator. Note that for the validation of the model the OTEC experimental set up is used as mentioned in section 1.5. In the set up water is used instead of seawater as a heating and cooling media. After validation seawater properties are calculated according to correlations gathered by Sharqawy et al. [51]. For the seawater properties the salinity is taken as 35 g/kg since that is the average salinity of seawater [39].

Table 2.1: Review of heat transfer correlations for single phase flow.

Investigator	Correlation	Validation range
Sinnott [53]	$\alpha_{sp,i} = \frac{\lambda_i}{d_e} 0.26 Re_i^{0.65} Pr_i^{0.4} $ (2.7)	Turbulent flow in a typical plate
VDI Heat Atlas [64]	$\alpha_{sp,i} = \frac{\lambda_i}{d_e} 1.615 [(\xi Re_{VDI,i}/64) Re_{VDI,i} Pr_i d_e/L_p]^{1/3} $ (2.8)	60 < Re < 30,000
Winkelmann [71]	$\alpha_{sp,i} = \frac{\lambda_i}{d_e} 0.60 Re_i^{0.51} Pr_i^c $ (2.9)	10 < Re < 450
	$\alpha_{sp,i} = \frac{\lambda_i}{d_e} 0.60 Re_i^{0.51} Pr_i^c $ $\alpha_{sp,i} = \frac{\lambda_i}{d_e} 0.22 Re_i^{0.68} Pr_i^c $ (2.9) (2.10)	450 < Re < 13,000
	c = 0.4 (2.11)	
	(if fluid is being heated)	
	c = 1/3 (2.12)	
	(if fluid is being cooled)	
Yan et al. [73]	$\alpha_{sp,i} = \frac{\lambda_i}{d_e} 0.2121 Re_i^{0.78} Pr_i^{1/3} $ $\alpha_{sp,i} = \frac{\lambda_i}{d_e} 0.2875 Re_i^{0.78} Pr_i^{1/3} $ (2.14)	Re > 200
Donowski and Kandlikar [15]	$\alpha_{sp,i} = \frac{\lambda_i}{d_e} 0.2875 Re_i^{0.78} Pr_i^{1/3} $ (2.14)	Re > 200

2.1. Heat exchangers 13

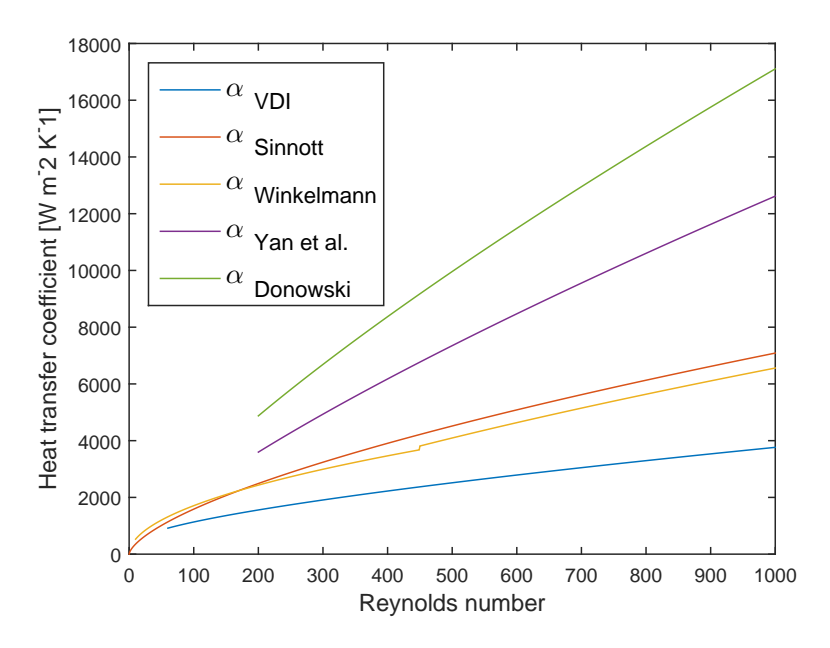


Figure 2.4: Comparison of heat transfer correlations for single phase flow.

2.1.1.2 Two phase flow

The correlations for two phase flow are similarly to the single phase flow correlations all of empirical nature. In the following sections a review of some of the correlations that have been proposed in literature are reviewed for condensation and evaporation.

2.1.1.2.1 Condensation

Table 2.2 shows a review of heat transfer correlations for condensation. Some of the correlations are a function of the equivalent Reynolds number which is expressed as

$$Re_{eq,i} = \frac{G_{eq,i}d_e}{\mu_l} \tag{2.15}$$

Where the equivalent mass flux is

$$G_{eq,i} = G[1 - q + q(\rho_l/\rho_v)^{1/2}]$$
(2.16)

Where q is the vapor quality and ρ the density.

The correlations were either fit to data for pure working fluids or mixture or both. In experiments done by Thonon and Bontemps [60] single component and binary mixtures of hydrocarbons in a welded cross-corrugated condenser were researched. The mixtures had a lower heat transfer coefficient for low Reynolds numbers but at higher Reynolds numbers (approximately above 2000) the mixtures were comparable with the pure fluids. The heat transfer coefficient was up to 4 times lower for the mixtures compared to the pure hydrocarbons which suggests that mass transfer plays a higher role for the mixtures at low Reynolds number. They only proposed a correlation for the pure fluids which is also valid for the mixtures at high Reynolds numbers. This contradicts the results of Palmer et al. who proposed heat transfer correlations for refrigerants R22, R290 and mixtures

R290-R600a and R32-R152a in a brazed plate heat exchanger [48]. They compared their experimental results to previously determined correlations, 13 for evaporation and 6 for condensation, but the agreement was found unsatisfactory with their data. The reason is probably that they used lower Reynolds numbers than the previous correlations namely in the range from 13 to 230. They concluded that the same correlation could be used for the pure fluids as well as the mixture R290-R600a but another correlation was used for the R32-R152a mixture since another lubricant was then used. This indicates that correlations for pure refrigerants might be accurate enough for mixtures. Winkelmann [71] also did experiments with condensation of pure fluids and mixtures in a plate heat exchanger. He proposed two different correlations one for pure fluids and one for mixtures. For the pure fluids Winkelmann did not get a more accurate fit by including the Reynolds number in the correlation. The correlation from Yan et al. [73] was fitted for data with refrigerant R134a.

A comparison of the condensation correlations proposed by Palmer et al. [48], the one for pure hydrocarbons by Thonon and Bontemps, the correlations by Winkelmann and the correlation proposed by Yan et al. is shown in figure 2.5. The comparison was made with properties for ammonia since it was used in the experiments. The Reynolds number is taken until a value of 1000. The plate geometry of the heat exchanger from the OTEC experimental set up were used similarly as for the single phase flow correlations. The pressure was set as 7 bar and the vapor quality as 50%.

It is seen that the correlation by Palmer et al., Yan et al., and the mixture correlation from Winkelmann have similar curves while the one by Thonon and Bontemps is more alike the correlation for pure fluid by Winkelmann. Also when looked more closely into the data from Palmer et al. it is seen that the mixtures do indeed have in most cases a lower heat transfer coefficient, see figure 2.6. As explained before Palmer et al. concluded that the heat transfer coefficient was likely lower in that case since another lubricant was then used however the explanation could also be that mass transfer is a more dominant phenomenon for the mixtures at low Reynolds numbers. The correlation from Palmer et al. might therefore be correlating more a mixture behaviour than a pure fluid behaviour for low Reynolds number and therefore shows similar results to the correlation from Winkelmann for mixtures. The correlation from Yan et al. seems to be showing more a mixture behaviour if compared to the mixture correlation from Winkelmann. The reason could be that the correlation was proposed for higher Reynolds numbers and the flow was kept turbulent.

2.1. HEAT EXCHANGERS 15

Table 2.2: Review of heat transfer correlations for condensation.

Investigator	Correlation		Validation range
Palmer et al. [48]	$\alpha_{cond,i} = \alpha_l^{0.387} \Phi_l^{0.0827} G a^{0.346} P_{red}^{1.5} \omega^{1.5}$	(2.17)	13 < Re < 230
	$\alpha_{l} = \frac{\lambda_{l}}{d_{e}} 0.16 Re^{0.89} Pr_{l}^{0.3}$	(2.18)	
	$P_{red} = P/P_c$	(2.19)	
	$\Phi_l = (1 + 12/X_{tt} + 1/X_{tt}^2)^{0.5}$	(2.20)	
	$X_{tt} = \left(\frac{1-q}{q}\right)^{0.9} \left(\frac{\rho_{\nu}}{\rho_{l}}\right)^{0.5} \left(\frac{\mu_{l}}{\mu_{\nu}}\right)^{0.1}$	(2.21)	
	$\omega = -log_{10}(P/P_c)$	(2.22)	
	$Ga = \rho_l(\rho_l - \rho_g)gd_e^3/\mu_l^2$	(2.23)	
Thonon and Bontemps [60]	$\alpha_{cond,i} = 1564Re_{eq,i}^{-0.76}\alpha_l$	(2.24)	50 < Re < 2000
	$\alpha_{l} = \frac{\lambda_{l}}{d_{e}} 0.347 Re^{0.653} Pr_{l}^{0.33}$ $\alpha_{cond,i} = \frac{\lambda_{l}}{d_{e}} 94 Co_{i}^{-0.46} Pr_{l,i}^{1/3}$	(2.25)	
Winkelmann [71]		(2.26)	10 < Re < 1100 (pure)
	$\alpha_{cond,i} = \frac{\lambda_l}{d_e} 16.8 Re_{eq,i}^{0.29} Pr_{l,i}^{1/3}$	(2.27)	10 < Re < 1100 (mixture)
Yan et al. [73]	$\alpha_{cond,i} = \frac{\lambda_l}{d_e} 16.8 R e_{eq,i}^{0.29} P r_{l,i}^{1/3}$ $\alpha_{cond,i} = 4.118 (\frac{\lambda_l}{d_e}) R e_{eq,i}^{0.4} P r_{l,i}^{1/3}$	(2.28)	Re > 200

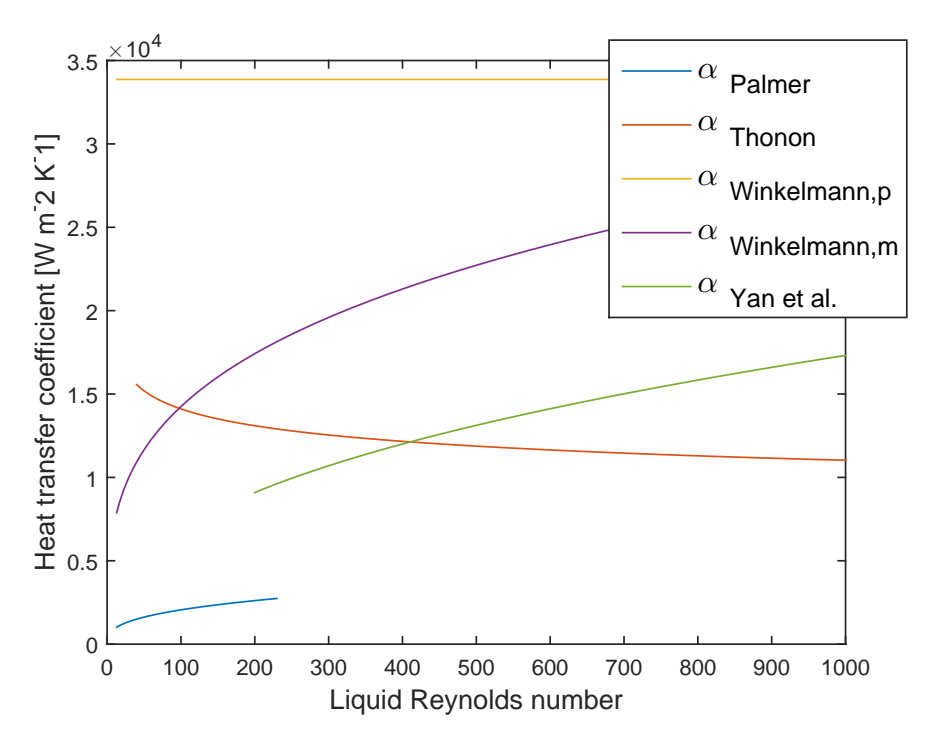


Figure 2.5: Comparison of the proposed heat transfer correlations for condensation. For the correlations from Winkelmann [71] p stands for pure fluid and m for mixture.

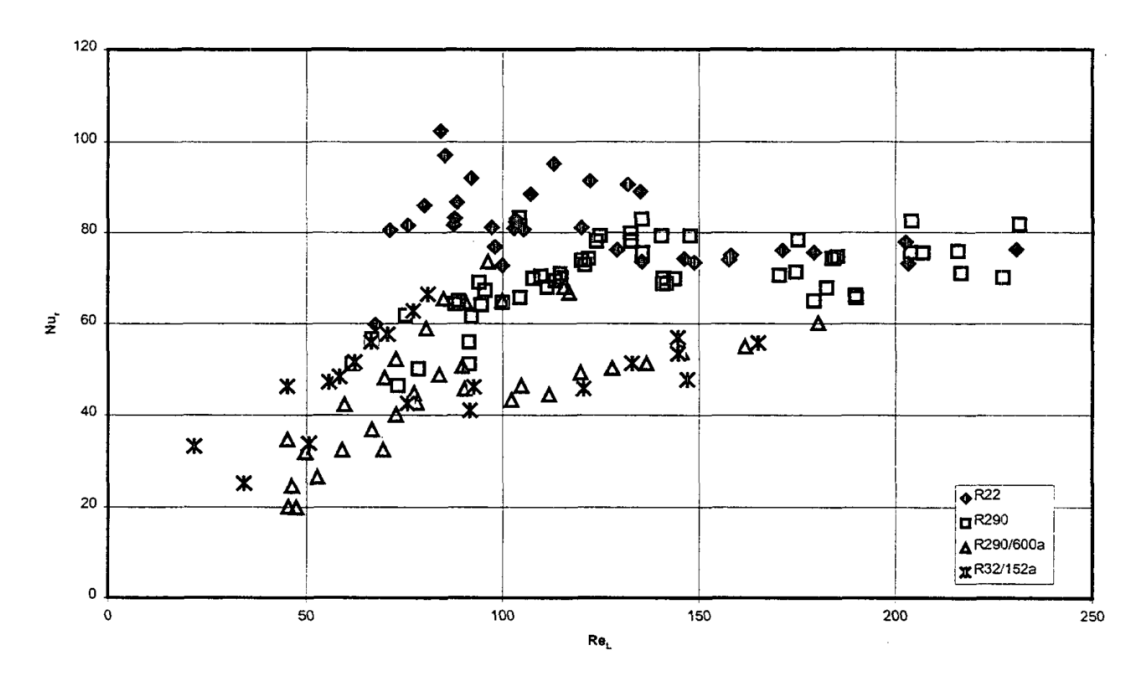


Figure 2.6: Data for condensation from Palmer et al. [48]. Here the Nusselt number is shown as a function of the liquid Reynolds numbers. The mixtures R290/600a and R32/152a have lower Nusselt numbers at lower Reynolds number than the pure fluids R22 and R290.

2.1. HEAT EXCHANGERS 17

2.1.1.2.2 Evaporation

Table 2.3 shows a review of heat transfer correlations for evaporation. These correlations are also of empirical nature. Kirkenier [31] noticed that correlation from Yan and Lin, which is based on experiments with refrigerant R134a, does not fit their own data except with an additional factor of 10. Donowski and Kandlikar [15] came to a similar conclusion and they proposed a new correlation based on Yan and Lin's data. The modified correlation was deemed promising by Huang [23].

Some of the proposed correlations are a function of the boiling number which is defined as

$$Bo = \frac{q''}{Gh_{In}} \tag{2.29}$$

Where q'' is the average imposed wall heat flux.

The correlation proposed by Ayub [6] is based upon experiments with ammonia and R22. Some correlations have been proposed for ammonia water mixtures which is a promising mixture for OTEC applications. Ventura [67] did some experiments in 2010 on evaporation of ammonia water mixture for low mass flux range 0.9 - 3.09 kg m⁻² s⁻¹ with a concentration of 0.93 to 0.99. Another correlation that has been proposed for ammonia water is one by Okamoto et al. [46]. They did experiments with ammonia water with concentration of ammonia from 90 to 100%. In the correlation E and m are constants that depend on the concentration of ammonia. For pure ammonia E and m are 13.6 and 0.6 respectively. For other concentrations the values were not given but from plots in the paper for ammonia concentrations of 0.9 and 0.95 the constants can be derived. For ammonia concentration of 0.95 (similar concentration to what has been proposed by Kirkenier [31] for OTEC application) the constants are approximately E=23 and m=0.33. Okamoto et al. varied the mass flux from 7.5 to 15 kg/m^2 s. At the lower mass flux range which corresponds to lower Reynolds numbers the difference in the local heat transfer coefficient was quite high with the heat transfer coefficient being lower for lower concentration of ammonia. For higher heat fluxes, which corresponds to higher Reynolds numbers, the difference in the heat transfer coefficient became smaller. This corresponds to the results of Thonon and Bontemps [60] described above.

A comparison of the correlations proposed for evaporation is given in figure 2.7. The figure was plotted for heat exchanger geometry of the OTEC experimental set up and ammonia was used for thermodynamic properties since that is the working fluid used in the OTEC set up. The pressure was taken as 6.75 bar, and the heat flux as 11000 W m⁻². When compared, it can be observed that the correlations divide roughly into two groups, that is those that show very high heat transfer coefficients and those that show much lower values. The higher ones are the correlations from Ayub, Yan and Lin with the correction factor of 10 and the correlation from Palmer et al. This might be because of different geometry and conditions during these experiments.

Table 2.3: Review of heat transfer correlations for evaporation.

Investigator	Correlation	Validation range
Yan & Lin [72]	$\alpha_{evap,i} = \frac{\lambda_l}{d_e} 1.926 Re_{eq,i} Re_i^{-0.5} Pr_{l,i}^{1/3} Bo_{eq,i}^{-0.3} $ (2.30)	Re > 200
Yan & Lin times factor 10	$\alpha_{evap,i} = \frac{\lambda_l}{d_e} 19.26 Re_{eq,i} Re_i^{-0.5} Pr_{l,i}^{1/3} Bo_{eq,i}^{-0.3} $ (2.31)	Re > 200
Donowski and Kandlikar [15]	$\alpha_{evap,i} = 1.055[1.056Co_i^{-0.4} + 1.02Bo_i^{0.9}]q^{-0.12}\alpha_l^{0.98} $ (2.32)	Re > 200
	$\alpha_{evap,i} = [1.184Co_i^{-0.3} + 225.5Bo_i^{2.8}](1-q)^{0.0003}\alpha_l $ (2.33)	Re > 200 (another fit)
	$Co = (\rho_g/\rho_l)^{0.5} ((1-q)/q)^{0.8}$ (2.34)	
	$\alpha_l = 0.02875 Re^{0.78} Pr^{1/3} \frac{\lambda_l}{d_e} $ (2.35)	
Ayub [6]	$\alpha_{evap,i} = 0.025C \frac{\lambda_l}{d_e} [Re_i^2 h_{lv}/L_p]^{0.4124} (P/P_c)^{0.12} (65/\beta)^{0.35} $ (2.36)	No limit defined
	C=0.1121 for flooded and thermo-syphon	
	C=0.0675 for direct expansion	
Okamota [46]	$\frac{\alpha_{evap,i}}{\alpha_l} = E(1/X_{tt})^m \tag{2.37}$	200 < Re < 400
	$\alpha_l = 0.023 \frac{\lambda_l}{d_e} \left[\frac{G(1-q)d_e}{\mu_l} \right]^{0.8} Pr_l^{0.4} $ (2.38)	
Ventura [67]	$\alpha_{evap,i} = 1.92 \frac{\lambda}{d_e} Re_{eq}^{0.885} Pr^{1/3} Bo_{eq}^{0.536} z^{-22.3} $ (2.39)	10 < Re < 200
Palmer et al. [48]	$\alpha_{evap,i} = 1.92 \frac{\lambda}{d_e} Re_{eq}^{0.885} P r^{1/3} B o_{eq}^{0.536} z^{-22.3} $ (2.39) $\alpha_{evap,i} = 2.7 \frac{\lambda}{d_e} Re_l^{0.55} P r_l^{0.5} $ (2.40)	13 < Re < 230

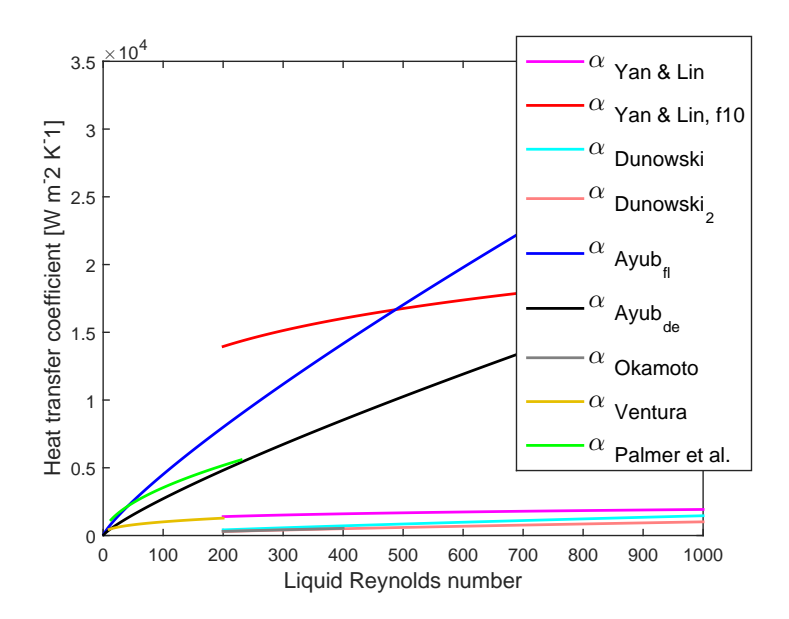


Figure 2.7: Comparison of heat transfer correlations for evaporation. Here two groups are observed, the correlations that show higher heat transfer coefficient which are the correlation from Yan & Lin [72] with a factor of 10, the one from Palmer et al. [48] and both of the proposed correlations from Ayub [6]. The other group that shows lower heat transfer coefficients are shown in more detail in figure 2.8.

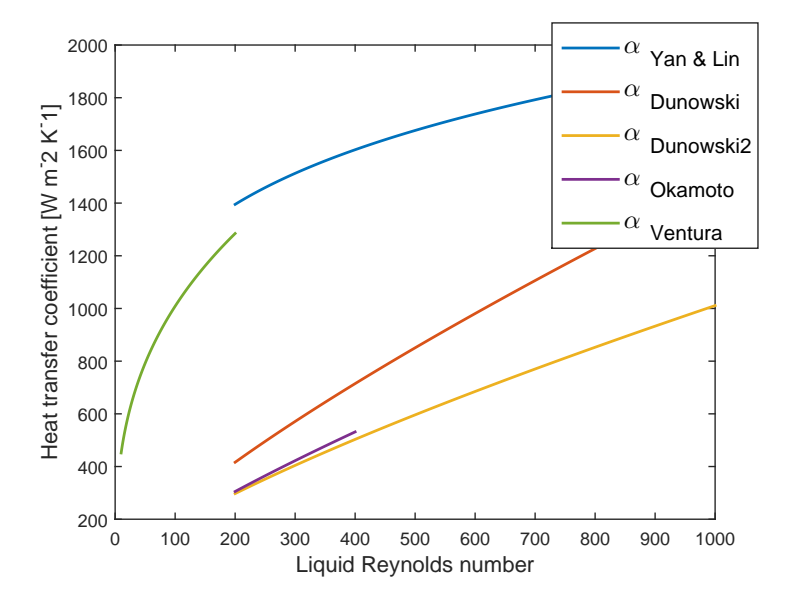


Figure 2.8: Comparison of heat transfer correlations for evaporation that show lower heat transfer coefficient, namely the correlation proposed by Yan & Lin [72] without a correction factor, the correlations proposed by Donowski and Kandlikar [15], the correlation proposed by Okamoto et al. [46] and the one proposed by Ventura [67].

2.1.2. Pressure Drop Correlations

The pressure drop for the heat exchangers can be divided into frictional pressure drop, pressure drop because of acceleration, elevation and pressure drop at inlet and exit manifolds and ports [72]

$$\Delta P_{total} = \Delta P_{frict} + \Delta P_{acc} + \Delta P_{ele} + \Delta P_{man}$$
 (2.41)

The pressure drop because of acceleration is determined as

$$\Delta P_{acc} = G^2 \nu_m \Delta q \tag{2.42}$$

Where the specific volume of the mixture is estimated as $v_m = [qv_g + (1-q)v_l]$. The pressure drop because of elevation as:

$$\Delta P_{ele} = \frac{gL}{\nu_m} \tag{2.43}$$

The pressure drop at inlet and exit manifolds and ports is determined as

$$\Delta P_{man} = 1.5(\frac{u_m^2}{2v_m})\tag{2.44}$$

Where $u_m = Gv_m$ is the mean flow velocity.

According to experiments made by Yan and Lin [72] on evaporation of R134a the frictional pressure drop was measured as 96 to 99% of the total pressure drop. Another set of experiments on condensation heat transfer by Yan et al. [73] the frictional pressure drop was measured as 93 to 99 % of the total pressure drop. Therefore some authors only consider the frictional pressure drop for plate heat exchangers [6]. The frictional pressure drop is given by:

$$\Delta P_{frict} = \frac{\xi G^2}{2\rho d_a} L_p = \frac{2fG^2}{\rho d_a} L_p \tag{2.45}$$

Where L_p is the length of the plates and ρ is the density of the fluid. ξ is the friction factor but in the literature it is also common to use the Fanning friction factor $f=\xi/4$. The friction factor depends on the plate design and many different correlations have been developed. A couple of them can be viewed in a literature survey by Ayub [6]. Most of those were in the form of a power law curve fit with the latest ones taking the chevron angle into account. Focke et al. [16] concluded after experiments with different chevron angles that the chevron angle is a major parameter influencing the pressure drop since it affects the flow structure through the plates. Therefore pressure drop correlations dependent on the chevron angle are chosen for further review.

2.1.2.1 Single phase flow

There are many correlations for single phase flow in plate heat exchangers. Couple of those take the effect of the chevron angle and are suitable for the conditions for OTEC. The chevron angle in the experimental set up was measured as 22° to the horizontal (see

2.1. HEAT EXCHANGERS 21

figure 2.3) and the chevron angle was assumed to be 30° measured from the horizontal in Kirkenier's thesis which is a common chevron angle [31]. A review of friction factors for single phase flow is shown in table 2.4. The correlations are a function of the chevron angle or were correlated for plate heat exchangers with chevron angle of 30° measured from the horizontal. Note that φ is the chevron angle of the plates measured from the vertical flow direction while β is the chevron angle measured from the horizontal flow direction.

Comparison between the correlations for the 30° chevron angle can be seen in figure 2.9 and for the 22° chevron angle in figure 2.10. All of the correlations show a similar trend, that is for higher Reynolds number a lower friction factor. The correlation from Thonon [61] seems to under predict the factor for turbulent flow and the correlation from the VDI Heat Atlas [64] might be over predicting the pressure drop for low Reynolds numbers for the 22° chevron angle. For single phase flow the correlation from the VDI Heat Atlas is chosen since it gives the most average results for the 30° chevron angle.

Table 2.4: Review of friction factor correlations for single phase flow.

Investigator	Correlation		Validation range
VDI Heat Atlas [64]	$\frac{1}{\sqrt{\xi}} = \frac{\cos(\varphi)}{\sqrt{0.18tan(\varphi) + 0.36sin(\varphi) + \xi_0(Re_{VDI})/c}}$	cos(φ)	Re _{VDI} < 2000
	$+rac{1-cos(arphi)}{\sqrt{3.8\xi_1(Re_{VDI})}}$	(2.46)	
	$\xi_0 = \frac{64}{Re_{VDI}}$	(2.47)	
	$\xi_1 = \frac{597}{Re_{VDI}} + 3.85$	(2.48)	
Kumar [35]	$f = 19.40Re^{-0.589}$	(2.49)	10 < Re <100
	$f = 2.990Re^{-0.183}$	(2.50)	Re > 100
			β ≤ 30°
Wanniarachchi et al. [68]	$f = [f_1^3 + f_t^3]^{1/3}$	(2.51)	1 < Re < 10,000
	$f_1 = 1774 \beta^{-1.026} \Phi^2 Re^{-1}$	(2.52)	20° < β < 62°
	$f_t = 46.6\beta^{-1.08}\Phi^{1+s}Re^{-s}$	(2.53)	
	$s = 0.00423\beta + 0.0000223\beta^2$	(2.54)	
Thonon [61]	$f = 45.57 Re^{-0.670}$	(2.55)	Re < 160
	$f = 0.370Re^{-0.172}$	(2.56)	Re > 160
Focke et al. [16]	$f = 45.57 Re^{-0.670}$	(2.57)	90 < Re < 400
	$f = 6.7Re^{-0.209}$	(2.58)	400 < Re < 16,000

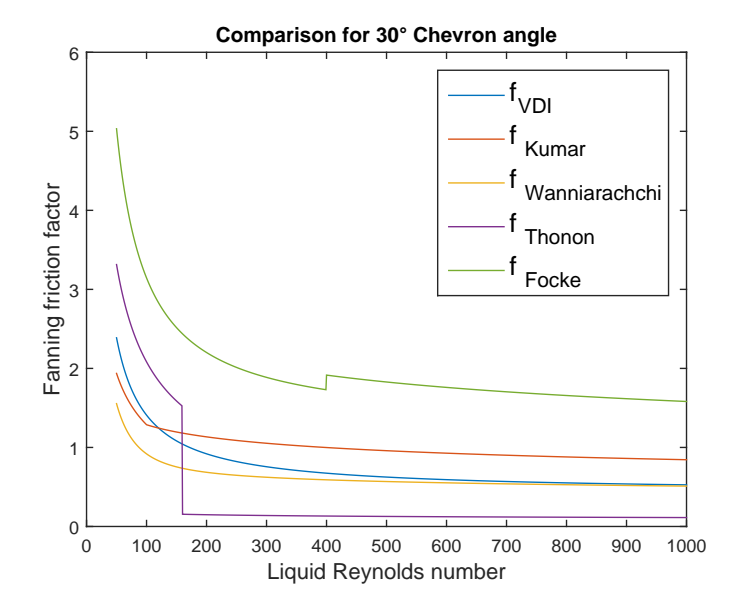


Figure 2.9: Comparison of the proposed correlations of the friction factors for single phase flow with chevron angle of 30° . The correlation from The VDI Heat Atlas [64] is chosen for 30° chevron angle since it gives the most average results compared to the other correlations.

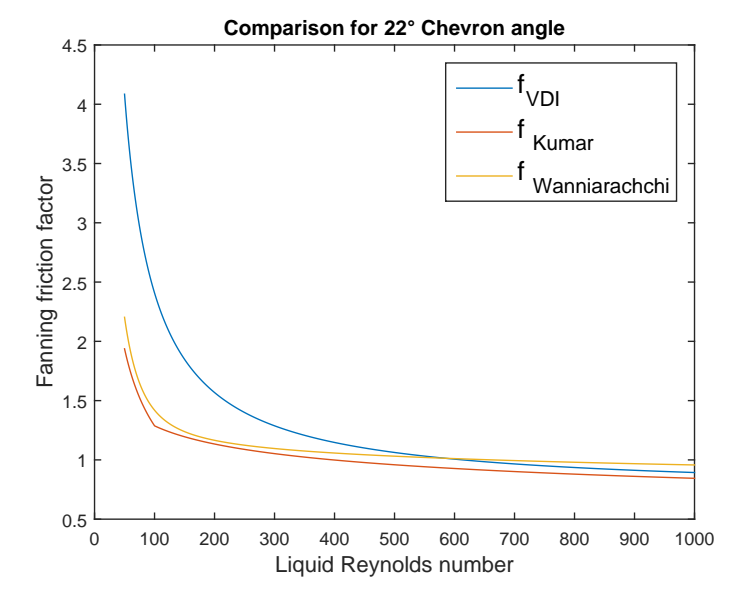


Figure 2.10: Comparison of the proposed correlations of the friction factors for single phase flow with chevron angle of 22°. The correlation proposed by the VDI Heat Atlas[64] might be over predicting the friction factor at low Reynolds numbers.

2.1. Heat exchangers 23

2.1.2.2 Two phase flow

For two phase flows there exist fewer correlations, especially correlations which include the effect of the chevron angle. Some of the correlations that have been proposed are based on the Lockhart-Martinelli approach but most of the proposed correlations are based on a homogeneous theory where the friction factor is a function of the vapor quality and liquid only Reynolds number [23]. A review of friction factor correlations for evaporation and condensation is shown in tables 2.5 and 2.6, respectively.

Comparison of the proposed correlations for condensation and evaporation can be seen in figures 2.12 and 2.11 respectively. Compared to the friction factors for single phase flow the values, especially for low Reynolds numbers, should be higher than for single phase flow due to unsteady motions caused by a phase of different density and the effective stresses [10]. Since the corrugation pitch is unknown of the heat exchangers in the OTEC experimental set up the correlations from Han et al. [21] are not used in the model. However if the corrugation pitch can be measured these correlations are promising and are therefore included in the comparison. For condensation the correlation from Yan et al. [73] is therefore chosen even though the friction factor is likely underestimated. For evaporation the correlation from Yan & Lin [72] is selected since the friction factor is likely underestimated by the correlation proposed by Ayub [6].

Table 2.5: Review of friction factor correlations for evaporation.

Investigator	Correlation		Validation range
Ayub [6]	$f = (2.99Re^{-0.137})(-1.89 + 6.56(\beta/30) - 3.69$	$(\beta/30)^2)$ (2.59)	Re < 4000
			30° < β <65°
Han et al. [20]	$f = Ge_3Re_{eq}^{Ge_4}$	(2.60)	250 < Re _{VDI} < 750
	$Ge_3 = 64,710(\frac{p_{co}}{d_e})^{-5.27}(\frac{\pi}{2} - \beta)^{-3.03}$	(2.61)	20° < β < 45°
	$Ge_4 = -1.314(\frac{p_{co}}{d_e})^{-0.62}(\frac{\pi}{2} - \beta)^{-0.47}$	(2.62)	
Yan and Lin [72]	$f = 6.947 \cdot 10^5 Re_{eq}^{1.109} Re^{-0.5}$	(2.63)	Re _{eq} < 6000
	$f = 31.21 Re_{eq}^{0.04557} Re^{-0.5}$	(2.64)	Re _{eq} < 6000

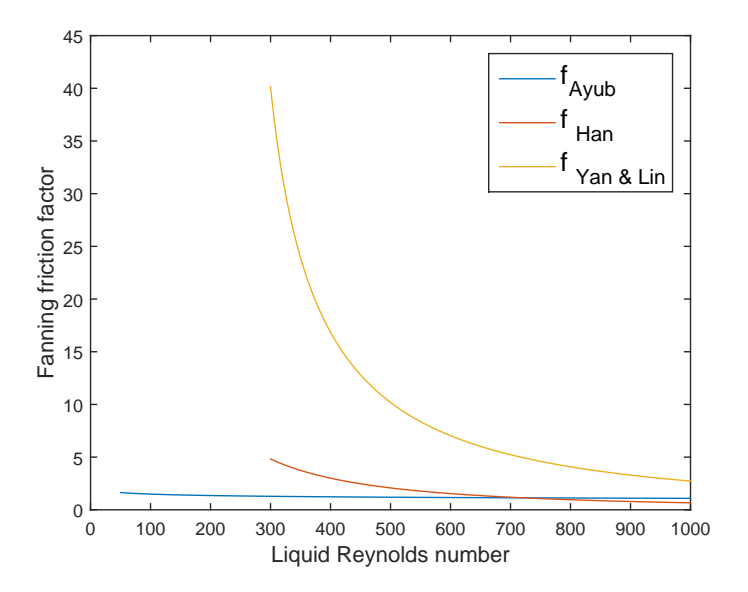


Figure 2.11: Comparison of the proposed correlations of the Fanning friction factors for evaporation. The correlation from Yan & Lin [72] is used in the model.

Table 2.6: Review of friction factor correlations for condensation.

Investigator	Correlation		Validation range
Han et al. [20]	$f = Ge_3Re_{eq}^{Ge_4}$	(2.65)	250 < Re _{VDI} < 750
	$Ge_3 = 3521.1(\frac{p_{co}}{d_o})^{4.17}(\frac{\pi}{2} - \beta)^{-7.75}$	(2.66)	20° < β < 45°
	$Ge_4 = -1.024 \left(\frac{p_{co}}{d_e}\right)^{0.0925} \left(\frac{\pi}{2} - \beta\right)^{-1.3}$	(2.67)	
Yan et al. [73]	$f_{cond,i} = 94.75 Re_{eq,i}^{-0.0467} Re_i^{-0.4} Bo_{eq,i}^{0.5} (\frac{P_m}{P_c})^{0.8}$	(2.68)	Re > 200
	$Bo_{eq} = \frac{q^{''}}{G_{eq}h_{lv}}$	(2.69)	

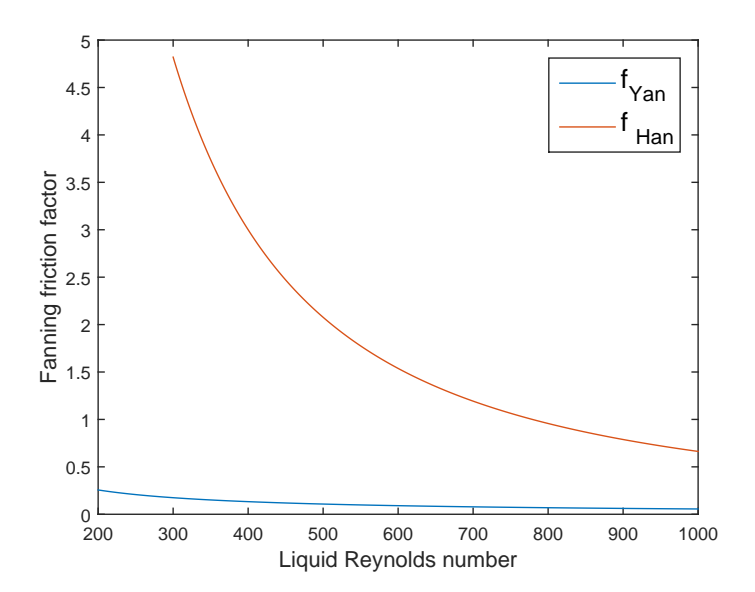


Figure 2.12: Comparison of the proposed correlations of the Fanning friction factors for condensation. The correlation from Yan et al. [73] is used in the model.

2.2. THERMODYNAMIC PROPERTIES

As mentioned in section 2 the thermodynamic properties of the fluids are imported from the REFPROP database[36]. However transport properties of some mixtures, like ammonia water, cannot by calculated by REFPROP. For the present study the relevant transport properties are the thermal conductivity and the viscosity. The correlations that are used are the ones that are suggested in the 7^{th} edition of the Chemical Engineers Handbook [49]. The correlation proposed for the viscosity of liquid mixtures is the following:

$$ln\mu_m = \sum_j x_j ln\mu_j \tag{2.70}$$

Here *x* is the mixture molar composition, and the subscript j stands for component j of the mixture. The thermal conductivity of a mixture is calculated with the following relation

$$\lambda_m = \sum_{j=1}^n \sum_{k=1}^n \phi_j \phi_k \lambda_{jk}$$
 (2.71)

Where the constant ϕ is calculated as

$$\phi_j = \frac{x_j V_j}{\sum_{k=1}^n x_k V_k}, \ \phi_k = \frac{x_k V_k}{\sum_{k=1}^n x_k V_k}$$
 (2.72)

and

$$\lambda_{jk} = \frac{2}{(1/\lambda_j) + (1/\lambda_k)} \tag{2.73}$$

Here the subscripts j and k stand for component j or k of the mixture and V is the liquid molar volume of each of the components.

In the experiments performed with the OTEC experimental set up normal water is used as a heating and cooling medium and then thermodynamic properties are easily imported from REFPROP. Seawater properties are not included in the REFPROP database and therefore for the larger scale calculations the seawater properties are calculated according to correlations gathered by Sharqawy et al. [51].

2.3. TURBINE

The turbine in the cycle expands the vapor from the separator and produces work. The turbine intended to be used in the OTEC experimental set up is a Tesla turbine. Unfortunately the turbine had some leakages and therefore instead of a turbine an expansion valve was used in the experimental set up. An axial turbine is the preferred choice for the 10 to 25 MW OTEC offshore plant. Because of the small temperature difference in OTEC systems the pressure and volume flow ratio in the turbine are small. This means that one stage turbine can be used and according to Macchi and Perdichizzi [41] the isentropic efficiency can be estimated from 89.5 to 89.8 %. Indeed the internal efficiency of the turbine was well over 80% in the operation of the 100 kW OTEC plant in the republic of Nauru [43]. Also an operating geothermal Kalina cycle with a gross power of 3.4 MW in Unterhaching Germany has a single stage turbine with an isentropic

2.4. PUMPS 27

efficiency of 84.9 %. This turbine is a modified steam turbine and it is operating over a higher pressure drop than would be possible in an OTEC system since the heating source is at a much higher temperature of over 120°C². Therefore it is likely that this efficiency could be possible and in the design the efficiency was estimated as 89.5 % and the efficiency of the generator as 95% [31]. The power output of the turbine, generator, can be calculated as:

$$\dot{W}_{T-G} = \dot{m}_{\nu} \eta_T \eta_G (h_{4r} - h_{5rs}) \tag{2.74}$$

Where η_T and η_G are the isentropic efficiencies of the turbine and the generator respectively, h is the enthalpy and \dot{m} the mass flow. The subscripts of the enthalpy values refer to certain points in the cycle as defined in figure 2.1. The isentropic efficiency of the turbine is calculated as follows:

$$\eta_T = \frac{h_{4r} - h_{5r}}{h_{4r} - h_{5rs}} \tag{2.75}$$

The turbine efficiency is an important parameter that varies with off-design conditions [19]. The turbine in an OTEC system operating with ammonia or ammonia water can be a modified steam turbine since the molar mass of ammonia is similar to that of water. As metioned above this is the case for the Unterhaching plant in Germany. Jüdes et al. [27] estimated the change in isentropic efficiency during off design operation for a steam turbine as follows:

$$\eta_{off} = \eta_{off,1} - \frac{1}{2} \Delta q_T \tag{2.76}$$

Where Δq_T is the change in outlet quality of the turbine, that is if the quality is lower then one and

$$\eta_{off,1} = \eta_{des} (-1.0176 \left(\frac{\dot{m}_{off}}{\dot{m}_{des}}\right)^4 + 2.4443 \left(\frac{\dot{m}_{off}}{\dot{m}_{des}}\right)^3 - 2.1812 \left(\frac{\dot{m}_{off}}{\dot{m}_{des}}\right)^2 + 1.0535 \left(\frac{\dot{m}_{off}}{\dot{m}_{des}}\right) + 0.701)$$
(2.77)

Here the subscript des refers to properties when the cycle is running under design conditions and of f when the operation is running off design.

2.4. PUMPS

The OTEC system needs three pumps. A cold seawater pump that pumps the cold seawater through the condenser, a hot seawater pump that pumps the warm seawater through the evaporator and a working fluid pump that increases the working fluid pressure and feeds it to the evaporator. The working fluid pump in the OTEC experimental set up is an oscillating displacement pump and therefore a damper is installed after the pump to decrease oscillations in the pressure. Since the temperature difference is small, relatively large seawater mass flows are needed to achieve the desired power output. Therefore the electricity consumption of the pumps is a large portion of the gross power output of the cycle. The isentropic efficiency of pumps are normally assumed in the range of 70-80% [5, 7, 42, 74]. In the design of the 10 to 25 MW system the isentropic efficiency of the seawater pump was assumed to be 80% and 70% for the working fluid. The isentropic efficiencies of the pumps in the OTEC experimental set up are unknown since the characteristics of the pumps are unknown and the electricity consumption was not

²Wolfgang Geisinger, personal communication, May 8, 2015

measured. The pressure levels before and after each pump were also unknown. The specific work required by the pumps is calculated as:

$$W_P = \frac{\Delta P}{\rho \eta_p} = \Delta h_p \tag{2.78}$$

The head loss of the cold and hot seawater pipes can be divided into pipe inlet and friction losses, and the pressure difference of the seawater in the heat exchanger. The pressure drop of the water side of the heat exchangers is calculated with the correlation from the VDI Heat Atlas [64] as stated in section 2.1.2. The inlet and friction losses of the warm water pipe have been estimated as 0.041 bar and as 0.344 for the cold water pipe by Kleute [32]. The losses are higher for the cold water pipe since that pipe goes down to 1000 m depth while the warm water pipe goes down to only 20 m depth.

2.5. SEPARATOR/MIXER

It is assumed that the separator splits the working fluid into pure vapor and liquid components. The mass balance for the separator is shown in equation 2.79 and the energy balance in equation 2.80, where the heat losses to the environment are considered to be negligible.

$$\dot{m}_{wf} = (1 - q)\dot{m}_{wf} + q\dot{m}_{wf} = \dot{m}_l + \dot{m}_v \tag{2.79}$$

$$\dot{m}_{wf}h_4 = \dot{m}_v h_{4r} + \dot{m}_l h_{4w} \tag{2.80}$$

Similar mass and energy balance equations apply for the mixer as for the separator.

The pressure drop for the separator can be estimated as one velocity head for the inlet pipe and half for the outlet pipe [9]. The pressure drop is then is calculated as

$$\Delta P = \frac{\dot{m}_{in}^2}{2\rho_{in}A_{in}^2} + \frac{\dot{m}_{out}^2}{4\rho_{out}A_{out}^2}$$
 (2.81)

The subscripts *in* and *out* stand for the inlet and outlet pipe respectively and A stands for the cross section area of each pipe. Note that the pressure drop will vary for the vapor and liquid streams from the separator since the outlet conditions vary.

2.6. Overall system calculations

The overall thermal efficiency of the cycle is estimated as the net power produced by the cycle divided by the heat duty of the evaporator:

$$\eta_{cycle} = \frac{\dot{W}_{net}}{\dot{Q}_{evap}} \tag{2.82}$$

The thermal efficiency can be compared to the Carnot efficiency which is the theoretical maximum efficiency of a heat engine [40]. For the OTEC cycle the Carnot efficiency is

$$\eta_{Carnot} = 1 - \frac{T_{cw}}{T_{hw}} \tag{2.83}$$

The net power of the cycle is calculated according to following equation:

$$\dot{W}_{net} = \dot{W}_{T-G} - \dot{W}_{TP} \tag{2.84}$$

Where \dot{W}_{T-G} is the power produced by the turbine-generator and \dot{W}_{TP} is the total electricity consumptions of the pumps:

$$\dot{W}_{TP} = \dot{W}_{hwp} + \dot{W}_{cwp} + \dot{W}_{wfp}$$
 (2.85)

Here the subscript hwp refers to the hot water pump, cwp to the cold water pump and wfp to the working fluid pump.

3

THE MODEL

A model is implemented in Matlab [59]. The model is a steady state "off design" model. That is the model uses a fixed design and can then be used to analyse the effects of different operating conditions than were used to obtain the design. As mentioned before a previous "on design" model was made to optimize an OTEC cycle by Kirkenier [31]. This optimisation was made for certain operating conditions. The most relevant is the seawater temperature. The surface temperature was assumed 27°C and the temperature at 1000 m depth as 5°C. These are typical conditions in the tropics which is a suitable location for OTEC applications. When the operating temperatures are different the effects on each optimized design are unknown. A new model is implemented to show these effects.

3.1. ASSUMPTIONS

The main assumptions used in the model are listed below

- 1. 0-dimensional except for heat exchanger calculations which are 1-dimensional so that pinch points can be identified (see page 10). There is not an interest in knowing the spatial distribution of the system but rather values at relevant states that can be used to describe the system except for in the evaporator and condenser where the change in conditions through both components are desired.
- 2. Each component of the power cycle is assumed to be in steady state.
- 3. Adiabatic components, it is assumed that the components have sufficient insulation to be assumed adiabatic.
- 4. The working fluid at the condenser outlet is assumed to be saturated.
- 5. The separator is assumed to separate the working fluid perfectly into its vapor and liquid components.
- 6. The pumps are assumed to have a given isentropic efficiency.
- 7. The turbine is assumed to have an isentropic efficiency that is dependent on the design and off design mass flow and the vapor quality at the turbine outlet.

32 3. The model

3.2. SOLUTION PROCEDURE

The model follows modularity to a certain degree. That is calculation of every state in the cycle has its own code. This makes it easier to evaluate individually each component of the cycle and to have a better overview of the cycle. These codes are then implemented as shown in figure 3.3. More detailed description is given below.

A schematic of the thermodynamic cycle that is being modelled is shown in figure 3.1. Before the modelling procedure starts the necessary inputs have to be defined. That is the cold and warm seawater temperature, all mass flows, the isentropic efficiencies of the pumps and the turbine, the heat exchangers geometry and in case of a mixture the mixture concentration. Additionally the pressures in state 1 and 3 in the cycle are assumed, the temperature in state 3 and the heat duties of the heat exchanger. Then the model starts by calculating through the evaporator. The temperature, pressure and vapor quality after the evaporator are calculated according to the heat exchanger procedure explained in figure 3.2. Thereafter the pressure and temperature in states 4r and 4w can be calculated. For a mixture the concentration in each state is also calculated. Then the pressure and temperature in state 5r after the turbine can be calculated. At this point the conditions in state 6w are not known. The conditions at the condenser outlet are however assumed saturated and therefore the conditions in state 7 can be calculated. Thereafter the pressure and temperature after the working fluid pump, state 2 in the cycle is calculated. Then the temperature and pressure in states 3 and 5w after the recuperator can be calculated according to the heat exchanger procedure. Now it is checked if the assumed temperature in state 3 is the same one as the calculated one. If not the temperature is replaced by the calculated value. Then temperature is calculated after the expansion valve in state 6w. There it is assumed that the enthalpy over the valve is constant and that the pressure expands to the same pressure as in state 5r. Now all states around the mixing point have been calculated and the energy balance over the connection from states 5r and 6w to state 7 is used to see if the initial estimate of the pressure in state 1 was assumed correctly. If the energy balance holds the script continues else the pressure is decreased or increased. Then to see if the initial estimate for the pressure before the evaporator is assumed correctly the energy balance of the cycle is checked. That is if the heat duty of the evaporator and the electricity consumption of the working fluid pump are equal to the heat duty of the condenser and the work produced by the turbine. If that holds the script ends else the pressure in state 3 is increased or decreased. All of the relevant equations used in the model were listed in chapter 2.

There were a couple of complications that arose during the development of the model. The most important one is the importance of accurate initial assumptions. For the model to run the pressure in states 1 and 3, the temperature in state 3 and the heat loads of the heat exchangers have to be estimated. If these assumptions are far off then the model will give an error. To minimize these effects there are couple of catch and try loops in the model. That is if the original assumptions are too far off they will be changed. For example if the heat loads of the heat exchangers are assumed too high they will be lowered by 20%. The model is also quite sensitive if the working fluid is fully evaporating. This is because of the fact that when the fluid starts superheating only small enthalpy change will cause a large

temperature difference. In these cases a sub model was added to more accurately estimate the pressure in state 3.

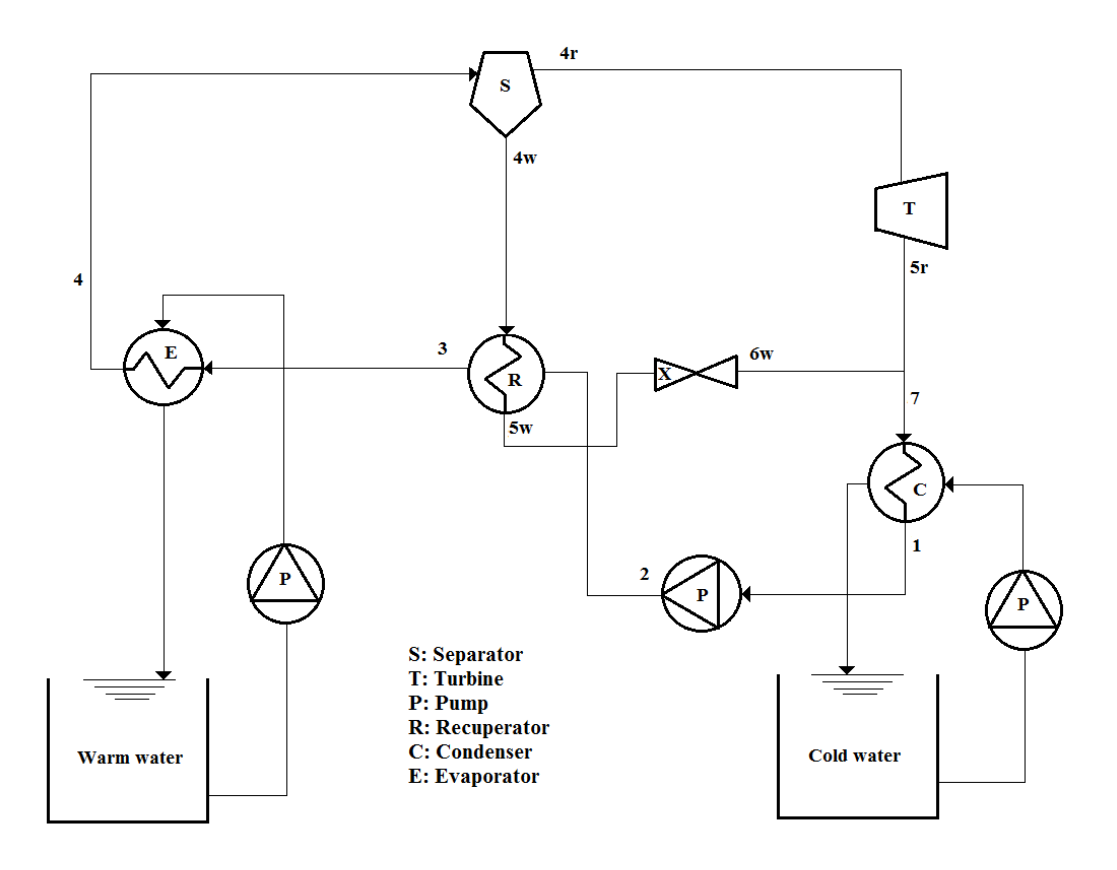


Figure 3.1: A schematic of the Otec cycle that is being modelled.

3. The model

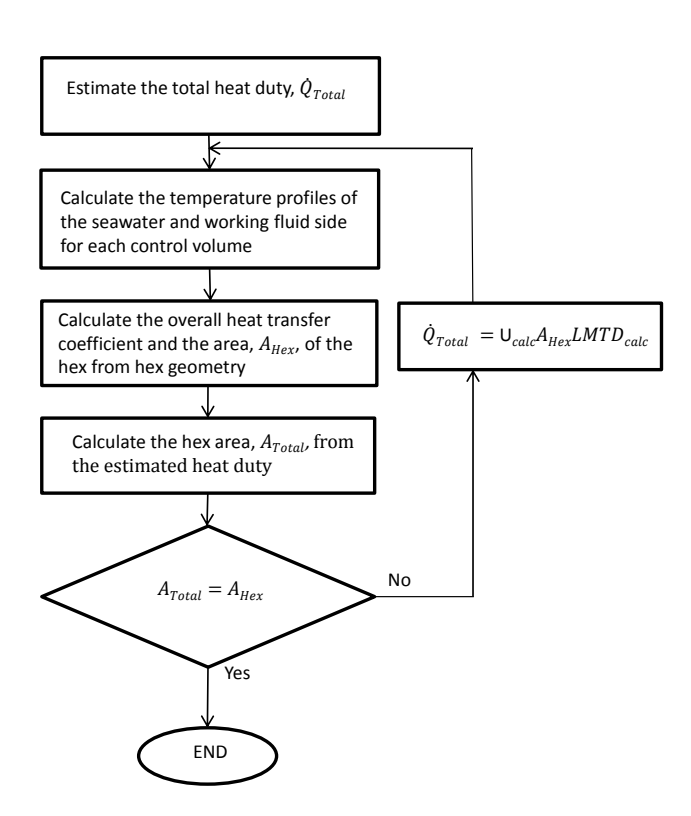


Figure 3.2: Heat exchangers solution procedure.

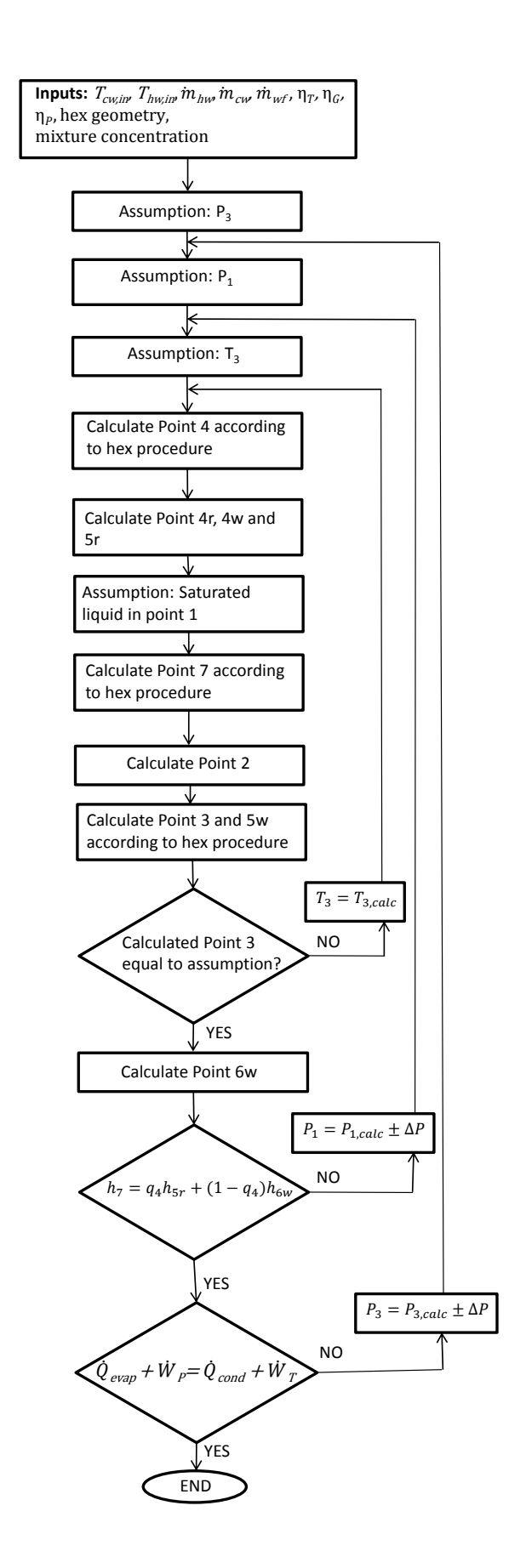


Figure 3.3: Solution procedure of the thermodynamic cycle.

4

DESIGN OF EXPERIMENTS

To validate the model of the thermodynamic cycle presented in this work experiments were executed with an OTEC experimental set up developed by Bluerise in collaboration with Delft University of Technology. The experimental set up is in principle the Kalina cycle as described at the beginning of chapter 2. A simplified Process and Instrumentation Diagram (P&ID) is shown in figure 4.1. The geometry of the heat exchangers in the set up is given in table 4.1. In the experiments the warm and cold water temperatures were varied as well as the working fluid mass flow. The experiments were executed with pure ammonia. Preferably ammonia water mixture would have also been used however since some of the sensors in the system were not installed yet the concentration would be hard to determine and therefore it was decided to use only pure ammonia for the experiments.

As explained in chapter 1 the seawater temperature has some fluctuations between seasons and the chosen geographical location. For this research the range of the cold water is selected from 4-7°C and the warm water temperature from 24-29°C since most of suitable OTEC locations are within this range. In the experiments the minimum and the maximum temperature differences are used (4 to 29°C and 7 to 24°C), and then the temperature difference from 5 to 27°C which was used in the optimization of the OTEC cycle by Kirkenier [31].

To decide which mass flows should be used the ratio of the size of the condenser in the experimental set up and the ratio of the condenser for pure ammonia in the results from Kirkenier [31] is used. The condenser area is used instead of for example the evaporator area since the condenser is the limiting heat exchanger. The working fluid has to condensate for the working fluid pump to work. The calculated ratio is 393,380. The resulting mass flows are listed in the first experiment in the list of experiments in table 4.2. The mass flow of the working fluid is then varied by approximately 10% in experiment 4 and 5. The mass flow of the warm water is significantly higher than the mass flow of the cold water. This is the result of the cost optimization done by Kirkenier [31] since the warm water is available at the sea surface it is cheaper than the cold water from 1000 m depth. Experiment 6 is performed to see the influence this might have on the efficiency of the cycle. The mass flows can be controlled with the working fluid pump speed (rpm).

Table 4.1:	OTEC Demo	heat e	exchangers	specifications.

	Condenser	Recuperator	Evaporator
Number of passes	1	1	1
Flow	Counterflow	Counterflow	Counterflow
Total number of channels	17	17	21
Number of channels in pass 1 hot	9	9	11
Number of channels in pass 1 cold	8	8	10
Surface enlargement factor*	1.17	1.17	1.17
Chevron angle [°]	22	22	22
Horizontal port centres distance [mm]	50	50	50
Vertical port centres distance [mm]	250	250	250
Plate thickness [mm]	0.4	0.4	0.4
Compressed plate pitch [mm]	2.42	2.42	2.42
Port diameter [mm]	23/30	23/30	23/30
Plate width [mm]	111	111	111
Total number of plates	18	18	22

Table 4.2: List of the planned experiments.

Test Nr.	\dot{m}_{cw} [kg/s]	\dot{m}_{hw} [kg/s]	\dot{m}_{wf} [kg/s]	T_{hw} [°C]	T_{cw} [°C]	%NH ₃
1	0.079	0.204	0.0018	29	5	100
2	0.079	0.204	0.0018	27	5	100
3	0.079	0.204	0.0018	24	7	100
4	0.079	0.204	0.0020	27	5	100
5	0.079	0.204	0.0016	27	5	100
6	0.079	0.079	0.0018	27	5	100

4.1. SENSORS

There are temperature, pressure, liquid level and flow sensors in the OTEC experimental set up. The location of each of the sensors is shown in the simplified P&ID (see figure 4.1). More details on the relevant sensors are listed below.

4.1.1. FLOW SENSORS

There are three flow meters in the system, one for the cold water flow, one for the warm water flow and one for the vapor flow after the separator.

The flow meter for the vapor flow is a thermal, bypass mass flow meter for pure ammonia. The accuracy of the flow meter when it is calibrated is 1% accuracy against full scale plus $\pm 1\%$ accuracy of the reading. The measuring range is from 0.0001 - 0.005 kg/s at T = 26.5 °C and P = 9.5 bar [11].

The flow meters for the warm and cold water flow are DF140 Flowsensors. The sensors are 3/4" and the flow velocity range is 30 - 3000 l/h (approximately 0.0083-0.83 kg/s for water). The accuracy of the sensors are supposed to be $\pm 1\%$ over the full range and $\pm 0.5\%$

4.1. Sensors 39

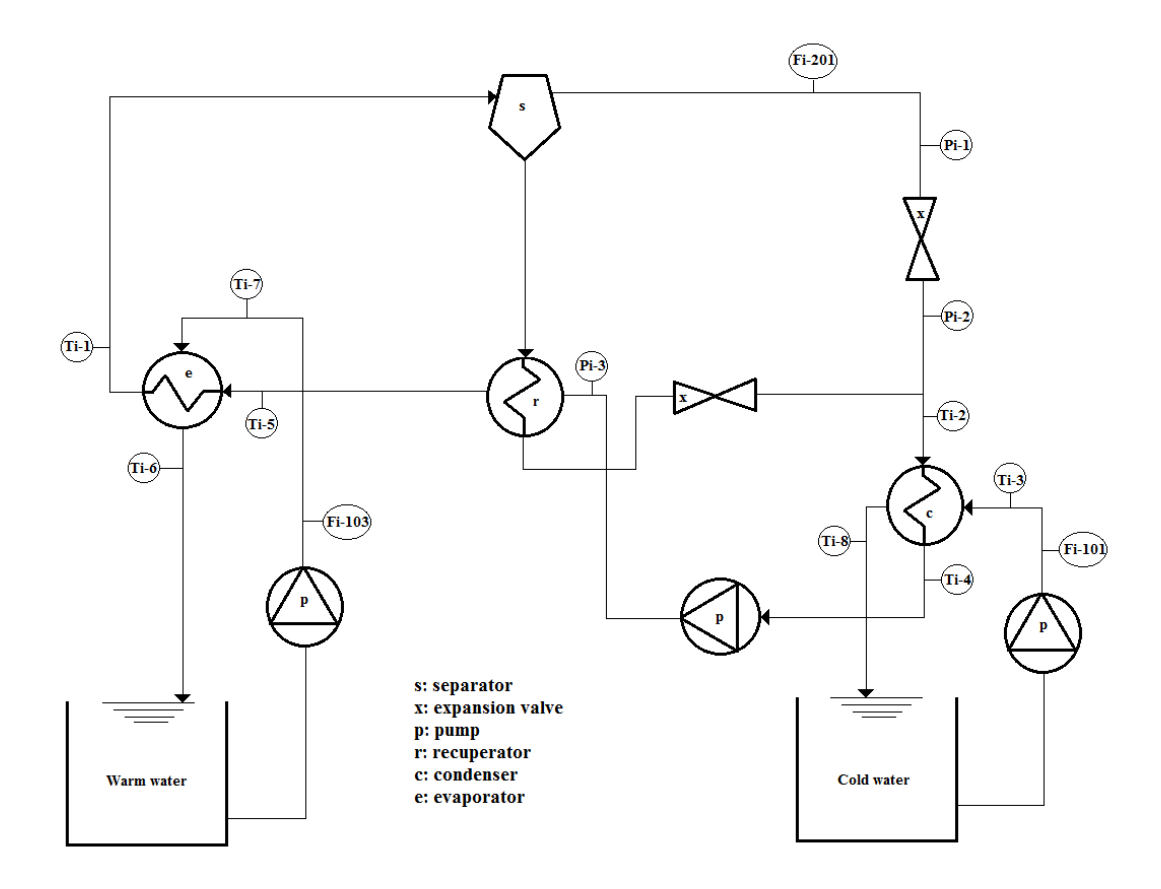


Figure 4.1: Simplified Process and Instrumentation diagram of the OTEC experimental set up where the location of the relevant sensors is shown. The pressure sensors are labeled with Pi-X, the temperature sensors with Ti-X and the flow sensors with Fi-XXX where X gives the sequence number.

repeatability [2].

The vapor flow sensor could not be calibrated. The water flow sensors were calibrated by making the water in the water circuits flow for a fixed amount of time into a bucket. The weight of the bucket was then measured before and after the water intake and the calculated value was compared to the average measured value for that time period. This was done four times at different flow speeds of approximately 500 l/h, 1000 l/h and 1500 l/h. The sensor in the warm water circuit showed an average offset of 0.58% between the measured and calculated value and the sensor in the cold water circuit showed an average offset of 0.71%. Both of the offsets are within the given accuracy range.

4.1.2. PRESSURE SENSORS

The pressure sensors are gauge pressure sensors with a span of 0 to 10 bar-g. They have the accuracy of 0.5 % of their span [57]. The pressure sensors would ideally have been calibrated with a dead weight calibration equipment. Since that was not available the pressure value was read at different pressures and the sensor that gave the average value

was used as a reference to calibrate the others. The pressure difference should therefore be approximately accurate while the absolute pressure might have more error.

4.1.3. TEMPERATURE SENSORS

The temperature sensors are resistance thermometers of the type TC Direct PT-100 class B. They have a tolerance of \pm 0.3 °C around 0 °C (\pm 0.8 °C around 100 °C) [58].

The temperature sensors were calibrated by using a controlled thermal bath and an already calibrated temperature sensor with an accuracy of 0.01 °C. The resistance and temperature of each of the sensors were read at 5 °C, 15 °C, 25 °C and 35 °C which is the desirable range for OTEC applications. Quadratic fit was then used to correct the temperature profiles. The temperatures were then within 0.01 °C from the calibrated sensor. Most of the sensors were successfully calibrated except sensor T1 which is situated in the working fluid flow after the evaporator and T7 which is situated in the water flow before the evaporator. T1 was calibrated as well as possible but due to a short wire of the sensor it was difficult to keep it stable in the heat bath. Sensor T7 was really off compared to the other sensors, approximately 1 K at each temperature, compared to the calibrated temperature sensor. This sensor was therefore replaced with a new sensor. There was not time to calibrate the new sensor before the start of the experiments and afterwards it broke down before calibration could be done. Since the sensor was new it is assumed that the measured value is inside the tolerance given by the manufacturer or around 0.4 °C.

EXPERIMENTS AND MODEL VALIDATION

5.1. OTEC EXPERIMENTS

Experiments were performed with the OTEC experimental set up from Bluerise. The Demo is shown in figure 5.1. A couple of complications rose during the experiments. These complications, the results and the validation of the model are further explained below.

5.1.1. COMPLICATIONS DURING EXPERIMENTS

For the first trial run of the experiments there was considerable preheating done by the recuperator even though the flow was fully evaporating or even superheating in the evaporator and the valve after the recuperator was kept closed. The most probable explanation was that some of the vapor escaped through the recuperator and condensed against the flow from the condenser. This caused over ten degree temperature increase through the recuperator before the evaporator. Extra valves were therefore added before the recuperator and before a liquid level sensor after the separator so that a organic Rankine cycle could be better simulated for the cases where full evaporation was preferred. This decreased the temperature difference to approximately 6K. To decrease it further the recuperator, the pipes from the condenser to the evaporator and an ammonia storage tank before the ammonia pump were insulated and that resulted in a decrease to about 2 to 3 K. The insulation can be seen in figure 5.1.

The working fluid pump was running at the lowest possible capacity or 0.1 % during the first experiments. This resulted in a larger mass flow than the suggested mass flow and therefore experiment number 5 could not be performed where the plan was to decrease the mass flow even further. The mass flow of the ammonia could not be tested beforehand since the pump could not be run until the experimental set up had been filled with ammonia.

Experiments number 2 and 4 could also not be performed as planned. The reason was that the vapor flow sensor did not show stable values at these conditions. A probable reason is mist flow. If droplets get into the vapor sensor it can influence the sensor greatly. The sensor started to show values with large fluctuations up to 3 times higher than expected



Figure 5.1: The OTEC Demo. The big steel tank on the left is the warm water tank and the plastic one on the right is the cold water tank. The recuperator is wrapped in silver insulation and insulated pipes go from the recuperator to the evaporator on the left and to the condenser on the right. The separator is a narrow vertical tank situated above the recuperator in the figure. The working fluid pump is the blue pump in the middle of the figure and the water pumps are the grey and yellow pumps in each corner.

values. This was not a problem during experiment 1 since then superheated vapor was formed at the end of the evaporator. This was also not a problem in experiments 3 and 6 where there was a definite two phase flow at the end of the evaporator. An experiment with warm water inlet temperature at 28°C was performed instead of experiment 2, then the flow at the end of the evaporator was superheated and then stable values could be obtained from the vapor flow sensor. Experiment number 4 was cancelled since there was not enough time was to perform a modified experiment for example with a higher inlet temperature.

Another complication that came up was that the control board for controlling the cold water temperature broke just before the experiments started. A new one took too long to get and therefore the cold water temperature was controlled with manual switches. The cold water temperature is achieved with two heat pumps, one slightly more powerful than the other. The switches turned on and off each heat pump. There was quite some delay when the heat pumps were turned on and off and this delay varied a bit. Also it was dependent on each operating condition how much cooling was needed to keep the cold water temperature relatively steady. These two facts made it quite difficult to achieve a steady temperature. The temperature was kept steady as much as possible but this did add some extra fluctuations to the data.

5.1.2. RESULTS

As explained in the section above there were in the end four experiments performed with the OTEC experimental set up. In the experiments steady state, or as close to steady state as possible, was maintained for approximately 15 to 20 minutes in each case. The average measured results from the experiments can be seen in table 5.1 and in figures 5.3 and 5.2 for test number 1. Appendix A contains figures with the results of the other tests.

Table 5.1: The average measured values from each of the experiments that were performed.

Sensor	Variable	Test 1	Test 2	Test 3	Test 6
Ti-1 [°C]	T_4 (evap out)	28.52	27.15	20.94	20.58
Ti-2 [°C]	T_7 (cond in)	17.79	15.75	14.81	15.71
Ti-3 [°C]	$T_{cw,in}$	3.92	4.50	7.17	5.30
Ti-4 [°C]	T_1 (cond out)	6.56	8.22	9.36	6.94
Ti-5 [°C]	T_3 (evap in)	9.79	10.51	13.63	11.98
Ti-6 [°C]	$T_{hw,out}$	26.17	25.15	21.70	20.87
Ti-7 [°C]	$T_{hw,in}$	29.0	27.9	24.0	27.0
Ti-8 [°C]	$T_{cw,out}$	11.72	12.40	13.41	11.86
Pi-1 [barg]	P_{4r} (turbine in)	8.65	8.72	7.82	7.71
Pi-2 [barg]	P_{5r} (turbine out)	5.73	5.88	6.12	5.78
Pi-3 [barg]	P_2 (pump out)	8.70	8.77	7.87	7.77
Fi-101 [l/h]	\dot{m}_{cw}	292	287	289	289
Fi-103 [l/h]	\dot{m}_{hw}	740	738	741	288
Fi-201 [kg/min]	$\dot{m}_{ u}$	0.122	0.124	0.094	0.103

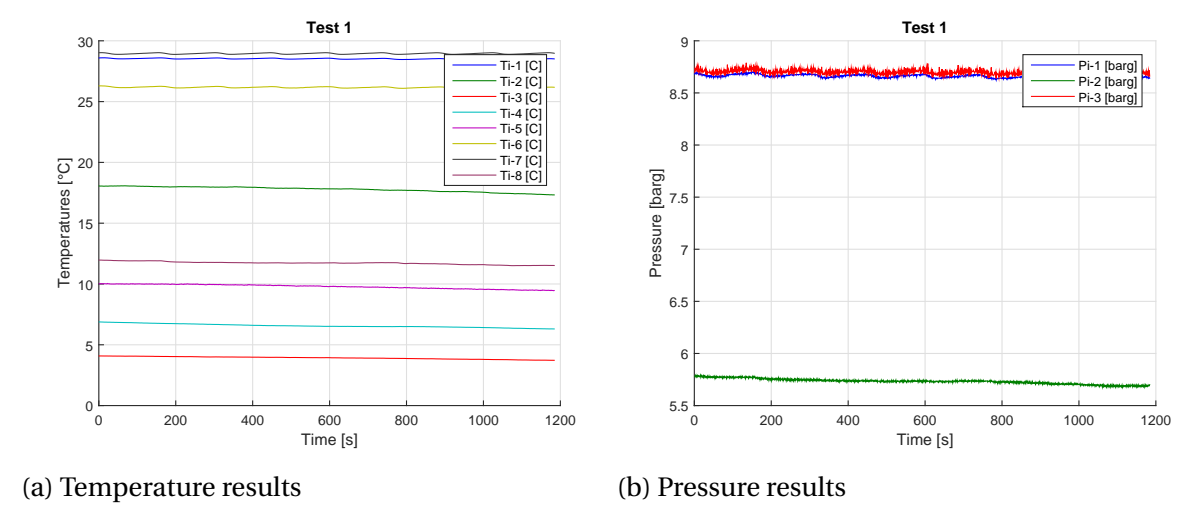


Figure 5.2: Measurement data for test 1, (a) temperature as a function of time; (b) pressure as a function of time.

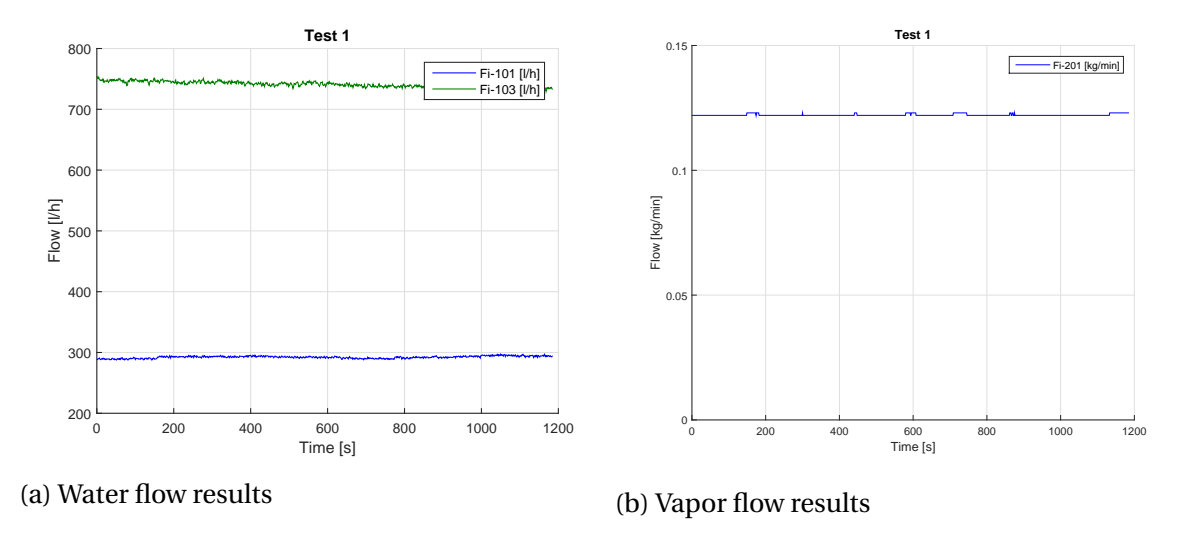


Figure 5.3: Measurement data for test 1, (a) water flow as a function of time; (b) vapor flow as a function of time.

5.1.3. UNCERTAINTY ANALYSIS

The uncertainty of the measurements are evaluated in a similar way as was done by Yuan et al. [76]. That is the Root - Sum - Square method is used to combine errors. The uncertainty of each measurement is determined by the accuracy of each sensor or in the case where calibration was done the accuracy after calibration. For the temperature values the uncertainty is assumed 0.05 °C, except for the value from sensor number 7, since the uncertainty of the calibrated sensor is likely to have deteriorated over time from the given 0.01 °C accuracy. The uncertainty of sensor 7 is estimated to be 0.4 °C as explained in section 4.1.3. The pressure sensors are assumed to have 0.05 bar accuracy. The water flow sensors are assumed to have the calibrated accuracy, or 0.58 % of the measured value for the warm water and 0.71 % for the cold water. The accuracy of the vapor flow sensor is 1 % of 0.005 kg/s and 1% of the measured value as explained in section 4.1.1. The energy balances over the heat exchangers are calculated to estimate the quality of the gathered data. The uncertainty of the calculated heat load from the working fluid side of the evaporator is estimated as

$$\frac{u_{\dot{Q}_{evap,wf}}}{\dot{Q}_{evap,wf}} = \sqrt{\left(\frac{u_{\dot{m}_{wf}}}{\dot{m}_{wf}}\right)^2 + \left(\frac{u_{h_4}}{h_4}\right)^2 + \left(\frac{u_{h_3}}{h_3}\right)^2}$$
(5.1)

Where the uncertainties of the enthalpies are determined as

$$u_h = \sqrt{(h(T + u_T, P) - h(T, P))^2 + (h(T, P + u_P) - h(T, P))^2}$$
(5.2)

The uncertainty of the heat load of the evaporator calculated from the water side is estimated as

$$\frac{u_{\dot{Q}_{evap,hw}}}{\dot{Q}_{evap,hw}} = \sqrt{\left(\frac{u_{\dot{m}_{hw}}}{\dot{m}_{hw}}\right)^2 + \left(\frac{u_{c_{p,hw}}}{c_{p,hw}}\right)^2 + \left(\frac{u_{T_{hw,in}}}{T_{hw,in}}\right)^2 + \left(\frac{u_{T_{hw,out}}}{T_{hw,out}}\right)^2}$$
(5.3)

Where the uncertainty of the heat capacity is estimated similar to the enthalpy as

$$u_{c_p} = \sqrt{(c_p(T + u_T, P) - c_p(T, P))^2 + (c_p(T, P + u_P) - c_p(T, P))^2}$$
(5.4)

The uncertainty of the condenser is calculated in the same way. The comparison of the energy balances for all the tests can be seen in table 5.2. The total mass flow of tests 3 and 6 was assumed to be the average mass flow from tests 1 and 2 since in all cases the working fluid pump was run at the same capacity. The energy balance of the cycle is

$$\dot{Q}_{cond} + \dot{W}_p = \dot{Q}_{evap} + \dot{W}_T \tag{5.5}$$

However since there is no turbine in the experimental set up and the electricity consumption of the working fluid pump is small compared to the heat duties of the heat exchangers the following balance should hold

$$\dot{Q}_{cond} \approx \dot{Q}_{evap}$$
 (5.6)

This balance approximately holds for all cases with the heat duty of the condenser slightly higher because of heat input from the working fluid pump.

When the energy balances are compared between the water and working fluid side of each heat exchanger it is seen that the balances for test 1 and 2 are within the error margin while tests 3 and 6 are not. This makes the data from test 3 and 6 less reliable. A possible explanation for this might be that in these cases there was flow through the recuperator. To keep this flow steady a needle valve located after the recuperator had to be fixed to the right position until the level in a storage tank before the ammonia pump was steady. The level in the tank was affected by the pulsation from the pump and therefore a fixed point was difficult to determine. This means that there might have been a small build up of liquid in the recuperator which would result in a reduced working fluid flow. The data is therefore still used for the validation but should be taken with more consideration.

Table 5.2: Energy balances over the heat exchangers from the measured data. The balances for tests 1 and 2 are within the error margin while for tests 3 and 6 they are not.

	Test 1	Test 2	Test 3	Test 6
$\dot{Q}_{evap,wf}$ [kW]	2.6 ± 0.5	2.6 ± 0.4	2.4 ± 0.2	
$\dot{Q}_{evap,hw}$ [kW]	2.44 ± 0.02	2.40 ± 0.02	1.96 ± 0.02	2.04 ± 0.02
$\dot{Q}_{cond,wf}$ [kW]			2.5 ± 0.2	
$\dot{Q}_{cond,cw}$ [kW]	2.65 ± 0.07	2.64 ± 0.07	2.10 ± 0.04	2.21 ± 0.05

5.2. HEAT EXCHANGERS VALIDATION

The pressure drop correlations for the heat exchangers could not be confirmed and the most promising ones were therefore chosen only based on comparison between the proposed correlations, see section 2.1.2. As previously stated the pressure drop correlation proposed by the VDI Heat Atlas [64] for single phase flow was selected, the one from Yan et al. [73] for condensation and for evaporation the correlation from Yan & Lin [72]. The evaporator and condenser were divided into 30 control volumes since further division did not improve the results to a great extent.

5.2.1. RECUPERATOR

There are not many sensors situated around the recuperator (see the simplified P&ID in figure 4.1). Still the temperatures can be estimated and the temperature between the recuperator and evaporator is measured (sensor Ti-5). The temperature in state 2 before the recuperator should be similar to the temperature in state 1 before the pump (sensor Ti-4). When there is flow through the recuperator the temperature in state 4w is similar to temperature in state 4 (sensor Ti-1). The temperature in state 5w is unknown but it cannot be smaller than the temperature in state 2 since the subsequent energy balance has to hold

$$\dot{Q}_{recup} = \dot{m}_{wf}(h_3 - h_2) = \dot{m}_{wf,l}(h_{4w} - h_{5w})$$
(5.7)

Using the data from test 3 and 6 where there was a clear flow through the recuperator an estimate of suitable single phase heat transfer correlation should be attained. Unfortunately since the Reynolds numbers are quite low or around 36-39 the only correlation that is valid in that range is the one proposed by Winkelmann [71]. The

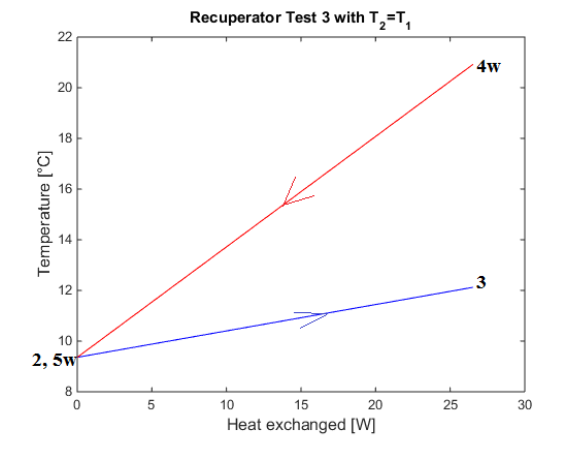
correlations that comes closest to be also valid is the one from the VDI Heat Atlas. When they are compared there is no noticeable difference in the results, that might stem from the fact that the heat load is quite low as well as the Reynolds numbers. The data can though be used to estimate the temperature increase because of the pump. The working fluid pump is largely oversized and it is uncertain how much heat it adds to the cycle. Since the liquid flow from the separator is much lower than the total flow on the other side the liquid flow is easily cooled down. As explained above the liquid flow can though never get colder than the inlet temperature of the opposite flow. In order to get the temperature in state 3 equal to the measured value the temperature in state 2 has to be approximately 2 K higher than the measured temperature in state 1 when the data from test 3 is viewed, see table 5.3. The increase is even higher or just over 3 K when the data from test 6 is viewed, see table 5.4. This temperature increase is much higher than expected from the working fluid pump. The pump is much larger than would be necessary and was operated as 0.1% capacity which is of course not an ideal operating capacity. This could also explain the high temperature increase from the condenser until the evaporator in tests 1 and 2 when the flow was completely evaporated. Test 1 and 6 were performed in the same day and in test 1 the temperature increase is approximately 3 K. Tests 2 and 3 were performed during another day and also observed is a approximately 2 K increase during test 2. This means that the isentropic efficiency is much lower than expected or around 2-3 %. In figure 5.4 the temperature profiles of the recuperator for test 3 are shown. The colder flow is only able to reach the measured value when there is 2 °C temperature increase over the pump. Since the warmer flows' mass flow is considerably lower than of the colder flow the working fluid is able to cool down to almost the same value as at the colder flows' inlet.

Table 5.3: **Recuperator test 3**: Comparison between the data for the recuperator and the model results for test 3. The comparison shows that the temperature in state 2 in the cycle has to be approximately 2 °C higher than the temperature in state 1 so that the temperature in state 3 matches with the measured value.

Variable	Measured data	Model with $T_2 = T_1$	Model with T_2 = T_1 + 2 ° C
$\overline{P_2}$ [bar]	8.88	8.88	8.88
T_2 [°C]	$9.36(T_1)$	9.36	11.36
T_3 [°C]	13.63	12.12	13.64
$\dot{m}_w f [\mathrm{kg}\mathrm{s}^{-1}]$	0.00205	0.00205	0.00205
\dot{m}_l [kg s ⁻¹]	0.000487	0.000487	0.000487
T_{4w} [°C]	20.94	20.91	20.91
T_5w [°C]		9.36	11.38
P_{4w} [bar]	~8.83	8.83	8.83
Heat Load [W]		26.5	21.9
$\Delta_{P,wf}$ [bar]		0.015	0.015
$\Delta_{P,l}$ [bar]		0.015	0.015
Re_{wf}		36.9	37.7
$Re_{wf,l}$		39.1	39.5

Table 5.4: **Recuperator test 6**: Comparison between the data for the recuperator and the model results for test 6. The comparison shows that the temperature in state 2 in the cycle has to be approximately 3.3 °C higher than the temperature in state 1 so that the temperature in state 3 matches with the measured value.

Variable	Measured data	Model with $T_2 = T_1$	Model with $T_2 = T_1 + 3.3$ ° C
$\overline{P_2 \text{ [bar]}}$	8.78	8.78	8.79
T_2 [°C]	$6.94(T_1)$	6.94	10.24
T_3 [°C]	11.98	9.17	11.92
$\dot{m}_w f [\text{kg s}^{-1}]$	0.00205	0.00205	0.00205
\dot{m}_l [kg s ⁻¹]	0.000333	0.000333	0.00333
T_{4w} [°C]	20.58	20.53	20.53
T_5w [°C]		6.94	10.24
P_{4w} [bar]	~8.72	8.72	8.72
Heat Load [W]		21.3	16.1
$\Delta_{P,wf}$ [bar]		0.015	0.015
$\Delta_{P,l}$ [bar]		0.015	0.015
Re_{wf}		36.0	37.3
$Re_{wf,l}$		38.5	39.2



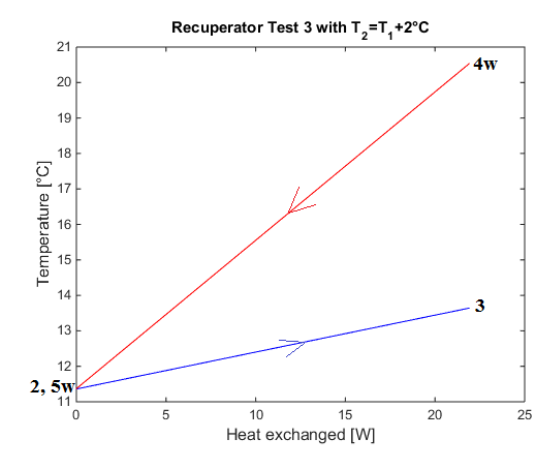


Figure 5.4: Temperature profiles for the recuperator from test 3. Left: the outlet temperature of colder flow does not reach the measured value in state 3, right: it does.

5.2.2. CONDENSER

There was some unexpected subcooling in the condenser of the experimental set up. The subcooling took up approximately 6 % of the total area. The area was calculated with the correlation that gave the best fit, see below. This was likely happening near the cold water entrance. The model was adjusted to take this into account. For the part in the condenser where the working fluid is condensing the heat transfer correlations from section 2.1.1.2.1 for condensation were implemented in the code. Where there was single phase flow the single phase heat transfer correlations from section 2.1.1.1 were implemented. The combination of correlation that gave the best fit to the data was the heat transfer correlation from Thonon & Bontemps [60] for condensation and the heat transfer correlation from Yan et al. [73] for the single phase flow. The results from test 3 with the single phase correlation from Yan et al. and the proposed heat transfer correlation for condensation can be seen in table 5.5. When the condenser correlations were coupled with the single phase correlation from the VDI Heat Atlas [64] the heat transfer was under predicted. This was also the case when they were coupled with the correlation from Coulson and Richardson's Chemical Engineering Design [53] and the one proposed by Winkelmann [71]. When the condensing heat transfer correlations were coupled with the single phase heat transfer correlation proposed by Donowski and Kandlikar [15] then the heat transfer was over predicted in most cases. It should be noted that the Reynolds numbers are lower than 200 which is the limit of the correlations from Yan et al. it is therefore likely that this correlations does not accurately predict the single phase heat transfer. However since it is only possible to validate the overall heat transfer this combination is used since it gives the closest fit to the data. In figure 5.6 the heat transfer coefficient of the cold water and the working fluid from all four experiments have been plotted with the correlations for single phase flow and condensation to show how they compare to the proposed correlations. In figure 5.5 the temperature profile for the condenser is shown for the different correlations that were proposed. All of them show a similar trend except they either over or underestimate the heat transfer.

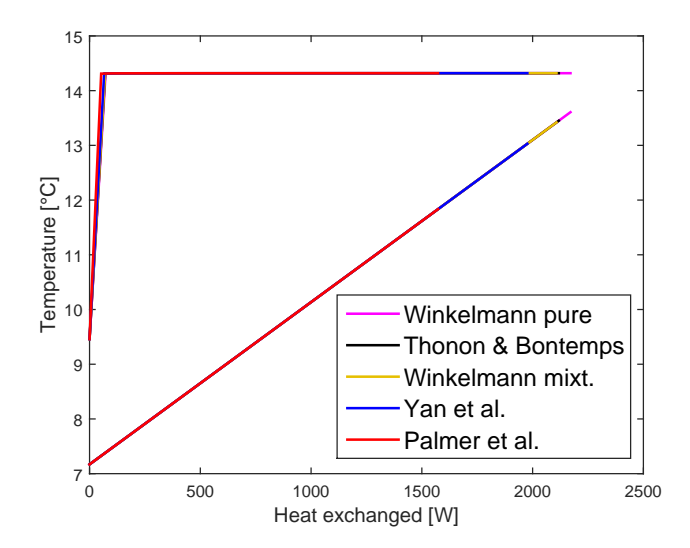


Figure 5.5: Comparison of temperature profiles in the condenser for different correlations for test 3.

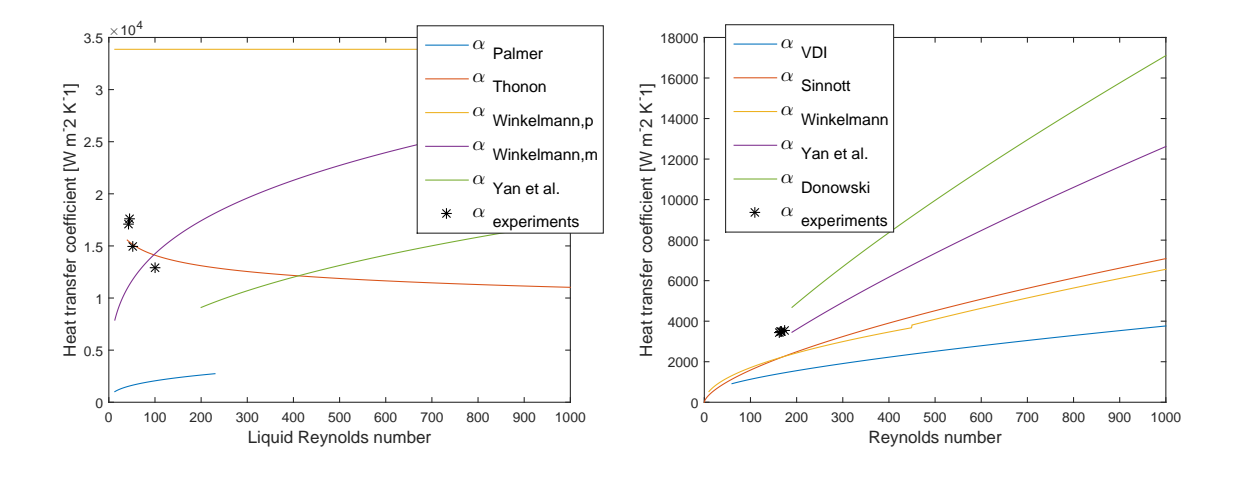


Figure 5.6: The heat transfer coefficients from the four experiments are here shown with regard to the proposed correlations. Left: condensation; right: water side.

Table 5.5: **Condenser test 3**: Comparison between the data for the condenser and the model results for test 3. The comparison is for the single phase correlation from Yan et al. [73] and the condenser correlation proposed in section 2.1.1. The comparison shows that the correlation from Thonon and Bontemps [60] gives the best fit to the data (see the cold water temperature, $T_{cw,out}$)

Variable	Measured data	Yan et al.	Palmer	Thonon & Bontemps	Winkelmann mixt.	Winkelmann pure
T ₇ [°C]	14.81	14.32	14.32	14.32	14.32	14.32
T_1 [°C]	9.358802	9.36	9.36	9.36	9.36	9.36
$T_{cw,in}$ [°C]	7.169662	7.17	7.17	7.17	7.17	7.17
$T_{cw,out}$ [°C]	13.41227	12.94	11.87	13.38	13.32	13.54
P_1 [bar]	~7.12	7.12	7.12	7.12	7.12	7.12
\dot{m}_{wf} [kg s ⁻¹]	0.00205	0.00205	0.00205	0.00205	0.00205	0.00205
$\dot{m}_{cw} [\text{kg s}^{-1}]$	0.080319	0.0803	0.0803	0.0803	0.0803	0.0803
$LMTD_{avg}$ [K]		4.14	4.73	3.94	3.95	3.85
Heat Load [W]		1947	1459	2096	2076	2149
$U_{avg} [{ m W} { m m}^{-2} { m K}^{-1}]$		1403	869	1805	1711	1910
$\alpha_{wf,avg} [{\rm W m^{-2} K^{-1}}]$		4724	1525	17606	10844	37540
$\alpha_{cw,avg} [{\rm W m^{-2} K^{-1}}]$		3557	3525	3567	3566	3571
$Re_{wf,avg}$		43	43	43	43	43
$Re_{cw,avg}$		171	168	172	172	173
$\Delta_{P,wf}$		0.0023	0.0024	0.0023	0.0023	0.0023
q_7		0.7628	0.6181	0.8227	0.8148	0.8439

5.2.3. EVAPORATOR

After a quick test it is obvious that the heat transfer correlations for evaporation that had heat transfer coefficients in the lower range in section 2.1.1.2.2 underestimate the heat transfer. The heat transfer correlations in the higher range were the ones from Yan and Lin [72] with an extra factor of 10, the heat transfer correlations from Ayub et al. [6] and the one from Palmer et al. [48]. In all cases, except for test 1, the best fit was the heat transfer correlation from Yan and Lin [72] for evaporation in combination with the single phase correlation from Donowski and Kandlikar [15]. In those cases all other combination of correlations underestimated the heat transfer. Test 1 stood out since this combination overestimated the heat transfer and the best fit was the correlation from Yan and Lin in combination with the single phase correlation from Winkelmann. Since in all other cases the other two were the best fit they were chosen as the appropriate heat transfer correlations. It should be noted that since the Reynolds numbers of the working fluid are very low the correlations from Yan & Lin is not valid in that range. However since the other correlations were really far off this correlation was still selected. The results of the model from test 2 with the single phase heat transfer correlation from Donowski and Kandlikar [15] coupled with the evaporation correlations from the higher range are listed in table 5.6. In the comparison it is clear that all of the combinations under predict the heat transfer however the evaporative correlation from Yan and Lin with the factor of 10 comes the closest. This is clear from figure 5.7 that shows the temperature profile for the different correlations that were proposed for test 2. In this case the working fluid should be superheated however none of the correlations show that. In figure 5.8 the heat transfer coefficient of the cold water and the working fluid from all four experiments have been plotted with the correlations for single phase flow and evaporation to show how they compare to the proposed correlations.

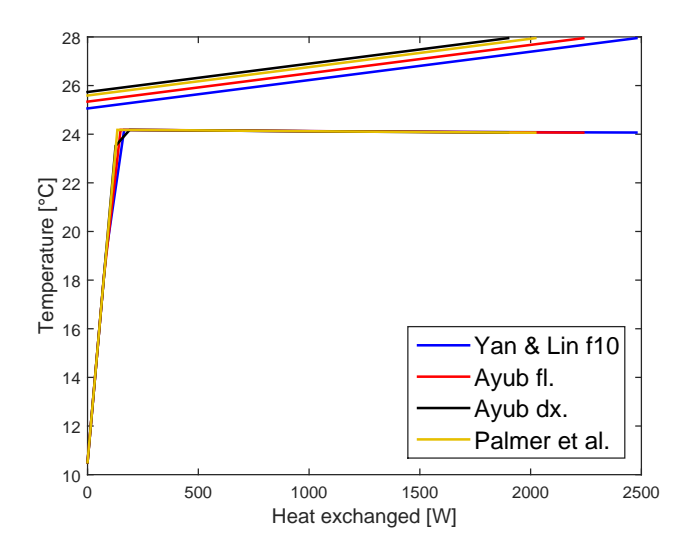


Figure 5.7: Comparison of temperature profiles in the evaporator for different correlations for test 2.

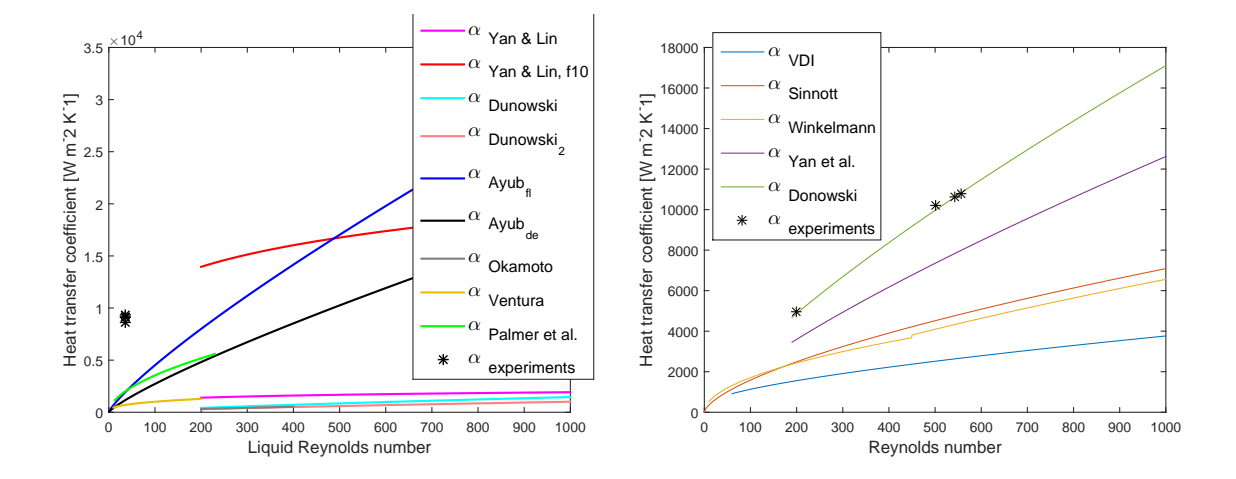


Figure 5.8: The heat transfer coefficients from the four experiments are here shown with regard to the proposed correlations. Left: evaporation; right: water side.

5.3. CYCLE VALIDATION 53

Table 5.6: **Evaporator test 2**: Comparison between the data for the evaporator and the model results for test 2. The comparison is for the single phase correlation from Donowski and Kandlikar [15] and the evaporative correlations with results in the higher range proposed in section 2.1.1. The comparison shows that the correlation from Yan and Lin [72] gives the best fit to the data (see the warm water outlet temperature, $T_{hw,out}$, and the vapor quality)

Variable	Measured data	Yan & Lin f10	Ayub fl.	Ayub dx.	Palmer et al.
P_3 [bar]	~9.78	9.78	9.78	9.78	9.78
T_4 [°C]	27.15	24.1	24.1	24.1	24.1
T_3 [°C]	10.51	10.51	10.51	10.51	10.51
$T_{hw,in}$ [°C]	27.95	27.95	27.95	27.95	27.95
$T_{hw,out}$ [°C]	25.15	25.21	25.4	25.69	25.63
\dot{m}_{wf} [kg s ⁻¹]	0.00206	0.00206	0.00206	0.00206	0.00206
\dot{m}_{hw} [kg s ⁻¹]	0.204939	0.205	0.205	0.205	0.205
$LMTD_{avg}$ [K]		2.79	2.94	3.16	3.12
Heat Load [W]		2347	2185	1939	1987
$U_{avg} [{ m W} { m m}^{-2} { m K}^{-1}]$		2329	1775	1380	1445
$\alpha_{wf,avg} [\text{W m}^{-2} \text{K}^{-1}]$		9108	3880	2362	2565
$\alpha_{hw,avg} [\text{W m}^{-2} \text{K}^{-1}]$		10216	10652	10669	10667
$Re_{wf,avg}$		36	36	36	36
$Re_{hw,avg}$		543	544	545	545
q_4	1	0.919	0.852	0.750	0.770

5.3. CYCLE VALIDATION

The results from the comparison of the data and the model for tests 1,2,3, and 6 is given in tables 5.7, 5.8, 5.9 and 5.10. When the subcooling in the condenser was included in the model the model quite well predicts the data even for datasets 3 and 6 which were deemed more unreliable because of the misfit of the energy balances over the heat exchangers (see table 5.2). The difference is though in most cases slightly more than the uncertainty of the measured values. This difference can at least partly be explained by the chosen heat transfer correlations. The correlations that were chosen as explained in the sections above were the ones that gave the best fit to the data. In both cases, that is for the condenser and the evaporator, none of the suggested correlations gave a perfect fit which could explain this difference. There is more difference between the data and the model for the evaporator than the condenser. That is partly explained with the heat transfer correlation misfit since the most noticeable difference is for high pressure in test 1 but then the selected heat transfer did not fit that well as explained in section 5.2.3. The difference might also be partly because of the subcooled and the superheated regions in the evaporator. In these regions the temperature changes quickly for a small change in the heat duty, that made the calculations more sensitive. It should be noted that separate single phase flow correlations were chosen for the evaporator and condenser. Of course this is not realistic but use of the same single phase flow correlation results in a worse fit. There was also no obvious way to determine which of the single phase flow heat transfer correlations would have been the most appropriate one. The most noticeable difference between the data and the model is for temperature T_7 (temperature before the condenser) in test 1 and 6. In the model the expansion valve from state 4r to 5r was assumed to be isenthalpic, that is no enthalpy difference over the valve. However temperature T_7 (sensor Ti-2) in test 1 and test 6 from the data indicate that there is a small enthalpy increase which might be because of a slight heat input from the environment to the pipe from the valve to the condenser. In that region the temperature of the working fluid was slightly lower than the environmental temperature which was around 20 °C. This slight enthalpy increase would explain the higher temperatures.

Table 5.7: Comparison of the average of the measured data from test 1 and the model results.

Sensor	Variable	Average measured data	Uncertanity	Model	Difference
Ti-1 [°C]	T_4	28.52	±0.05	28.36	0.16
Ti-2 [°C]	T_7	17.79	± 0.05	15.75	2.04
Ti-3 [°C]	$T_{cw,in}$	3.92	± 0.05	3.92	0.00
Ti-4 [°C]	T_1	6.56	± 0.05	6.46	0.10
Ti-5 [°C]	T_3	9.79	± 0.05	10.22	0.43
Ti-6 [°C]	$T_{hw,out}$	26.17	± 0.05	25.99	0.18
Ti-7 [°C]	$T_{hw,in}$	29.0	± 0.4	29.0	0.00
Ti-8 [°C]	$T_{cw,out}$	11.72	± 0.05	11.65	0.07
Pi-1 [bar]	P_{4r}	9.66	± 0.05	10	0.34
Pi-2 [bar]	P_{5r}	6.74	± 0.05	6.72	0.02
Pi-3 [bar]	P_2	9.70	± 0.05	10.07	0.37
Fi-101 [$kg s^{-1}$]	\dot{m}_{cw}	0.0810	± 0.0006	0.0810	0.00
$Fi-103 [kg s^{-1}]$	\dot{m}_{hw}	0.206	± 0.001	0.206	0.00
Fi-201 [kg s $^{-1}$]	\dot{m}_{v}	0.00204	± 0.00007	0.00204	0.00

5.3. CYCLE VALIDATION 55

Table 5.8: Comparison of the average of the measured data from test 2 and the model results.

Sensor	Variable	Average measured data	Uncertanity	Model	Difference
Ti-1 [°C]	T_4	27.15	±0.05	27.27	0.11
Ti-2 [°C]	T_7	15.75	± 0.05	15.96	0.21
Ti-3 [°C]	$T_{cw,in}$	4.50	± 0.05	4.50	0.00
Ti-4 [°C]	T_1	8.22	± 0.05	8.14	0.09
Ti-5 [°C]	T_3	10.51	± 0.05	11.35	0.84
Ti-6 [°C]	$T_{hw,out}$	25.15	± 0.05	24.98	0.16
Ti-7 [°C]	$T_{hw,in}$	27.9	± 0.4	27.9	0.00
Ti-8 [°C]	$T_{cw,out}$	12.40	± 0.05	12.36	0.04
Pi-1 [bar]	P_{4r}	9.73	± 0.05	9.67	0.06
Pi-2 [bar]	P_{5r}	6.89	± 0.05	6.87	0.02
Pi-3 [bar]	P_2	9.78	± 0.05	9.73	0.06
Fi-101 [$kg s^{-1}$]	\dot{m}_{cw}	0.0800	± 0.0006	0.080	0.00
Fi-103 [kg s $^{-1}$]	\dot{m}_{hw}	0.205	± 0.001	0.205	0.00
Fi-201 [kg s ⁻¹]	\dot{m}_{v}	0.00206	±0.00005	0.00206	0.00

Table 5.9: Comparison of the average of the measured data from test 3 and the model results.

Sensor	Variable	Average measured data	Uncertanity	Model	Difference
Ti-1 [°C]	T_4	20.94	±0.05	20.60	0.34
Ti-2 [°C]	T_7	14.81	± 0.05	14.28	0.53
Ti-3 [°C]	$T_{cw,in}$	7.17	± 0.05	7.17	0.00
Ti-4 [°C]	T_1	9.36	± 0.05	9.16	0.20
Ti-5 [°C]	T_3	13.63	± 0.05	13.13	0.50
Ti-6 [°C]	$T_{hw,out}$	21.70	± 0.05	21.59	0.11
Ti-7 [°C]	$T_{hw,in}$	24.0	± 0.4	24.0	0.00
Ti-8 [°C]	$T_{cw,out}$	13.41	± 0.05	13.34	0.07
Pi-1 [bar]	P_{4r}	8.83	± 0.05	8.74	0.09
Pi-2 [bar]	P_{5r}	7.13	± 0.05	7.11	0.02
Pi-3 [bar]	P_2	8.88	± 0.05	8.79	0.09
Fi-101 [kg s $^{-1}$]	\dot{m}_{cw}	0.0800	± 0.0006	0.080	0.00
Fi-103 [kg s $^{-1}$]	\dot{m}_{hw}	0.206	± 0.001	0.206	0.00
Fi-201 [kg s $^{-1}$]	\dot{m}_{v}	0.00156	± 0.00005	0.00167	0.00011

Table 5.10: Comparison of the average of the measured data from test 6 and the model results.

Sensor	Variable	Average measured data	Uncertanity	Model	Difference
Ti-1 [°C]	T_4	20.58	±0.05	20.14	0.43
Ti-2 [°C]	T_7	15.71	± 0.05	12.77	2.94
Ti-3 [°C]	$T_{cw,in}$	5.30	± 0.05	5.30	0.00
Ti-4 [°C]	T_1	6.94	± 0.05	6.977	0.05
Ti-5 [°C]	T_3	11.98	± 0.05	11.63	0.35
Ti-6 [°C]	$T_{hw,out}$	20.87	± 0.05	20.60	0.27
Ti-7 [°C]	$T_{hw,in}$	27.0	± 0.4	27.0	0.00
Ti-8 [°C]	$T_{cw,out}$	11.86	± 0.05	11.70	0.16
Pi-1 [bar]	P_{4r}	8.72	± 0.05	8.61	0.11
Pi-2 [bar]	P_{5r}	6.79	± 0.05	6.76	0.03
Pi-3 [bar]	P_2	8.79	± 0.05	8.66	0.11
Fi-101 [$kg s^{-1}$]	\dot{m}_{cw}	0.0800	± 0.0006	0.080	0.00
Fi-103 [kg s $^{-1}$]	\dot{m}_{hw}	0.080	± 0.0005	0.080	0.00
Fi-201 [kg s $^{-1}$]	\dot{m}_v	0.00172	± 0.00005	0.00172	0.00

5.4. HÚSAVÍK CONDENSER

The model has also been validated making us of data from a former geothermal plant. The Húsavík Kalina plant operated in Húsavík, Iceland, from 2000 to 2008 [70]. The plant operated on similar principles as an closed OTEC cycle except with a geothermal heat source. The hot side temperature is higher and therefore an extra recuperator stage was used compared to the Kalina cycle for OTEC applications. The heat exchangers used in the plant were shell and tube and plate heat exchangers. The evaporator and the high temperature recuperator were a shell and tube heat exchangers while the low temperature recuperator and the condenser were plate heat exchangers [56]. The condenser of the plant is similar to what has been proposed in the use for OTEC. The working fluid was ammonia water with the base concentration of around 82% [70]. A validation of the condenser part of the model with this condenser can give an useful insight into the effects of using an ammonia water mixture. The geometry and the specification of the condenser from the Húsavík plant are shown in table 5.11. The conditions at the outlet of the condenser are claimed to be 5.4 bar and 12.4°C [56]. The mixture is not fully condensed at these conditions compared to the REFPROP database and therefore first there is a comparison with 5.4 bar pressure at the outlet and then with a outlet pressure of 5.45 bar. At 5.4 bar the saturation temperature is around 12.1 °C but at 5.45 bar the saturation temperature is approximately 12.4 °C.

The pressure drop from the Húsavík plant is a design specification and can therefore not be used to validate the pressure drop correlations. The correlations that were used were the one from the VDI Heat Atlas [64] for single phase flow and the one from Yan et al. [73] for two phase flow. These correlation were used since they showed promising results when compared to other correlations, see section 2.1.2. The temperatures and outlet pressure have however been reported after operation started [56] and therefore this data can give a good estimate of which heat transfer correlation is appropriate for this condition.

As explained in section 5.2 the best fit to the data obtained from the experiments with pure ammonia was the combination of the single phase flow correlation from Yan et al. [73] and the two phase flow correlation from Thonon & Bontemps [60] for the condenser. When the single phase flow correlation from Yan et al. is used for the condenser from Húsavík all of the correlations highly over estimate the heat transfer. The results when the single phase flow heat transfer correlation proposed by Sinnott in the Coulson and Richardson's Chemical Engineering Design [53] is used are listed in tables 5.12 and 5.13 for 5.4 bar and 5.45 bar outlet pressures, respectively. The heat transfer correlation from Palmer et al. [48] is not used since it is based on a much lower Reynolds numbers. The correlation for pure fluids proposed by Winkelmann [71] is also not used since it did not converge for these conditions (over estimated the heat transfer).

The comparison between the heat transfer correlations for the 5.4 bar outlet pressure in table 5.12 shows that the correlations that comes closest to the correct heat transfer is the one by Yan et al. [73] This correlation under predicts the heat transfer as well as the correlation by Thonon & Bontemps [60]. The correlation from Winkelmann for mixtures [71] over predicts the heat transfer. The deviation of the results when the outlet pressure is

5.45 bar, see table 5.13, is quite significant. Here the correlation from Thonon & Bontemps gives the closest results. The correlation from Winkelmann in this case did not converge and both the correlations from Yan et al. and Thonon & Bontemps over predict the heat transfer. The difference seems to stem from the fact that for the higher pressure value the LMTD becomes higher. In figure 5.10 the temperature profile is shown when the correlation from Yan et al. is used with an outlet pressure of 5.4 bar. The figure clearly shows how the temperature glide of the ammonia water mixture follows the cooling water profile. In figure 5.9 the heat transfer correlations that were proposed are compared to the results from the best fit for 5.45 bar oulet pressure. That is the condensation correlation from Thonon & Bontemps and the single phase correlation from Sinnott. In the figure it is clear that there is a large difference between the single phase correlation proposed by Sinnott and the one from Yan et al. It should be noted that in chapter 2 the correlations were plotted for the geometry of the heat exchangers from the experimental set up while here they are plotted for the geometry from the Húsavík condenser.

Table 5.11: Húsavík condenser geometry and specifications

Number of passes	1
Flow	Counterflow
110	
Total number of channels	480
Number of channels in pass 1 hot	240
Number of channels in pass 1 cold	240
Surface enlargement factor*	1.076
Chevron angle [°]	60/29
Horizontal port centres distance [m]	0.486
Vertical port centres distance [m]	2.003
Plate thickness [mm]	0.5
Compressed plate pitch* [m]	0.00338
Port diameter [m]	0.243
Plate width [m]	0.989
Total area [m ²]	754.44
Total number of plates	481
*Calculated	

Table 5.12: Comparison of the Húsavík condenser and the model with outlet pressure of 5.4 bar with the single phase flow correlation proposed by Sinott [53].

Variable	Unit	Húsavík	Yan et al.	Thonon & Bontemps	Winkelmann mixt.
$T_{wf,cond,in}$	[°C]	37.6	34.2	27.6	110.7
$T_{wf,cond,out}$	[°C]	12.4	12.1	12.1	12.1
$T_{cw,cond,in}$	[°C]	5	5	5	5
$T_{cw,cond,out}$	[°C]	25.3	24.5	22.2	46.2
$P_{wf,out}$	[bar]	5.4	5.4	5.4	5.4
ΔP_{wf}	[bar]	0.0552	0.0158	0.0142	0.0277
ΔP_{cw}	[bar]	0.207	0.0624	0.0609	0.0712
\dot{m}_{wf}	$[kg s^{-1}]$	8.149	8.149	8.149	8.149
\dot{m}_{cw}	$[kg s^{-1}]$	85	85	85	85
$LMTD_{avg}$	[°C]	4.5	4.0	3.51	22.8
Heat load	[W]	7,207,667	6,959,000	6,150,000	14,707,000
Overall coefficient, U_{avg}	$[W m^{-2} K^{-1}]$	2682	2914	2841	3607
$Re_{wf,avg}$	-	-	490	473	790
$Re_{cw,avg}$	-	-	858	831	1147

Table 5.13: Comparison of the Húsavík condenser and the model with outlet pressure of 5.45 bar with the single phase flow correlation proposed by Sinott [53].

Variable	Unit	Húsavík	Yan et al.	Thonon & Bontemps
$T_{wf,cond,in}$	[°C]	37.6	89.9	43.5
$T_{wf,cond,out}$	[°C]	12.4	12.4	12.4
$T_{cw,cond,in}$	[°C]	5	5	5
$T_{cw,cond,out}$	[°C]	25.3	39.0	26.8
$P_{wf,out}$	[bar]	5.4	5.4	0
ΔP_{wf}	[bar]	0.0552	0.0231	0.0163
ΔP_{cw}	[bar]	0.207	0.0677	0.0621
\dot{m}_{wf}	$[kg s^{-1}]$	8.149	8.149	8.149
\dot{m}_{cw}	$[kg s^{-1}]$	85	85	85
$LMTD_{avg}$	[°C]	4.5	16.2	5.2
Heat load	[W]	7,207,667	12,146,000	7,810,000
Overall coefficient, U_{avg}	$[W m^{-2} K^{-1}]$	2682	3162	2739
$\alpha_{wf,avg}$	$[W m^{-2} K^{-1}]$	-	11936	9380
$\alpha_{cw,avg}$	$[W m^{-2} K^{-1}]$	-	5210	4971
$Re_{wf,avg}$	-	-	704	517
$Re_{cw,avg}$	-	-	1047	888

The main difference between the operating conditions of the condenser for the Húsavík plant and proposed for OTEC plants are the ammonia concentration which is lower and the ratio of mass flows between the working fluid and the cold water is lower as well for the Húsavík plant. This results in higher Reynolds numbers on the working fluid side than in the optimized design of the OTEC cycle by Kirkenier [31]. The fact that the correlations that fit best for pure ammonia, that is the correlation for condensation proposed by Thonon & Bontemps [60] in combination with the single phase flow correlation from Yan et al. [73], do over predict the heat transfer in this case suggests that indeed that mass transfer becomes a more prominent phenomenon for mixtures. For OTEC applications there is a question if this still holds because of the different operating concentration level, however this comparison suggests that the heat transfer might be even lower for OTEC applications since then the Reynolds numbers of the working fluid are even lower. Further experiments need to be done to verify that.

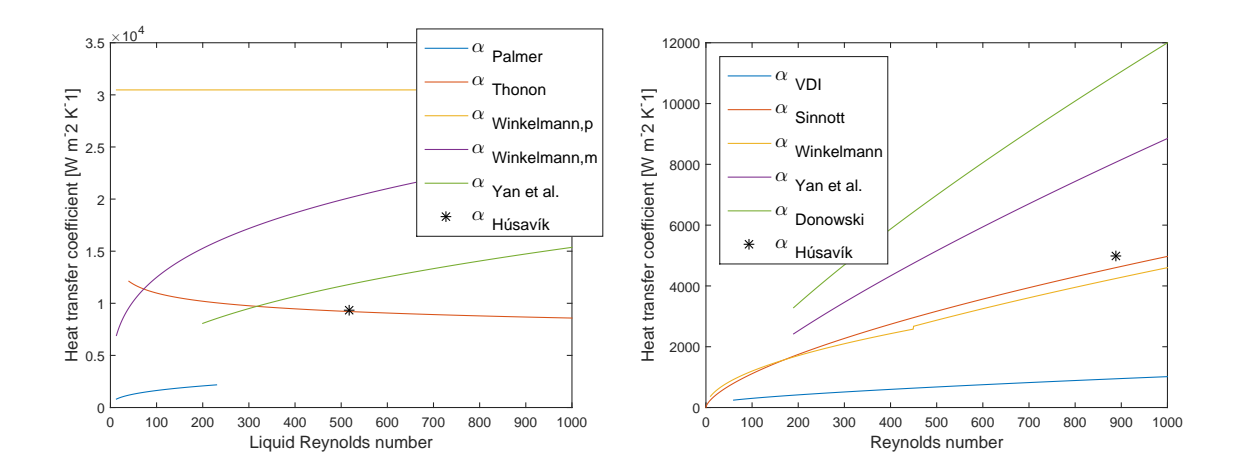


Figure 5.9: The heat transfer coefficients from the Húsavík condenser that gave the best fit for outlet pressure of 5.45 bar are here shown with regard to the proposed correlations. Left: condensation; right: water side.

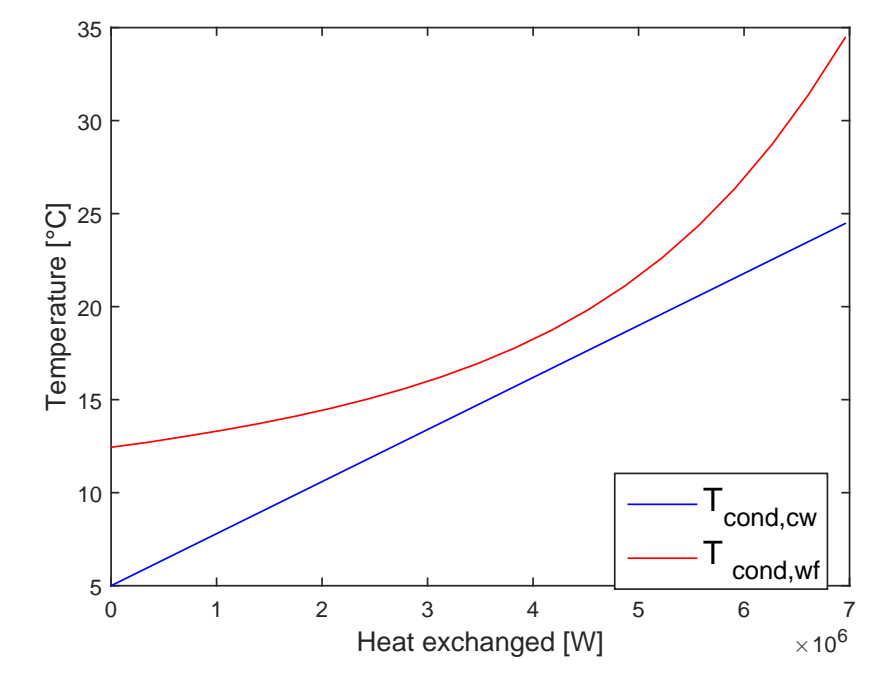


Figure 5.10: The calculated temperature profile for the Húsavík condenser with the two phase flow correlation from Yan et al.[73] and the single phase flow correlation from from Coulson and Richardson's Chemical Engineering Design [53]. The figure shows how the temperature glide of the ammonia water mixture follows the cooling water profile.

6

SENSITIVITY ANALYSIS

A sensitivity analysis is made for the three cases discussed in chapter 2. That is for a cycle with pure ammonia, a cycle with R32 - R134a mixture and a cycle with ammonia - water mixture. The analysis is to identify the influences on the net power output and the thermal efficiency when there are variations in the sea water temperature. As mentioned before the model is based on an optimized design made by Kirkenier [31]. The heat exchanger sizes in the case for pure ammonia, ammonia water and R32 - R134a are shown in table 6.1. In the optimization only the length of each plate and the total width was determined but not the width of each plate. Since in the calculations only the width times the number of channels is used the width of each plate does not have effect on the calculations outcome. It was therefore assumed that the width would be one third of the length of each plate and from the total width the number of channels and plates were determined. In the case of the recuperator only the total area was calculated in the optimization. The length and width were therefore both assumed. The optimized mass flows are also listed in the table. The optimal concentration for the ammonia water mixture according to the research of Kirkenier was 95.29 % of ammonia versus 4.71 % water, mass based. For the R32 - R134a mixture the concentration was 53.67 % R32 versus 46.33 % R134a, mass based.

In the optimization made by Kirkenier the LCOE of each optimized design was calculated. The LCOE is of course affected by the net power output. However since in the following analysis the effects of extreme temperature fluctuations are researched rather then the temperature fluctuations of specific locations the change in LCOE is not analysed.

During the analysis an error was noticed in the optimization from Kirkenier. In the calculations of the heat transfer coefficient for the evaporator and the condenser the thermodynamic properties of water were used for both sides, that is for the water and the working fluid side. Since these components are relatively large compared to other components this can potentially have quite high impact on the results. Therefore it is likely that the results from Kirkeniers are not the real optimum for each working fluid. Therefore the results of the analysis do not give the best indication of which working fluid should be selected. However the results do show how each particular design is affected by temperature fluctuations of the seawater.

Table 6.1: Heat exchangers specifications.

	Pure an	nmonia	I	Ammonia wat	er	R32 - R134a	
	Evaporator	Condenser	Evaporator	Condenser	Recuperator	Evaporator	Condenser
Number of water channels	185774	58205	170194	53947	730	181798	54627
Number of working fluid channels	185773	58205	170194	53947	730	181798	54627
Chevron angle [°]	30	30	30	30	30	30	30
Plate width* [m]	0.441	0.704	0.489	0.830	0.667	0.462	0.808
Vertical port centres distance [m]	1.323	2.111	1.466	2.492	2.000*	1.3862	2.424
Plate thickness [mm]	0.6	0.6	0.6	0.6	0.6	0.6	0.6
Compressed plate pitch [m]	0.0039	0.0039	0.0039	0.0039	0.0039	0.0039	0.0039
Total number of plates*	371548	116410	340389	107895	1464	363597	109255
Total area [m ²]	216810	172970	243850	223310	1984	232890	214040
Working fluid mass flow [kg s ⁻¹]	687.53	687.53	1097.39	1097.39	1097.39	4144.6	4144.6
Cold water mass flow [kg s ⁻¹]	-	30908.3	-	30908.3	-	-	30908.3
Warm water mass flow [kg s ⁻¹]	79730.48	-	76573.31	-	-	79730	
*Assumed							

6.1. AMMONIA

In figures 6.1 and 6.2 the effects of the seawater temperature on the delivered power and thermal efficiency are shown respectively. As expected the net power and efficiency increase with increasing temperature difference since the pressure drop over the turbine increases. It is also clear from figure 6.1 that for the same temperature difference the power output is comparable. That is for 24 and 4 °C and for 27 and 7 °C the net power is similar and the same applies for 27 and 5 °C and 29 and 7 °C. This means that fluctuations in the cold seawater temperature have similar effect to fluctuations in the warm seawater temperature and the net power and the thermal efficiency are proportional to the temperature difference. The increase in net power is approximately 2.3 MW for each degree increase in temperature difference.

As stated in chapter 2 the thermal efficiency can be compared to the Carnot efficiency which is the theoretical maximum for a heat engine. The thermal efficiency is approximately 26 % of the Carnot efficiency for the minimum temperature difference up to 42 % for the maximum temperature difference. The thermal efficiency for couple of binary geothermal plants can be found in a paper by DiPippo [14]. As explained in section 5.4 the thermodynamic cycle of binary geothermal plants are similar to the OTEC cycle. The thermal efficiencies for the geothermal plants were from 26 % of the Carnot efficiency up to 51 % with the average around 34 %. The results are therefore comparable.

In tables 6.2 and 6.3 the Reynolds numbers, LMTD, heat transfer coefficients and the pressure drop over the evaporator and condenser are listed. From the tables it is clear that the Reynolds numbers of the working fluid are lower for OTEC application than for geothermal applications like the Húsavík plant, see section 5.4. The overall heat transfer coefficient should be a good estimation of the real value because of the validation with the data for pure ammonia from the experiments. The heat transfer coefficients of the water and the ammonia separately might however be less accurate since only the combination of heat transfer correlation for single phase flow and two phase flow could be validated. The temperature profiles of the evaporator and the condenser for temperature difference of 22 K ($T_{hw} = 27$ °C and $T_{cw} = 5$ °C) are shown in figure 6.3.

6.1. Ammonia 65

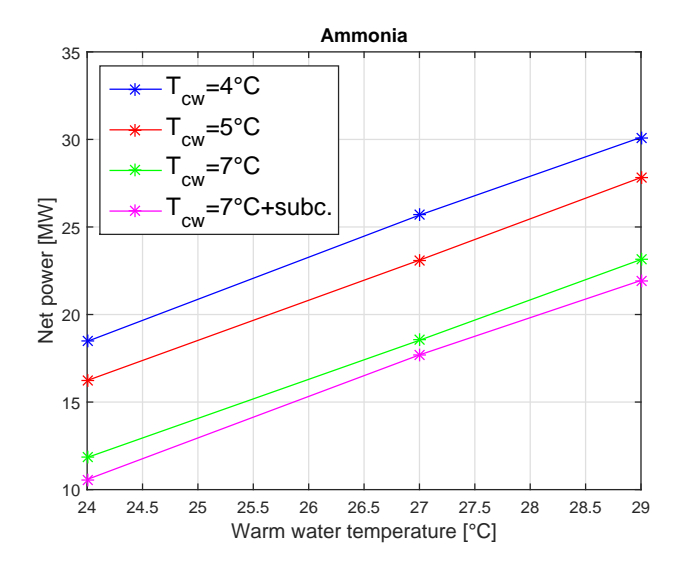


Figure 6.1: Net power output as a function of the seawater temperature for a cycle operating with pure ammonia.

The effects of subcooling in the condenser are also included in the figures for cold water temperature of 7 °C (note that the effects are not included in table 6.3). As explained in chapter 5 there was some subcooling in the condenser during the experiments. The subcooling covered approximately 6 % of the total area during the experiments and the same ratio was used here. The subcooling caused an increase in the lower pressure level which resulted in a lower net power output and thermal efficiency. Therefore if it is possible to modify the heat exchanger design so that subcooling can be avoided, for example by increasing the working fluid mass flow, that should be done.

Table 6.2: Results from the evaporator calculations for pure ammonia. Here the average Reynolds numbers, the LMTD, the heat transfer coefficients and pressure drops are listed from the lowest to the highest seawater temperature difference.

$\Delta T [K]$	$Re_{wf,avg}$	$Re_{hw,avg}$	U_{avg} [W m ⁻² K ⁻¹]	LMTDavg [K]	$\alpha_{wf,avg} [\mathrm{W}\mathrm{m}^{-2}\mathrm{K}^{-1}]$	$\alpha_{hw,avg} [\text{W m}^{-2}\text{K}^{-1}]$	ΔP_{wf} [bar]	ΔP_{hw} [bar]
17	113	1929	2605	1.99	9277	18129	0.0021	0.0012
19	117	1931	2530	2.01	8697	18141	0.0020	0.0012
20 (24-4)	116	1931	2530	2.05	8716	18138	0.0020	0.0012
20 (27-7)	120	2062	2555	2.13	8852	18766	0.0019	0.0011
22 (27-5)	119	2061	2558	2.17	8918	18759	0.0037	0.0021
22 (29-7)	121	2154	2547	2.17	8685	19190	0.0020	0.0011
23	118	2061	2551	2.24	8857	18759	0.0020	0.0012
24	120	2153	2540	2.26	8646	19188	0.0021	0.0011
25	127	2149	2551	2.39	8760	19170	0.0021	0.0012

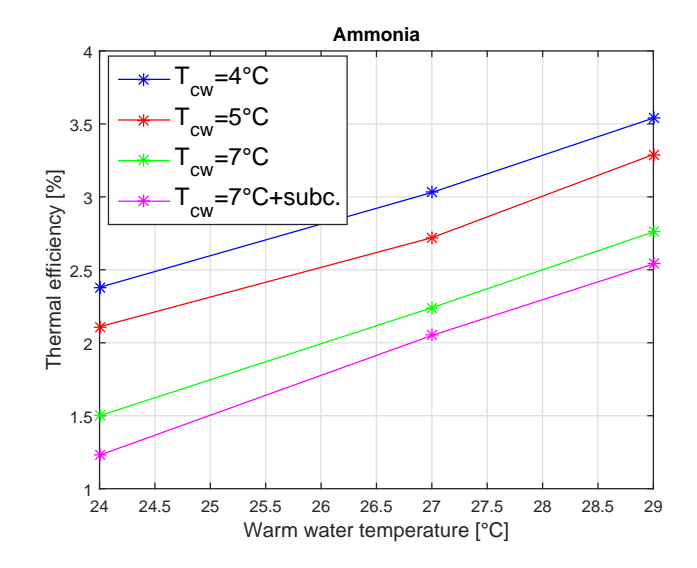


Figure 6.2: Thermal efficiency as a function of the seawater temperature for a cycle operating with pure ammonia.

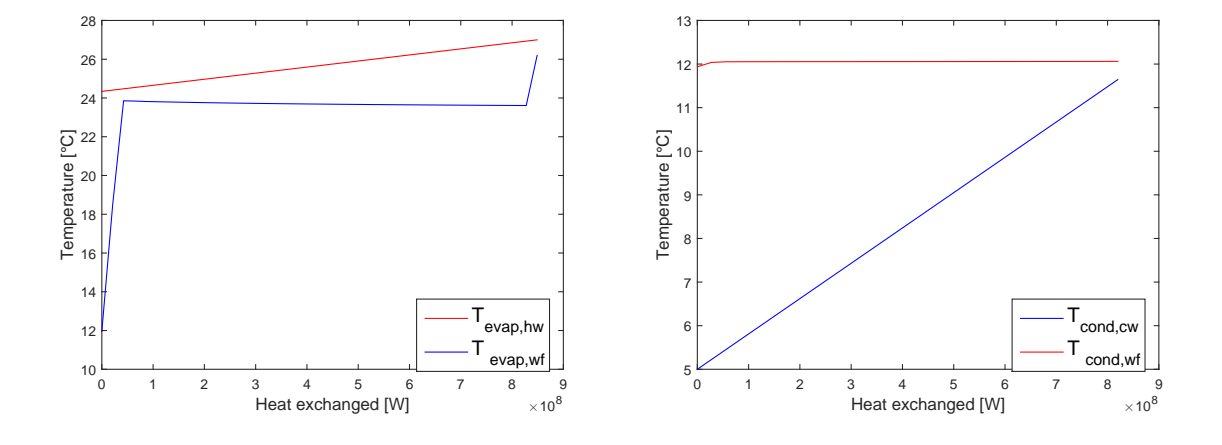


Figure 6.3: Temperature profiles for 22 K temperature difference. Left: temperature profile in the evaporator; right: temperature profile in the condenser.

6.1. Ammonia 67

Table 6.3: Results from the condenser calculations for pure ammonia. Here the average Reynolds numbers, the LMTD, the heat transfer coefficients and pressure drops are listed from the lowest to the highest seawater temperature difference.

$\Delta T [K]$	$Re_{wf,avg}$	$Re_{cw,avg}$	$U_{avg} \ [{ m W m^{-2} K^{-1}}]$	$LMTD_{avg}$ [K]	$\alpha_{wf,avg} [\mathrm{W}\mathrm{m}^{-2}\mathrm{K}^{-1}]$	$\alpha_{cw,avg} [\mathrm{W} \mathrm{m}^{-2} \mathrm{K}^{-1}]$	ΔP_{wf} [bar]	ΔP_{cw} [bar]
17	227	1085	2220	3.48	8564	9293	0.026	0.0003
19	222	1022	2212	3.37	8692	9011	0.027	0.0003
20 (24-4)	220	993	2200	3.42	8651	8880	0.027	0.0002
20 (27-7)	228	1089	2206	3.63	8389	9310	0.027	0.0003
22 (27-5)	224	1031	2180	3.73	8288	9051	0.027	0.0002
22 (29-7)	228	1090	2203	3.67	8346	9315	0.027	0.0002
23	221	1001	2173	3.72	8304	8914	0.027	0.0002
24	224	1030	2184	3.69	8332	9046	0.027	0.0002
25	236	1006	2173	3.93	8277	8938	0.026	0.0002

6.1.1. POSSIBLE IMPROVEMENTS

To keep the benefits of a simpler cycle, that is an organic Rankine cycle instead of the Kalina cycle the ammonia has to fully evaporate in each case. When the temperature difference is at its lowest the ammonia is not fully evaporating for the current design without modification. By lowering the mass flow of the ammonia this can be solved. In the worst case when the deep seawater is 7 °C and the surface water is at 24 °C (17 K temperature difference) this can be solved by decreasing the mass flow by 5%. Then the working fluid fully evaporates and the net power output is similar to what it was before (around 11.8 MW) however the thermal efficiency is though slightly lower. This gives a good insight also into part load operation. If the mass flow is lowered further the working fluid will continue to fully evaporate but the net power and the thermal efficiency of the system will decrease.

In the best case, that is when the temperature difference is at maximum the net power output can be slightly improved by increasing the total ammonia mass flow and still have the working fluid fully evaporating in the evaporator. However the thermal efficiency decreases so there is an optimum. When the working fluid mass flow is increased by 5% then the net power increases from 30.1 MW to around 30.5 MW however if it is increased by 6 % the net power is only around 30.4 MW and the thermal efficiency has decreased from approximately 3.5 % to 3.4 %. The efficiency decreases since both the higher pressure level and the isentropic efficiency of the turbine decrease. At one point this decrease has more effect than the gain from the increased mass flow.

The mass flow of the working fluid can be varied by changing the speed of the working fluid pump. However to be able to increase the mass flow the pump has to have a higher capacity than for the designed case. This method is for example used in a 1.3 MW organic Rankine cycle plant in Svartsengi, Iceland. Svartsengi is a traditional geothermal plant were the Rankine cycle plant is used to further utilize waste heat from the first stage of the plant. The temperature of the waste heat source can vary and then the power output of the Rankine cycle plant is optimized by varying the mass flow of the working fluid 1 .

¹Albert Albertsson (Chief Engineer, HS Energy), personal communication, June 30, 2015

6.2. R32 - R134a

In figure 6.4 and 6.5 the effects of the seawater temperature on the net power and thermal efficiency are shown, respectively. Similar trend is seen here as for the pure ammonia. The net power is proportional to the temperature difference like before, the increase is approximately 2.5 MW for each degree increase in temperature. As in the case for pure ammonia and ammonia water the warm and cold seawater temperature have similar effects on the net power output and the thermal efficiency. When the thermal efficiency of R32 - R134a is compared to the thermal efficiency of pure ammonia, see figure 6.2, it is noted that the thermal efficiency is higher for the pure ammonia. This is surprising since according to the results of Kirkenier [31] this mixtures should have the best results. This is due to the fact that the thermodynamic properties of the working fluids in the heat transfer coefficient calculations were accidentally calculated for water in all cases by Kirkenier as explained before. When the correct properties are used according to the REFPROP database [36] the heat transfer coefficient is considerably lower than for pure ammonia, see tables 6.3 and 6.2 for ammonia compared to tables 6.5 and 6.4 for R32 - R134a. For this mixture the temperature glide during evaporation and condensation is not enough to overcome this difference in the heat transfer coefficient. The temperature profiles for 22 K temperature difference are shown in figure 6.7. To get a better comparison the same heat exchanger sizing as for the mixture R32 - R134a is used for pure ammonia, see figure 6.6. Then the difference between the thermal efficiency of the ammonia versus R32 - R134a is similar as before. This shows that the error in Kirkeniers model has considerable effects on the outcome.

In tables 6.5 and 6.4 another interesting parameters are the Reynolds numbers. The Reynolds numbers for R32 - R134a mixture are a lot higher than in the case for the pure ammonia and the ammonia water mixture. This stems from the fact that the optimum mass flow of the working fluid was higher and the dynamic viscosity is lower compared to the other working fluids. This might be beneficial for the heat transfer correlation, that is the correlation might be closer to a pure fluid correlation than ammonia water for example. This does however not make this mixture more beneficial than ammonia since the correlations for pure ammonia were used in the calculations.

6.2. R32 - R134a 69

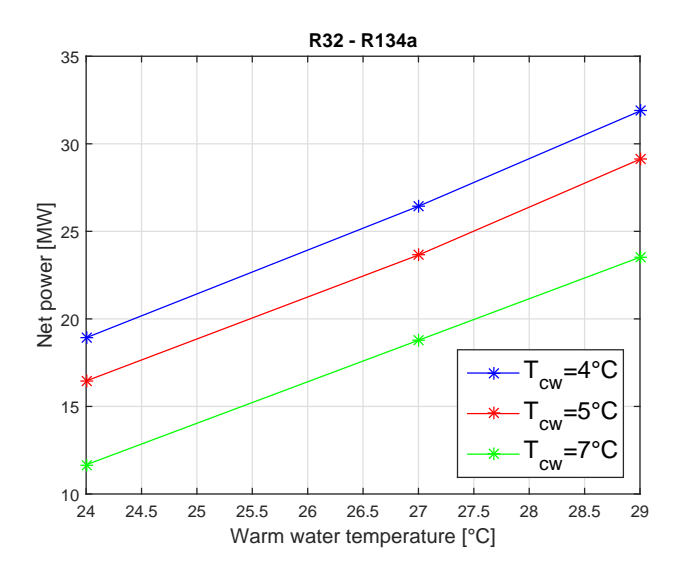


Figure 6.4: Net power output as a function of the seawater temperature for a cycle operating with R32 - R134a mixture.

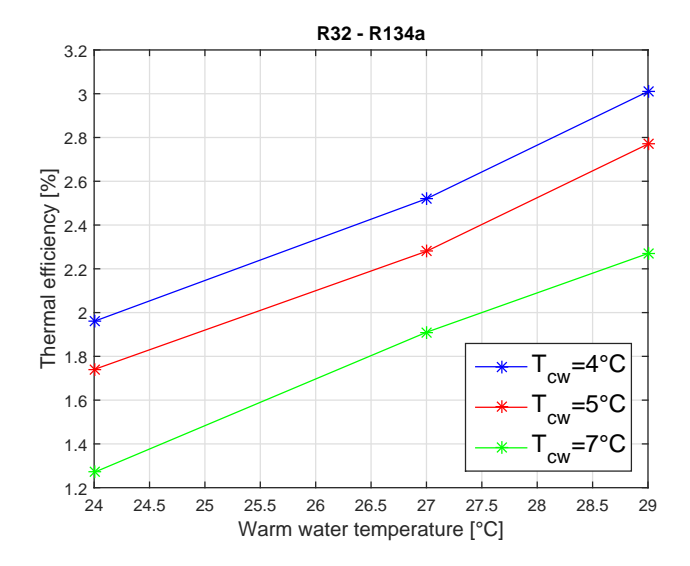


Figure 6.5: Thermal efficiency as a function of the seawater temperature for a cycle operating with R32 - R134a mixture.

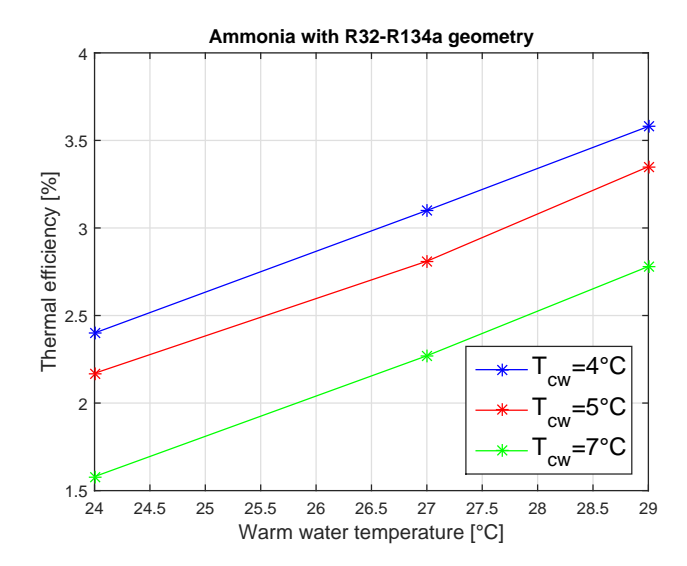


Figure 6.6: Thermal efficiency as a function of the seawater temperature for a cycle operating with ammonia with the same heat exchanger design as the R32 - R134a mixture.

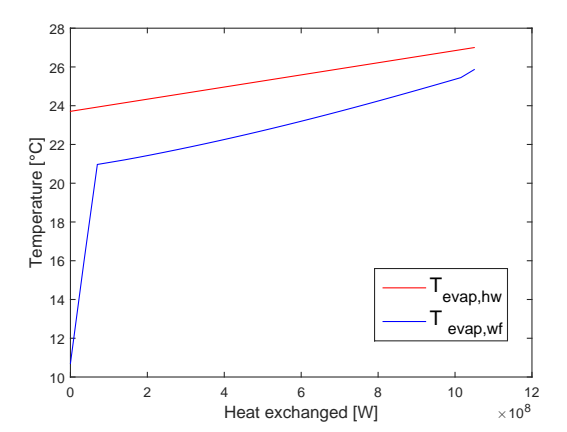
Table 6.4: Results from the evaporator calculations for R32 - R134a mixture. Here the average Reynolds numbers, the LMTD, the heat transfer coefficients and pressure drops are listed from the lowest to the highest seawater temperature difference.

$\Delta T [K]$	$Re_{wf,avg}$	$Re_{hw,avg}$	$U_{avg} \ [{ m W m^{-2} K^{-1}}]$	$LMTD_{avg}$ [K]	$\alpha_{wf,avg} [\mathrm{W}\mathrm{m}^{-2}\mathrm{K}^{-1}]$	$\alpha_{hw,avg} [\mathrm{W}\mathrm{m}^{-2}\mathrm{K}^{-1}]$	ΔP_{wf} [bar]	ΔP_{hw} [bar]
17	647	1874	1899	2.28	4026	17742	0.0077	0.0033
19	667	1872	1889	2.41	3983	17734	0.0071	0.0031
20 (24-4)	664	1870	1893	2.49	4007	17727	0.0071	0.0031
20 (27-7)	687	2002	1888	2.50	3945	18360	0.0068	0.0030
22 (27-5)	682	1996	1919	2.71	4102	18332	0.0076	0.0033
22 (29-7)	698	2087	1894	2.74	4000	18756	0.0069	0.0029
23	678	1996	1899	2.81	4056	18330	0.0070	0.0030
24	691	2086	1886	2.87	3976	18751	0.0074	0.0031
25	687	2085	1882	2.95	3963	18749	0.0075	0.0031

6.2. R32 - R134a 71

Table 6.5: Results from the condenser calculations for R32 - R134a mixture. Here the average Reynolds numbers, the LMTD, the heat transfer coefficients and pressure drops are listed from the lowest to the highest seawater temperature difference.

ΔT [K]	$Re_{wf,avg}$	$Re_{cw,avg}$	$U_{avg} \ [{ m W m^{-2} K^{-1}}]$	$LMTD_{avg}$ [K]	$\alpha_{wf,avg} [\mathrm{W}\mathrm{m}^{-2}\mathrm{K}^{-1}]$	$\alpha_{cw,avg}$ [W m ⁻² K ⁻¹]	ΔP_{wf} [bar]	ΔP_{cw} [bar]
17	1233	1023	1446	3.32	2843	8835	0.0101	0.0009
19	1207	969	1431	3.42	2820	8593	0.0102	0.0009
20 (24-4)	1196	943	1421	3.51	2799	8475	0.0102	8000.0
20 (27-7)	1237	1027.52	1432	3.47	2792	8855	0.0102	0.0009
22 (27-5)	1220	981	1396	3.88	2697	8643	0.0099	8000.0
22 (29-7)	1246	1036	1406	3.80	2704	8891	0.0099	0.0009
23	1206	953	1392	3.90	2698	8517	0.0099	8000.0
24	1219	980	1398	3.85	2704	8640	0.0099	8000.0
25	1206	953	1393	3.88	2700	8516	0.0100	0.0008



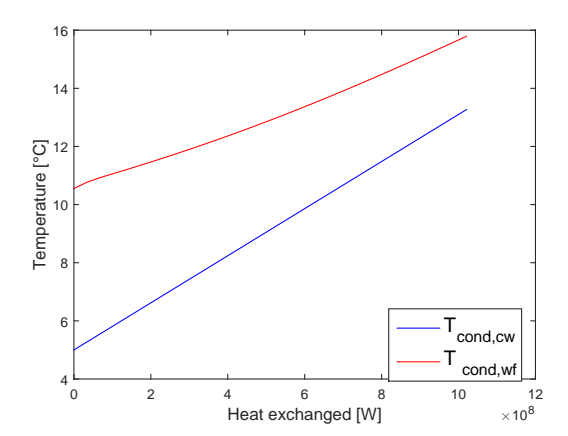


Figure 6.7: Temperature profiles for 22 K temperature difference. Left: temperature profile in the evaporator; right: temperature profile in the condenser.

6.2.1. Possible improvements

For the same reason as for the pure ammonia the R32 - R134a mixture has to fully evaporate so that the benefits of having a simpler cycle can be utilized. To make sure that the mixture fully evaporates at the lower temperature difference the mass flow of the mixture can be decreased or the concentration can be changed. To change the concentration of the mixture is in practice more difficult than to change the working fluid mass flow. If there is not discovered a way to change the concentration while the plant is in operation any benefits of changing the concentration will unlikely make up for losses during shut down of the plant. However this possibility is still reviewed in the case that a method will be discovered.

For the smallest temperature difference a decrease in the mass flow of 5% will make sure that the mixture fully evaporates, however the net power decreases from 11.7 MW to 10.5 MW and the thermal efficiency from 1.3 % to 1.06 %. Since R32 is the more volatile component, that is evaporates more easily, the concentration of R32 has to be increased to have the mixture fully evaporate. Again for the smallest temperature difference, when the deep seawater is at 7 °C and the surface water is at 24 °C, the concentration of R32 is

increased from 53.67% to 55%. This results in the mixture fully evaporating but the power output decreases from approximately 11.7 MW to 9.5 MW and the efficiency decreases from 1.3 % to 0.91 %. The better option in this case seems to be to decrease the mass flow rather than increase the concentration of R32 since in this case it seems that it does not lead to a more favourable temperature glide in the heat exchangers.

For the best case scenario, that is when the warm seawater temperature is at 29 °C and the cold at 4 °C, lowering the mass flow or the concentration of R32 only lowers the net power output and thermal efficiency and is therefore not recommended in this case. This might be due to the fact that the design is not the optimum design or that the temperature glide in the heat exchangers becomes less favourable.

6.3. AMMONIA WATER

In figures 6.8 and 6.9 the effects of the seawater temperature on the power and efficiency are shown, respectively. The trend is similar as in the case of the other working fluids. In tables 6.6 and 6.7 the Reynolds numbers, LMTD, heat transfer coefficients and the pressure drop over the evaporator and condenser are listed. By comparing the tables to the tables for pure ammonia it is noticed that the heat transfer coefficient is slightly lower for ammonia water in the evaporator. It should be noted that the same heat transfer correlations were used as in the case for pure ammonia however it is likely that the heat transfer coefficients will be even lower for ammonia water because of increase in mass transfer resistance. That has to be confirmed with further experiments.

The effects of the error in Kirkeniers model can also be seen here. The ammonia - water mixture gave better results in Kirkeniers results however when compared to pure ammonia the thermal efficiency is only higher for the lower seawater temperature differences. For the higher temperature differences the pure ammonia becomes a better option. However since the design in both cases is likely not the optimum design a conclusion whether the ammonia - water mixture performs better than the pure ammonia one cannot be drawn. That is if the benefits of the temperature glide during evaporation and condensation will make up for a lower heat transfer coefficient. In figure 6.10 the temperature glides in the heat exchangers are shown for 22 K temperature difference.

6.3. Ammonia water 73

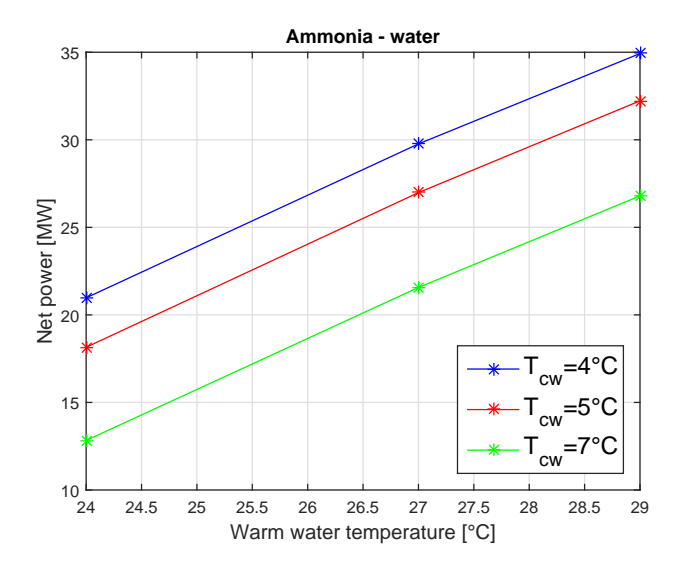


Figure 6.8: Net power output as a function of the seawater temperature for a cycle operating with ammonia water mixture.

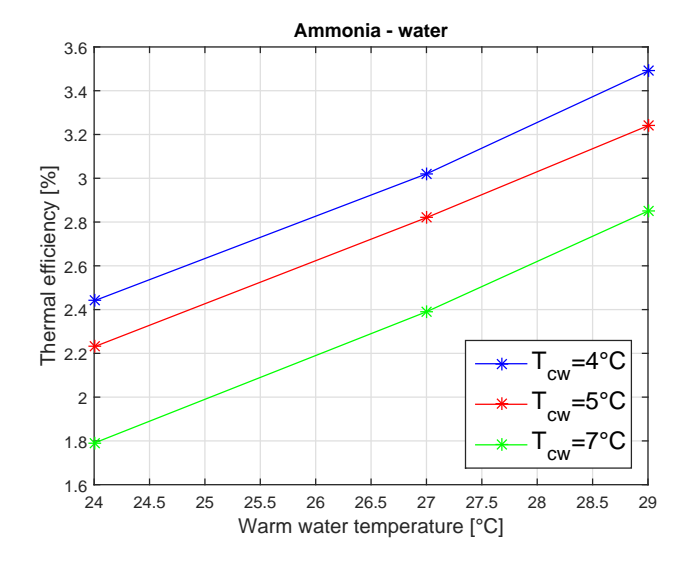


Figure 6.9: Thermal efficiency as a function of the seawater temperature for a cycle operating with ammonia water mixture.

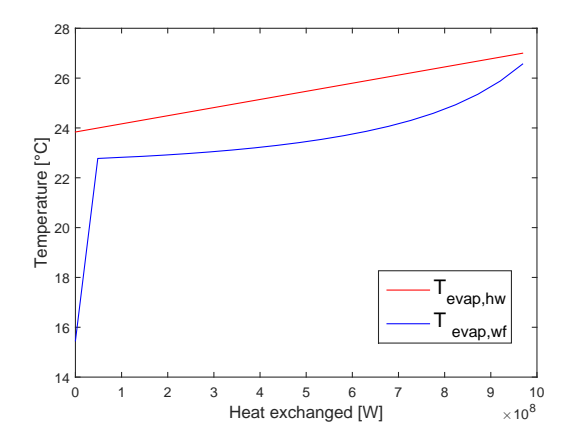
Table 6.6: Results from the evaporator calculations for ammonia water mixture. Here the average Reynolds numbers, the LMTD, the heat transfer coefficients and pressure drops are listed from the lowest to the highest seawater temperature difference.

ΔT [K]	$Re_{wf,avg}$	$Re_{hw,avg}$	$U_{avg} [{ m W m^{-2} K^{-1}}]$	$LMTD_{avg}$ [K]	$\alpha_{wf,avg} [\mathrm{W} \mathrm{m}^{-2} \mathrm{K}^{-1}]$	$\alpha_{hw,avg} [\mathrm{W} \mathrm{m}^{-2} \mathrm{K}^{-1}]$	ΔP_{wf} [bar]	ΔP_{hw} [bar]
17	171	1827	2372	1.51	7218	17370	0.0051	0.0039
19	170	1821	2458	1.54	7831	17338	0.0062	0.0048
20 (24-4)	170	1818	2483	1.59	8102	17323	0.0071	0.0056
20 (27-7)	176	1942	2502	1.62	8161	17927	0.0090	0.0069
22 (27-5)	176	1938	2533	1.78	8522	17904	0.0151	0.0117
22 (29-7)	180	2026	2516	1.73	8231	18322	0.0130	0.0095
23	175	1937	2535	1.84	8572	17898	0.0174	0.0135
24	178	2026	2507	1.73	8160	18322	0.0124	0.0091
25	178	2025	2473	1.86	8125	18317	0.0125	0.0092

Table 6.7: Results from the condenser calculations for ammonia water mixture. Here the average Reynolds numbers, the LMTD, the heat transfer coefficients and pressure drops are listed from the lowest to the highest seawater temperature difference.

$\Delta T [K]$	$Re_{wf,avg}$	$Re_{cw,avg}$	$U_{avg} \ [{ m W m^{-2} K^{-1}}]$	$LMTD_{avg}$ [K]	$\alpha_{wf,avg} [\mathrm{W}\mathrm{m}^{-2}\mathrm{K}^{-1}]$	$\alpha_{cw,avg}$ [W m ⁻² K ⁻¹]	ΔP_{wf} [bar]	ΔP_{cw} [bar]
17	326	1076	2331	2.47	10070	9255	0.0230	0.0004
19	322	1027	2277	2.75	9504	9034	0.0202	0.0003
20 (24-4)	320	1003	2251	2.87	9261	8923	0.0188	0.0002
20 (27-7)	331	1098	2263	2.92	9033	9349	0.0163	0.0002
22 (27-5)	326	1045	2223	3.11	8728	9114	0.0140	0.0002
22 (29-7)	332	1103	2250	3.00	8851	9369	0.0148	0.0002
23	323	1017	2209	3.14	8659	8987	0.0138	0.0002
24	325	1042	2234	3.04	8877	9097	0.0154	0.0002
25	322	1014	2220	3.099	8803	8970	0.0150	0.0002

6.3. Ammonia water 75



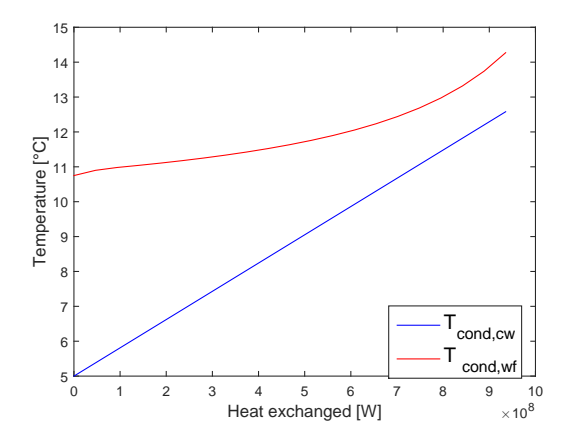


Figure 6.10: Temperature profiles for 22 K temperature difference. Left: temperature profile in the evaporator; right: temperature profile in the condenser.

6.3.1. Possible improvements

The ammonia - water mixture does not need to fully evaporate like the other working fluids, however still some improvements can be made to increase the net power output during off design operation.

For the largest temperature difference of 25 K the net power can be improved slightly by increasing the mass flow of the working fluid. By increasing the mass flow by 3 % the net power output can be increased from 34.8 MW to 35.1 MW however in this case the thermal efficiency decreases and if the mass flow is increased further then the net power output will start to decrease as well. The net power output can similarly be increased slightly for the smallest temperature difference by decreasing the mass flow, by decreasing it by 5% the net power output can be increased by approximately 0.7 MW and the thermal efficiency also increases. If the mass flow is decreased further the thermal efficiency starts to decrease.

The concentration of the ammonia - water mixture can also be varied to try to find a new optimum of the temperature glide for each temperature difference. For the best case the concentration was lowered to 95 % however then the net power output decreased. By lowering the concentration even less, an increase might be the result or the benefits of the temperature glide wont make up for the fact that the thermal efficiency and the efficiency of the turbine decrease when working under off design conditions. Similar effects were seen when the concentration was increased to 95.5 % for the smallest temperature difference.

CONCLUSIONS AND RECOMMENDATIONS

7.1. CONCLUSIONS

The main conclusion is as expected that when the temperature difference of the warm and cold seawater changes it has a large effect on the net power output and the thermal efficiency of an OTEC cycle. This stems from the fact that the total temperature difference is relatively low. Fluctuations in the warm or cold temperature seem to have similar effects. To improve the performance of the cycle during off design conditions the mass flow of the working fluid should be varied. However this can only improve the performance by a small degree. It should be noted that the temperature fluctuations that are researched in the report are the extremes for suitable OTEC locations and most locations have smaller fluctuations. For example an average 25 MW plant with fluctuations in the warm seawater temperature of 2°C and no fluctuations in the cold seawater temperature has fluctuations of approximately 5 MW or around 20 %. This shows that seasonal fluctuations have quite an impact on the net power produced which has to be taken into account in the economical evaluation of each location.

The model was validated with experiments for pure ammonia and should be fairly accurate also for scaled up OTEC plants operating with pure ammonia since the thermodynamics of the system stay similar for a larger plant. Whether the model is still valid for other working fluids is debatable since for example the selected heat transfer correlations might not give a good fit for other working fluids, especially in the case of mixtures. The heat transfer correlations that gave the best fit in the case of pure ammonia were the combination of the single phase flow heat transfer correlation proposed by Yan et al. [73] and the condensation correlation proposed by Thonon & Bontemps [60] for the condenser. For the evaporator the combination of the single phase flow correlation proposed by Donowski and Kandlikar [15] and the evaporation correlation by Yan and Lin [72] with an extra factor of 10 gave the best fit.

As mentioned in chapter 6 there was an error made in the previous optimization and therefore the optimized designs used in the analysis were not the real optima. This makes it hard to determine if ammonia or ammonia water will perform better taking off design into account. However as mentioned in section 5.2 the heat transfer correlations

for evaporation that were in the group with a lower heat transfer coefficient highly underestimated the heat transfer. Two of these correlations were made for ammonia - water mixture. This suggest that the heat transfer coefficient is indeed a lot lower for ammonia water and for mixtures in general because of the increased part of mass transfer at low Reynolds numbers. The validation of the condenser from the Húsavík plant in section 5.4 further supports this conclusion since when the single phase flow correlation proposed by Yan et al. [73] was coupled with the proposed condensation correlations the heat transfer was over predicted. Therefore ammonia - water and other mixtures might not be an attractive choice as the optimization by Kirkenier suggested [31]. A mixture that results in higher Reynolds number might be a better option than ammonia water however the benefits of a higher Reynolds number will have to overcome the disadvantage of a lower heat transfer coefficient.

7.2. RECOMMENDATIONS FOR FUTURE WORK

First of all it is recommended to combine this model with an optimization model for OTEC. Then the optimal design of the OTEC cycle for each suitable location could be determined for the entire year. Also the model should optimize modifications in mass flow and concentration that could further increase the net power of the cycle.

The OTEC experimental set up is being modified with more sensors. After the modification there will be temperature and pressure sensors before and after every component in the cycle. A Coriolis flow sensor that can measure the flow and concentration of a mixture is also added. It is therefore recommended that more experiments should be performed. These experiments could verify which pressure drop correlations are most appropriate for the heat exchangers. This also brings the opportunity to do measurements with mixtures like ammonia - water. Then it could be confirmed if the same heat transfer correlations can be used as for a pure ammonia or if the heat transfer coefficient does indeed drop as the validation from the Húsavík plant suggests. If a turbine will be installed it is also recommended to explore further how the turbine will be affected during off design conditions. It is also recommended if possible to do experiments to confirm which single phase flow heat transfer correlation is the best fit for OTEC operating conditions. This could be done with water on both sides of the heat exchangers for example. Then more accurate two phase flow correlations could be determined suitable for OTEC applications.

Also since incorrect thermal properties were used in heat exchanger calculations by Kirkenier [31] the most economical working fluids for OTEC should be researched again. The mixture R32 - R134a is for example not the best choice. Thereafter this model could be used to see how the working fluids that really give the best results perform under off design conditions. Another recommendation is to find a quicker equation of state for ammonia water calculations than the one used by REFPROP since the calculations for ammonia water were significantly slower than for pure ammonia and R32-R134a.



MEASUREMENTS RESULTS

In the following figures the measurement results from tests 2, 3 and 6 are shown.

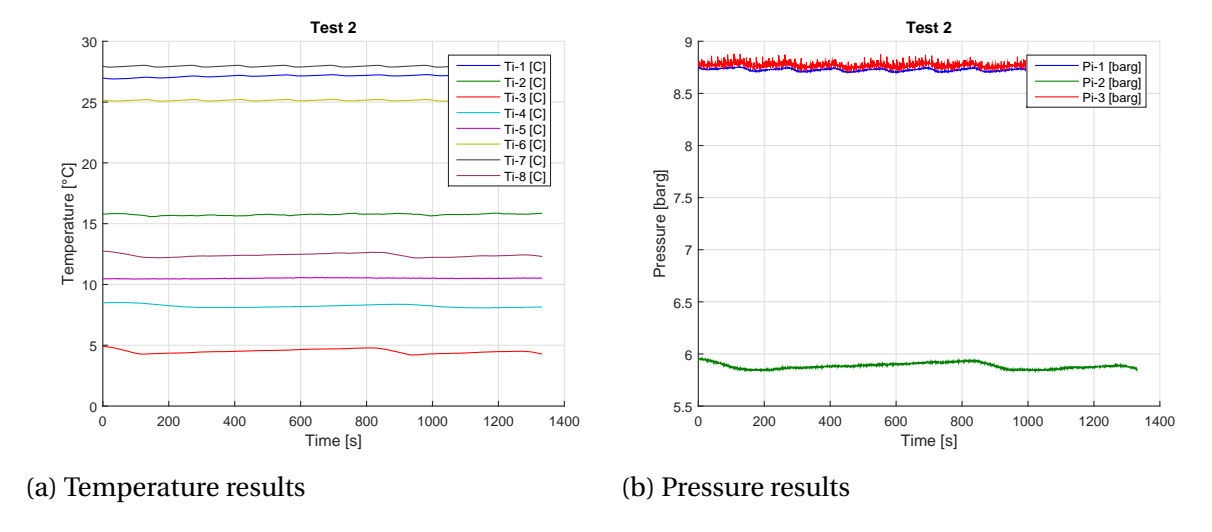


Figure A.1: Measurement data for test 2, (a) temperature as a function of time; (b) pressure as a function of time.

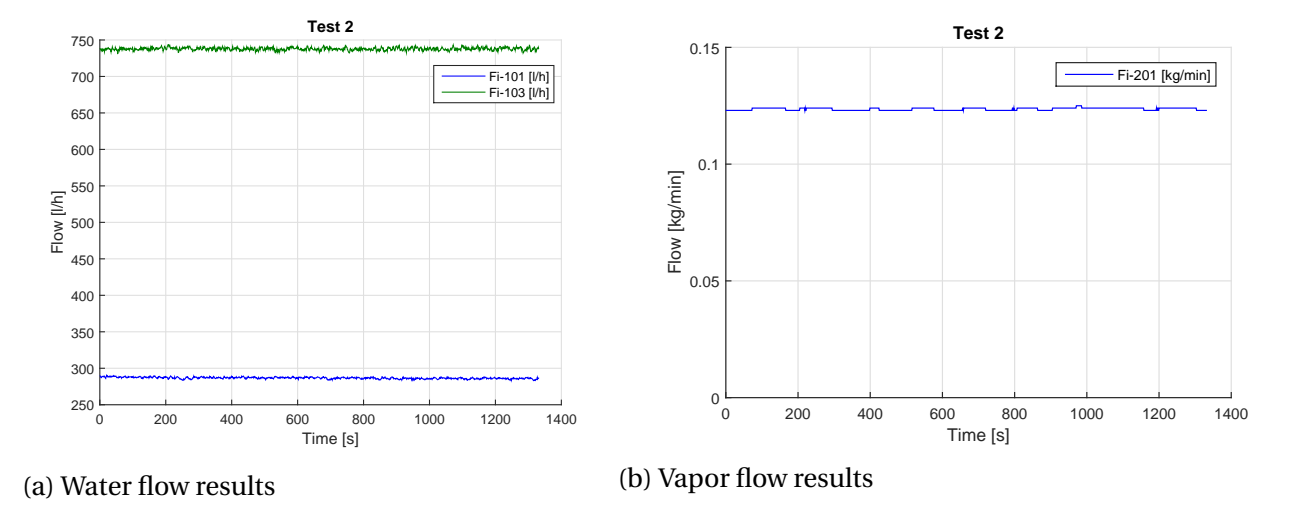


Figure A.2: Measurement data for test 2, (a) water flow as a function of time; (b) vapor flow as a function of time.

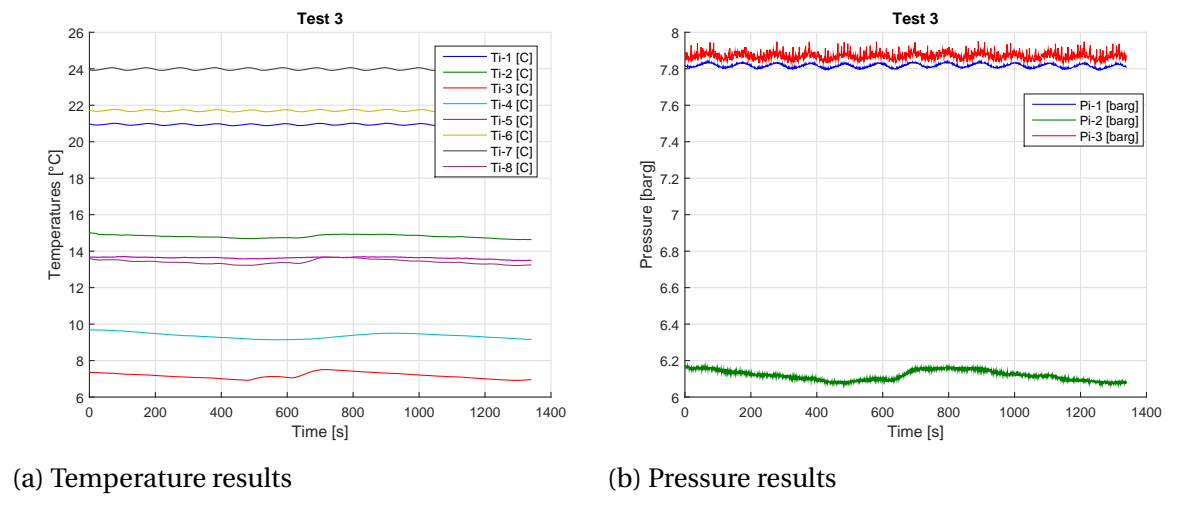


Figure A.3: Measurement data for test 3, (a) temperature as a function of time; (b) pressure as a function of time.

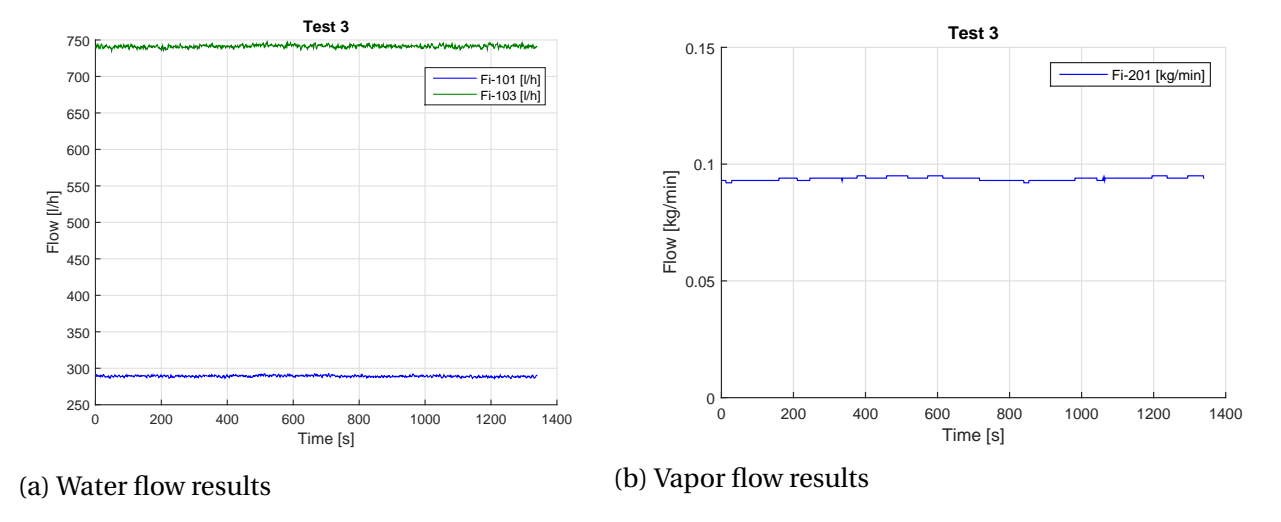


Figure A.4: Measurement data for test 3, (a) water flow as a function of time; (b) vapor flow as a function of time.

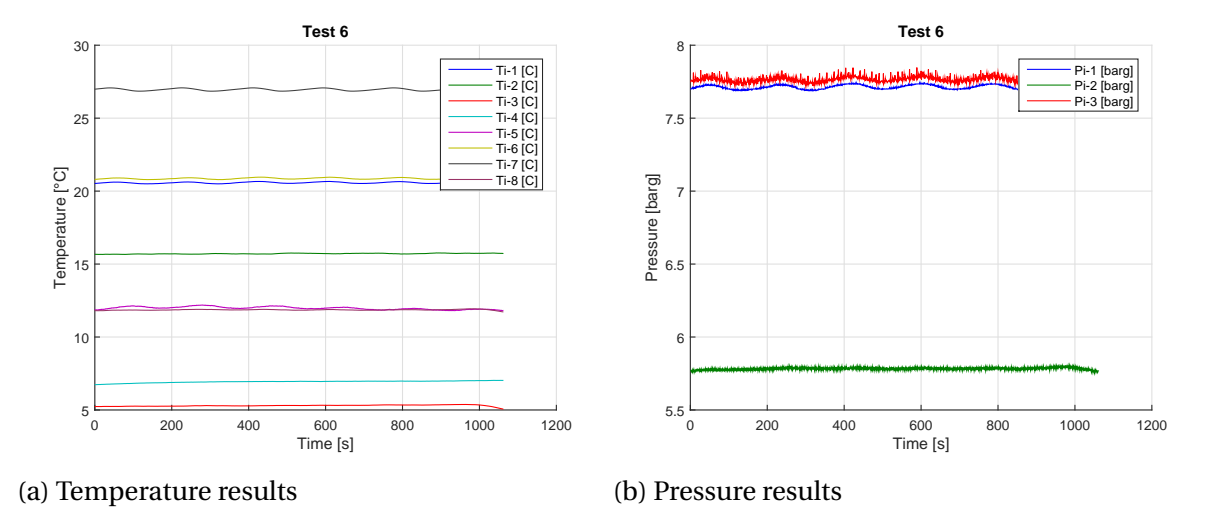


Figure A.5: Measurement data for test 6, (a) temperature as a function of time; (b) pressure as a function of time.

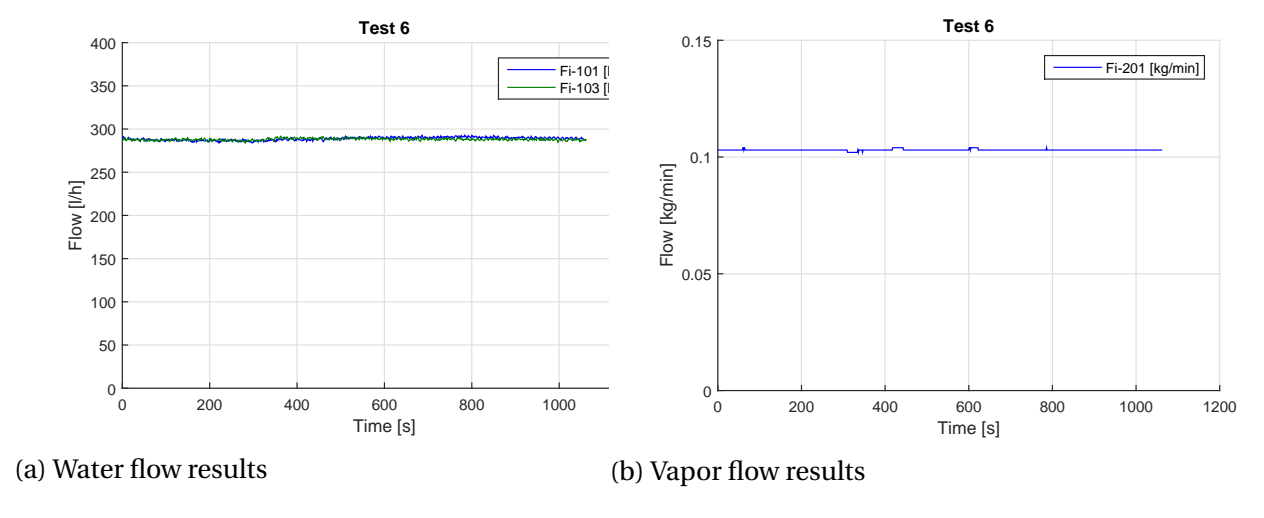


Figure A.6: Measurement data for test 6, (a) water flow as a function of time; (b) vapor flow as a function of time.

BIBLIOGRAPHY

- [1] ACEVEDO, D., BASKAR, Y., PROCHAZKA, T., AND HERMANS, K. *Ecopark for Curacao*. Technical report, Bluerise BV and Delft University of Technology, 2012.
- [2] AE SENSORS BV. DF140 Flowsenosr. Datasheet, n.d.
- [3] ANGELINO, G., AND COLONNA DI PALIANO, P. Multicomponent working fluids for organic Rankine cycles (ORCs). *Energy 23*, 6 (1998), 449–463.
- [4] AVERY, W. H., AND WU, C. Renewable Energy from the Ocean: A Guide to OTEC. Oxford University Press, Inc, 1994.
- [5] AYDIN, H., LEE, H. S., KIM, H. J., SHIN, S. K., AND PARK, K. Off-design performance analysis of a closed-cycle ocean thermal energy conversion system with solar thermal preheating and superheating. *Renewable Energy* 72 (2014), 154–163.
- [6] AYUB, Z. H. Plate Heat Exchanger Literature Survey and New Heat Transfer and Pressure Drop Correlations for Refrigerant Evaporators. *Heat Transfer Engineering 24*, 5 (Sept. 2003), 3–16.
- [7] BHARATHAN, D. Staging Rankine Cycles Using Ammonia for OTEC Power Production Staging Rankine Cycles Using Ammonia for OTEC Power Production. Technical report, National Renewable Energy Laboratory, 2011.
- [8] BLOKKER, R. COST REDUCTION OF OCEAN THERMAL ENERGY CONVERSION: Exploratory analysis of a Supercritical Rankine Cycle. Master's thesis, Technical University of Delft, 2012.
- [9] Branan, C. R. *Rules of Thumb for Chemical Engineers*, 3rd ed. Gulf Professional Publising, 2002.
- [10] Brennen, C. E. Fundamentals of Multiphase Flows. Cambridge University Press, 2005.
- [11] Bronkhorst Nederland. T14-AGD-44-E. Receipt, 2013.
- [12] Cox, N. A Novel Working Fluid for Ocean Thermal Energy Conversion. 2012.
- [13] CROSSLEY, M., AND SPRAGUE, T. Education for sustainable development: Implications for small island developing states (SIDS). *International Journal of Educational Development* 35 (Mar. 2014), 86–95.
- [14] DIPIPPO, R. Ideal thermal efficiency for geothermal binary plants. *Geothermics* 36, 3 (2007), 276–285.

84 Bibliography

[15] DONOWSKI, V., AND KANDLIKAR, S. *Correlating evaporation heat transfer coefficient of refrigerant R-134a in a plate heat exchanger*. Paper presented at the Engineering Foundation Conference on Pool and Flow Boiling, Alaska, May, 2000.

- [16] FOCKE, W., ZACHARIADES, J., AND OLIVIER, I. The effect of the corrugation inclination angle on the thermohydraulic performance of plate heat exchangers. *International Journal of Heat and Mass Transfer 28*, 8 (1985), 1469–1479.
- [17] FUJITA, R., MARKHAN, A. C., DIAZ, J. E. D., GARCIA, J. R. M., SCARBOROUGH, C., GREENFIELD, P., BLACK, P., AND AGUILERA, S. E. Revisiting ocean thermal energy conversion. *Marine Policy* 36 (2012), 463–465.
- [18] GANIC, E. N., AND WU, J. ON THE SELECTION OF WORKING FLUIDS FOR OTEC POWER PLANTS. *Energy Conv. & Mgmt. 20* (1980), 9–22.
- [19] GRITTON, E. C., PEI, E. C., AROESTY, J., BALABAN, M. M., GAZLEY, C., HESS, R. W., AND KRASE, W. H. A Quantitative Evaluation of Closed Cycle Ocean Thermal Energy Conversion (OTEC) Technology in Central Station Applications, 1980.
- [20] HAN, D. H., LEE, K. J., AND KIM, Y. H. Experiments on the characteristics of evaporation of R410A in brazed plate heat exchangers with different geometric configurations. *Applied Thermal Engineering* 23, 10 (2003), 1209–1225.
- [21] HAN, D. H., LEE, K. J., KIM, Y. H., AND MUTHURAMAN, S. The Characteristics of Condensation in Brazed Plate Heat Exchangers with Different Chevron Angles. *Journal of the Korean Physical Society* 43, 1 (2003), 66–73.
- [22] HIROYUKI, T., AKINOBU, M., AND TAKENOBU, K. Sensitivity analysis of ocean-based closed cycle OTEC power system. *Electrical Engineering in Japan 107*, 1 (Jan. 1987), 68–78.
- [23] HUANG, J. PERFORMANCE ANALYSIS OF PLATE HEAT EXCHANGERS USED AS REFRIGERANT EVAPORATORS. PhD thesis, University of the Witwatersrand, Johannesburg, 2010.
- [24] IKEGAMI, Y., AND FURUGEN, K. 100 kW CC-OTEC Plant and Deep Ocean water Applications in Kumejima, Okinawa, Japan. Presented at the Hawai'i Convention Center, Honolulu, Hawai'i, USA, 2013.
- [25] ISLEGEN, Z., AND REICHELSTEIN, S. Carbon Capture by Fossil Fuel Power Plants: An Economic Analysis. *Management Science* 57, 1 (2011), 21–30.
- [26] JOURNOUD, A., SINAMA, F., AND LUCAS, F. *Experimental Ocean Thermal Energy Conversion (OTEC) project on the Reunion Island.* Presented at the 4th International Conference on Ocean Energy, 17th October, Dublin, 2012.
- [27] JÜDES, M., VIGERSKE, S., AND TSATSARONIS, G. Optimization of the Design and Partial-Load Operation of Power Plants Using Mixed-Integer Nonlinear Programming. Tech. rep., 2009. Techniche Universitat Berlin.

BIBLIOGRAPHY 85

[28] KALINA, A. I. Generation of Energy by Means of a Working Fluid and Regeneration of a Working Fluid. US Patent, 4346561, 1982.

- [29] KEMPENER, R., AND NEUMANN, F. *OCEAN THERMAL ENERGY CONVERSION: TECHNOLOGY BRIEF.* Technical report, IRENA, 2014.
- [30] KIM, N. J., NG, K. C., AND CHUN, W. Using the condenser effluent from a nuclear power plant for Ocean Thermal Energy Conversion (OTEC). *International Communications in Heat and Mass Transfer* 36, 10 (Dec. 2009), 1008–1013.
- [31] KIRKENIER, J. A. *Techno-economic optimization of Organic Rankine Cycle using working fluid mixtures for 10 to 25 MW OTEC power plants.* Master's thesis, Technical University of Delft, 2014.
- [32] KLEUTE, B. J. Safety Reports Experimental Units OTEC demo. Tech. rep., 2011.
- [33] KLEUTE, B. J., AND VROOM, M. *Offshore ocean thermal energy conversion: Feasibility study of a 10 MW installation*. Technical report, Bluerise BV, 2014.
- [34] KOBAYASHI, H., JITHSUAHARA, S., AND UEHARA, H. *The Present Status and Features of OTEC and Recent Aspects of Thermal Energy Conversion Technologies*. http://www.nmri.go.jp/main/cooperation/ujnr/24ujnr_paper_jpn/Kobayashi.pdf. Accessed December 17, 2014.
- [35] KUMAR, H. The Plate Heat Exchanger: Construction and Design. *Institute of Chemical Engineering Symposium series*, no. 86 (1984), 1275–1288.
- [36] LEMMON, E. W., HUBER, M. L., AND MCLINDEN, M. O. NIST Standard Reference Database 23: Reference Fluid Thermodynamic and Transport Properties-REFPROP, Version 9.1, National Institute of Standards and Technology, Standard Reference Data Program, Gaithersburg, 2013.
- [37] LI, S., AND DAI, Y. Thermo-economic comparison of Kalina and CO₂ transcritical power cycle for low temperature geothermal sources in China. *Applied Thermal Engineering* 70, 1 (Sept. 2014), 139–152.
- [38] LOCAMINI, R. A., MISHONOV, J. I., ANTONOV, T. B., CARCIA, H. E., BARANOVA, O. K., ZWENG, M. M., AND JOHNSON, D. R. World Ocan Atlas 2009, Volume 1: Temperature. Tech. rep., 2010. S. Levitus, Ed. NOAA Atlas NESDIS 68, U. S. Government Printing Office, Washington, D. C., 184 pp.
- [39] LOÁICIGA, H. A. Modern-age buildup of CO₂ and its effecs on seawater acidity and salinity. *Geophysical Research Letters* 33 (2006).
- [40] LUCIA, U. Carnot efficiency: Why? *Physica A: Statistical Mechanics and its Applications* 392, 17 (2013), 3513–3517.
- [41] MACCHI, E., AND PERDICHIZZI, A. Efficiency prediction for axial flow turbines operationg with non-conventional fluids. *ASME J Eng Power 17* (1981), 712–724.

86 Bibliography

[42] Mellado, A. *Design of Turbine for an OTEC Application*. Master's thesis, Technical University of Delft.

- [43] MITSUI, T., ITO, F., SEYA, Y., AND NAKAMOTO, Y. Outline of the 100kW OTEC Pilot Plant in the Republic of Nauru. *IEEE Transactions on Power Apparatus and Systems* 9 (1983), 3167–3171.
- [44] MURALIDHARAN, S. *Assessment of Ocean Thermal Energy Conversion*. Master's thesis, Massachusetts Institute of Technology, 2012.
- [45] NAJAFI, A., REZAEE, S., AND TORABI, F. Sensitivity analysis of a closed cycle ocean thermal energy conversion power plant. *2012 Second Iranian Conference on Renewable Energy and Distributed Generation* (Mar. 2012), 1–6.
- [46] OKAMOTO, A., ARIMA, H., AND IKEGAMI, Y. Characteristic of local boiling heat transfer of ammonia and ammonia / water binary mixture on the plate type evaporator. *Journal of Thermal Science 20*, 4 (July 2011), 332–342.
- [47] OTEC FOUNDATION. Akuo Energy, DCNS and Entrepose to work together to develop onshore OTEC plant for Martinique. http://www.otecnews.org/2014/12/akuo-energy-dcns-entrepose-work-together-develop-onshore-otec-plant-\martinique/. Accessed December 30, 2014.
- [48] PALMER, S. C., PAYNE, W. V., AND DOMANSKI, P. A. Evaporation and Condensation Heat Transfer Performance of Flammable Refrigerants in a Brazed Plate Heat Exchanger. National Institute of Standards and Technology Gaithersburg, July, 2000.
- [49] PERRY, R. H., AND GREEN, D. W. Perry's Chemical Engineers' Handbook, 7th ed. McGraw-Hill, 1999.
- [50] RAJAGOPALAN, K., AND NIHOUS, G. C. Estimates of global Ocean Thermal Energy Conversion (OTEC) resources using an ocean general circulation model. *Renewable Energy* 50 (Feb. 2012), 532–540.
- [51] SHARQAWY, M. H., LIENHARD V, J. H., AND ZUBAIR, S. M. Erratum to Thermophysical properties of seawater: A review of existing correlations and data. *Desalination and Water Treatment* 29, 1-3 (2011), 355–355.
- [52] Shin, J. Y., Kim, M. S., and Ro, S. T. *Correlation of Evaporative Heat Transfer Coefficients for Refrigerant Mixtures*. Presented at the International Refrigeration and Air Conditioning Conference, West Lafayette, Indiana, 1996.
- [53] SINNOTT, R. *Coulson ad Richardson's Chemical Engineering Design, Volume 6.* Elsevier Butterworth-Heinemann, 4th Edition, 2005.
- [54] SOERENSEN, H. C., AND WEINSTEIN, A. Ocean Energy: Position paper for IPCC. Paper for the IPCC Scoping Conference on Renewable Energy, Lübeck, Germany, 2008.
- [55] SOTO, R., AND VERGARA, J. Thermal power plant efficiency enhancement with Ocean Thermal Energy Conversion. *Applied Thermal Engineering* 62, 1 (Jan. 2014), 105–112.

BIBLIOGRAPHY 87

- [56] STARR, F. Kalina Cycle Geothermal Power Plant. OMMI 1, 2 (2002), 1–10.
- [57] TC DIRECT. Industrial Pressure Transmitter. http://www.tcdirect.nl/Default.aspx?level=2&department_id=355/1&searchterm=716-218. Accessed May 11, 2015.
- [58] TC DIRECT. Klantspecifiek: Pt-100 met overgangshuls. Datasheet, n.d.
- [59] THE MATHWORKS INC. MATLAB Release R2014b, Natick, Massachusetts, United States, 2014.
- [60] Thonon, B., and Bontemps, A. Condensation of Pure and Mixture of Hydrocarbons in a Compact Heat Exchanger: Experiments and Modelling. *Heat Transfer Engineering* 23, March 2015 (2002), 3–17.
- [61] THONON, M. Design Method for Plate Evaporators and Condensers. *1st Internationa Conference on Process Intensification for the Chemical Industry*, BHR Group Conference Series Publication, no 18 (1995), 37–47.
- [62] UEHARA, H., AND IKEGAMI, Y. Optimization of a Closed-Cycle OTEC System. *J. Sol. Energy Eng. 112* (1990), 247–256.
- [63] U.S. ENERGY INFORMATION ADMINISTRATION. *International Energy Statistics*. http://www.eia.gov/cfapps/ipdbproject/iedindex3.cfm?tid=2&pid=2&aid=2&cid=ww,&syid=2007&eyid=2011&unit=BKWH. Accessed January 2, 2015.
- [64] VDI GESELLSCHAFT VERFAHRENSTECHNIK UND CHEMIEINGENIEURWESEN. *VDI Heat Atlas*, 2nd ed. Springer, 2010.
- [65] VEGA, L. Ocean Thermal Resources off the Hawaiian Islands, 2009.
- [66] VEGA, L. E. Ocean Thermal Energy Conversion Primer. *Marine Technology Society Journal* 6 (2002), 25–35.
- [67] VENTURA, I. Evaporation heat transfer coefficients of ammonia with a small content of water in a plate heat exchanger in an absorption refrigeration machine. Instituto Superior Técnico, Lisbon, Portugal, 2010.
- [68] WANNIARACHCHI, A. S., RATNAM, U., TILTON, B. E., AND DUTTA-ROY, K. Approximate Correlations for Chevron-Type Plate Heat Exchangers. *30th National Heat Transfer Conference*, vol 12, HTD vol 314, ASME, New York (1995), 145–151.
- [69] WEISSER, D. On the economics of electricity consumption in small island developing states: a role for renewable energy technologies? *Energy Policy 32* (2004), 127–140.
- [70] WHITTAKER, P. Corrosion in the Kalina cycle: An investigation into corrosion problems at the Kalina cycle geothermal power plant in Húsavík, Iceland. Master's thesis, the School for Renewable Energy Science in affiliation with the University of Iceland & the University of Akureyri, 2009.
- [71] WINKELMANN, D. *Condensation of pure refrigerants and their zeotropic mixtures in plate heat exchangers.* PhD thesis, Technical University of Berlin, 2010.

88 Bibliography

[72] YAN, Y., AND LIN, T. Evaporation Heat Transfer and Pressure Drop of Refrigerant R-134a in a Plate Heat Exchanger. *Transactions of the ASME 121*, February 1999 (1999).

- [73] YAN, Y.-Y., LIO, H.-C., AND LIN, T.-F. Condensation heat transfer and pressure drop of refrigerant R-134a in a plate heat exchanger. *International Journal of Heat and Mass Transfer* 42 (1999), 993–1006.
- [74] YANG, M., AND YEH, R. Analysis of optimization in an OTEC plant using organic Rankine cycle. *Renewable Energy 68* (2014), 25–34.
- [75] YOON, J., SON, C., BAEK, S., YE, B. H., KIM, H., AND LEE, H. Performance characteristics of a high-efficiency R717 OTEC power cycle. *Applied Thermal Engineering* 72 (2014), 304–308.
- [76] YUAN, H., MEI, N., HU, S., WANG, L., AND YANG, S. Experimental investigation on an ammonia-water based ocean thermal energy conversion system. *Applied Thermal Engineering 61*, 2 (Nov. 2013), 327–333.
- [77] YUAN, H., MEI, N., AND ZHOU, P. Performance analysis of an absorption power cycle for ocean thermal energy conversion. *Energy Conversion and Management* 87 (2014), 199–207.
- [78] ZHANG, X., HE, M., AND ZHANG, Y. A review of research on the Kalina cycle. *Renewable and Sustainable Energy Reviews 16*, 7 (Sept. 2012), 5309–5318.